

# NAVAL POSTGRADUATE SCHOOL MONTEREY, CALIFORNIA



## THESIS

### SOURCE DEVELOPMENT FOR A SEISMO- ACOUSTIC SONAR

by

Sean M. Fitzpatrick

December 1998

Thesis Advisors:

Thomas G. Muir  
Steven R. Baker  
Anthony J. Healey

Approved for public release; distribution is unlimited.

1 999021 9 09 2

QUALITY INSPECTED 4

| REPORT DOCUMENTATION PAGE  |  |   | Form Approved OMB No. 0704-0188  |  |
|--|--|---|----------------------------------|--|
| Public reporting burden for this collection of information is estimated to average 1 hour per response, including the time for reviewing instruction, searching existing data sources, gathering and maintaining the data needed, and completing and reviewing the collection of information. Send comments regarding this burden estimate or any other aspect of this collection of information, including suggestions for reducing this burden, to Washington Headquarters Services, Directorate for Information Operations and Reports, 1215 Jefferson Davis Highway, Suite 1204, Arlington, VA 22202-4302, and to the Office of Management and Budget, Paperwork Reduction Project (0704-0188) Washington DC 20503.  |  |   |                                  |  |
| 1. AGENCY USE ONLY (Leave blank)   | 2. REPORT DATE<br>December 1998                          | 3. REPORT TYPE AND DATES COVERED<br>Master's Thesis     |                                  |  |
| 4. TITLE AND SUBTITLE OF THESIS<br>SOURCE DEVELOPMENT FOR A SEISMO-ACOUSTIC SONAR  |  | 5. FUNDING NUMBERS                                      |                                  |  |
| 6. AUTHOR(S) Sean M. Fitzpatrick   |  |   |                                  |  |
| 7. PERFORMING ORGANIZATION NAME(S) AND ADDRESS(ES)<br>Naval Postgraduate School<br>Monterey CA 93943-5000  |  | 8. PERFORMING ORGANIZATION REPORT NUMBER                |                                  |  |
| 9. SPONSORING/MONITORING AGENCY NAME(S) AND ADDRESS(ES)<br>Office of Naval Research, Code 321<br>Dr. Douglas Todoroff, Program Manager<br>800 N. Quincy St.<br>Arlington, VA   |  | 10. SPONSORING/MONITORING AGENCY REPORT NUMBER          |                                  |  |
| 11. SUPPLEMENTARY NOTES The views expressed in this thesis are those of the author and do not reflect the official policy or position of the Department of Defense or the U.S. Government.   |  |   |                                  |  |
| 12a. DISTRIBUTION/AVAILABILITY STATEMENT<br>Approved for public release; distribution is unlimited.  |  | 12b. DISTRIBUTION CODE                                  |                                  |  |
| 13. ABSTRACT (maximum 200 words)<br>Buried mines in the beach and surf zone hinder Naval power projection beach assault operations and endanger humans. In this research, it is demonstrated that seismic interface waves on the surface of a natural beach can be used to detect buried, mine-like objects. A seismic sonar system, employing guided interface waves known as Rayleigh or Scholte waves has been proposed for detecting shallow, buried ordnance and is the subject of an ongoing, ONR-sponsored research program at the Naval Postgraduate School. The primary purpose of this research was to develop an improved seismic source to evaluate further the concept of using a seismo-acoustic sonar to detect buried ordnance in the beach and surf zone. The developed source was based upon a linear magnetic force actuator. Additionally, testing procedures were developed for follow-on research. Seismic interface waves were generated with two, 25-lb force-controlled linear actuators operated as shakers. The waves were measured with a two-element horizontal array of three axis seismometers. Buried, mine-like objects, ranging from 71kg to 290kg, and at ranges of up to 5 meters were echo-located by visual examination of the raw, recorded seismic signal, and by the use of polarization filtering signal processing. |  |   |                                  |  |
| 14. SUBJECT TERMS<br>Mine warfare, mine detection, buried ordnance detection, seismo-acoustic sonar, seismic surface waves, Rayleigh waves, Scholte waves  |  |   | 15. NUMBER OF PAGES<br>109       |  |
|  |  |   | 16. PRICE CODE                   |  |
| 17. SECURITY CLASSIFICATION OF REPORT<br>Unclassified  | 18. SECURITY CLASSIFICATION OF THIS PAGE<br>Unclassified | 19. SECURITY CLASSIFICATION OF ABSTRACT<br>Unclassified | 20. LIMITATION OF ABSTRACT<br>UL |  |



Approved for public release; distribution is unlimited

**SOURCE DEVELOPMENT FOR A SEISMO-ACOUSTIC SONAR**

Sean M. Fitzpatrick  
Lieutenant, United States Navy  
B.A., University of California at Berkeley, 1990

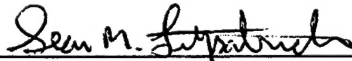
Submitted in partial fulfillment  
of the requirements for the degree of

**MASTER OF SCIENCE IN APPLIED PHYSICS  
MASTER OF SCIENCE IN MECHANICAL ENGINEERING**

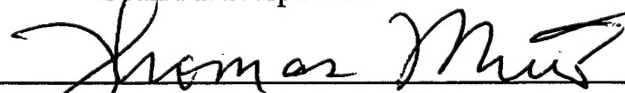
from the

**NAVAL POSTGRADUATE SCHOOL  
December 1998**

Author:


  
Sean M. Fitzpatrick

Approved by:

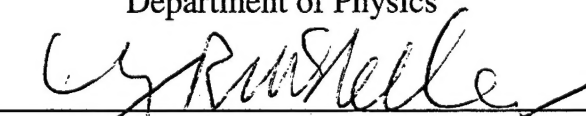
  
Thomas G. Muir, Thesis Advisor

  
Steven R. Baker, Thesis Advisor

  
Anthony J. Healey, Thesis Advisor

  
William B. Maier, Chairman

Department of Physics

  
Terry R. McNelley, Chairman  
Department of Mechanical Engineering



## **ABSTRACT**

Buried mines in the beach and surf zone hinder Naval power projection beach assault operations and endanger humans. In this research, it is demonstrated that seismic interface waves on the surface of a natural beach can be used to detect buried, mine-like objects. A seismic sonar system, employing guided interface waves known as Rayleigh or Scholte waves has been proposed for detecting shallow, buried ordnance and is the subject of an ongoing, ONR-sponsored research program at the Naval Postgraduate School. The primary purpose of this research was to develop an improved seismic source to evaluate further the concept of using a seismo-acoustic sonar to detect buried ordnance in the beach and surf zone. The developed source was based upon a linear magnetic force actuator. Additionally, testing procedures were developed for follow-on research. Seismic interface waves were generated with two, 25-lb force-controlled linear actuators operated as shakers. The waves were measured with a two-element horizontal array of three axis seismometers. Buried, mine-like objects, ranging from 71kg to 290kg, and at ranges of up to 5 meters were echo-located by visual examination of the raw, recorded seismic signal, and by the use of polarization filtering signal processing.



## TABLE OF CONTENTS

|   |    |
|---|----|
| I. INTRODUCTION.....                                | 1  |
| A. RESEARCH MOTIVATION.....                         | 2  |
| B. CURRENT AND EMERGING MINEHUNTING METHODS.....    | 4  |
| II. PREVIOUS RESEARCH.....                          | 9  |
| A. ARL:UT (1996).....                               | 9  |
| B. NAVAL POSTGRADUATE SCHOOL (1997).....            | 10 |
| III. THEORY OF SEISMIC WAVES.....                   | 13 |
| A. ELASTIC BODY WAVES.....                          | 13 |
| B. ELASTIC SURFACE WAVES.....                       | 15 |
| 1. Rayleigh waves.....                              | 15 |
| 2. Scholte waves.....                               | 20 |
| IV. DESCRIPTION OF EXPERIMENTAL EQUIPMENT.....      | 21 |
| A. SEISMIC SOURCE.....                              | 21 |
| 1. Actuator Modifications.....                      | 24 |
| 2. Electronic Control Unit (ECU) Modifications..... | 28 |
| 3. Relative Source Gain.....                        | 29 |
| B. SEISMIC SENSORS.....                             | 30 |
| C. DATA ACQUISITION.....                            | 32 |
| D. SIGNAL PROCESSING.....                           | 33 |
| E. TRANSPORTATION.....                              | 34 |
| V. TESTING PROCEDURES.....                          | 37 |
| A. BEACH TEST SITE.....                             | 37 |
| B. SEDIMENT CHARACTERIZATION.....                   | 38 |
| C. AMBIENT NOISE SPECTRA.....                       | 39 |
| D. SOURCE EMPLOYMENT.....                           | 40 |
| 1. Placement and Orientation.....                   | 41 |
| 2. Phasing.....                                     | 44 |

|  |    |
|--|----|
| E. TESTING CHRONOLOGY.....                                 | 46 |
| 1. Frequency.....  | 48 |
| 2. Wavespeed.....  | 50 |
| 3. Background Data.....                                    | 50 |
| 4. Target Data.....  | 51 |
| 5. Signal Processing.....                                  | 51 |
| VI. TEST RESULTS (VERTICAL SOURCE).....                    | 53 |
| A. ATTENUATION.....  | 53 |
| B. VELOCITY AND DISPLACEMENT.....                          | 54 |
| C. TARGET DETECTION.....                                   | 56 |
| D. UNDERWATER TEST.....                                    | 61 |
| VII. CONCLUSIONS AND RECOMMENDATIONS .....                 | 63 |
| A. CONCLUSIONS.....  | 63 |
| B. RECOMMENDATIONS.....                                    | 63 |
| APPENDIX A. MANUFACTURER SPECIFICATION SHEETS.....         | 67 |
| APPENDIX B. UNDERWATER ACTUATOR CABLES AND CONNECTORS..... | 79 |
| APPENDIX C. EXPERIMENTAL SETUPS.....                       | 85 |
| APPENDIX D. COMPUTER PROGRAMS AND SUBROUTINES.....         | 93 |
| LIST OF REFERENCES.....                                    | 95 |
| INITIAL DISTRIBUTION LIST.....                             | 97 |

## **ACKNOWLEDGMENT**

The author would like to thank George Jaksha & Gary Beck for their insight and help in developing the seismo-acoustic sonar used in this study. I would also like to especially thank Professor Tom Muir for his overall guidance and assistance during the field research phase and Professors Steve Baker and Anthony Healey for their help. Most importantly, I would like to thank my wife, Laure, for her continuous support. This work was supported by the Office of Naval Research, Code 321, Dr. Douglas Todoroff, Program Manager.



## I. INTRODUCTION

Buried mines are a hindrance to Naval beach assault operations. An unknown, buried mine, can disrupt, delay, and in some cases, halt Naval operations. In order to maintain the relative superiority and capability that U.S. Naval Forces have to project power ashore, it is critical that our forces have the ability to counter and neutralize buried mines in stride. This capability begins with the detection of buried mines, both in the beach and in the surf zone. The proposed concept by the Applied Research Laboratories of the University of Texas at Austin (ARL:UT) to use a seismo-acoustic sonar and "guided" seismic interface waves to detect shallow, buried ordnance in the beach and surf zone offers promise in providing the ability to detect buried mines. This concept will further enable our Naval Forces to effectively project power ashore.

Buried mines are not only a threat to U.S. military forces, they are also a serious hazard to civilians and non-combatants. For example, there are more than 100 million buried landmines worldwide and more than 150 people are killed or maimed each week. In fact, the casualty rate is so high that one in every 470 Angolans and 1 in every 1,000 Somalis is an amputee. Cambodia alone has an amputee population of more than 30,000. [Ref. 1] The concept of a seismo-acoustic sonar that can effectively detect buried mines is encouraging and would help reduce the number of landmines and casualties caused by buried landmines worldwide.

The research reported in this thesis is one step towards the development and fielding of a seismo-acoustic sonar for detecting buried ordnance. This research is presented in seven chapters. The introductory chapter outlines the motivation for developing a seismo-acoustic sonar including a brief discussion on continuing plans to develop improved Mine Countermeasure (MCM) capabilities for U.S. Naval Forces. Also included is a short summary of current and emerging minehunting (MH) methods and technologies. The second chapter describes previous research efforts, which helped provide guidance for source development and testing procedures. The third chapter presents a brief overview on seismic wave theory including a discussion on the advantages of using seismic interface waves for detecting buried ordnance. The fourth chapter outlines the design and development of the seismo-acoustic sonar and equipment

used in this experiment. The fifth and sixth chapters describe the field testing procedures and experimental results, respectively. The final chapter contains concluding remarks and recommendations for further testing and development.

## **A. RESEARCH MOTIVATION**

Mine warfare (MIW) has been a part of U.S. warfighting since the American Revolution. [Ref. 2] Since that time, U.S. MIW experiences have been infrequent and the lessons learned arguably ambiguous. It is partly because of this ambiguity that mine countermeasures for U.S. Naval Forces are less than ideal, as evidenced by the damage to the USS PRINCETON and USS TRIPOLI by Iraqi mines during DESERT STORM. [Ref. 3]

The reality of an increasing, modern mine threat is not surprising considering that most mines are relatively inexpensive and simple to manufacture. The low cost of developing an offensive or defensive mining capability combined with its effectiveness both tactically and psychologically, make MIW particularly attractive to nations with few resources to devote to more expensive, sophisticated weaponry. As a result, mine proliferation is becoming a worldwide problem, with more than 49 countries possessing mining capabilities, and with 30 of these demonstrating mine production capabilities, and 20 of these attempting to export their MIW systems. [Ref. 2]

The increasing mine threat, combined with a downsizing Navy and dwindling resources, have driven efforts to develop more flexible and robust minehunting systems and capabilities for U.S. Naval Forces. The modernization plan for the U.S. Navy is outlined in the *United States Naval Mine Warfare Plan* [Ref 2] which describes the requirement for an organic MCM capability consistent with Navy and Marine Corps doctrine, "Maneuver warfare...from the Sea".

Power projection operations, including the effective delivery of U.S. Amphibious Forces, from the sea, require the avoidance or neutralization of any possible mine threat, particularly in the vulnerable regions where amphibious forces transition from shallow water, through the surf zone, and onto the beach. Naval mines like the "Manta" bottom

mine (see Figure 1.1) that damaged the USS PRINCETON typically “scour” below the surface and in this process are buried, due to water action. Similarly, beach and surf zone mines are purposely hidden or become buried due to erosion and wind action, making their detection and neutralization more difficult. These types of buried mines clearly pose a serious threat to amphibious forces, particularly during an opposed, amphibious landing. A flexible, dedicated or organic minehunting capability to detect these buried mines in the shallow water surf zone and in the beach is needed to effectively neutralize the mine threat to U.S. amphibious landing forces.



Figure 1.1. “Manta” bottom mine similar to the mine that damaged the USS PRINCETON during DESERT STORM [Ref. 2]

Currently, U.S. capabilities to detect and localize buried mines in both the shallow water surf zone and in the beach are limited and no one system is optimally capable of operating in both environments. The successful development and fielding of a seismo-acoustic sonar would provide an additional minehunting capability that could cover the

critically vulnerable gap from the surf zone to the beach and help neutralize the mine threat for our amphibious landing forces.

## **B. CURRENT AND EMERGING MINEHUNTING METHODS**

The critically vulnerable regions for amphibious forces as they transition from sea to land are the shallow water surf zone and the beach. U.S. amphibious forces are vulnerable to buried ordnance in these regions partly because there is no MH system that can seamlessly transition from the sea, through the surf zone, and on to the beach while continuously hunting for buried mines. While there are a variety of methods and systems available to U.S. Naval Forces for hunting mines, no single system is capable of detecting buried mines both in the shallow water surf zone and in the beach. Some of the more common MH methods are listed below in Tables 1.1 and 1.2 respectively.

| <b>MINEHUNTING METHODS – SHALLOW WATER SURF ZONE</b> |
|--|
| Navy EOD and SEAL divers                             |
| USMC reconnaissance combat swimmers                  |
| Marine mammals (U.S. Navy dolphins)                  |
| Towed sweep gear                                     |
| Remote Minehunting (RMS) Sonar system                |
| Airborne Laser Mine Detection System (ALMDS)         |

Table 1.1. Current minehunting methods in the shallow water surf zone

| <b>MINEHUNTING METHODS – BEACH</b> |
|------------------------------------|
| Hand-held probes                   |
| Manual metal detectors             |
| Ground penetrating radar           |
| Mechanical breaching equipment     |
| Explosive breaching nets           |
| Trained dogs                       |

Table 1.2. Current minehunting methods on the beach

Each of the methods and capabilities listed in Tables 1.1 and 1.2 has distinct advantages and disadvantages. For example, manual minehunting methods are generally very accurate and have low false alarm rates. However, they are also relatively slow and dangerous, as illustrated by the EOD technician probing for buried mines with a hand-held probe in Figure 1.2. Additionally, none of the current methods listed in Tables 1.1 and 1.2 are capable of detecting and locating buried ordnance in the shallow water surf zone and in the beach.



Figure 1.2. EOD technician with a hand-held probe [Ref. 4]

There are a number of emerging technologies and systems being considered to combat the increasing mine threat to amphibious forces. One of these systems, the Coastal Battlefield Reconnaissance & Analysis (COBRA) minefield reconnaissance system (see Figure 1.3), an unmanned aerial vehicle (UAV) optical-based sensor system, offers promise in that it can detect shallow, underwater mines and is capable of surveying large areas. While the COBRA system offers relative improvements in minehunting, it is still unable to detect buried ordnance, both underwater and in the beach.

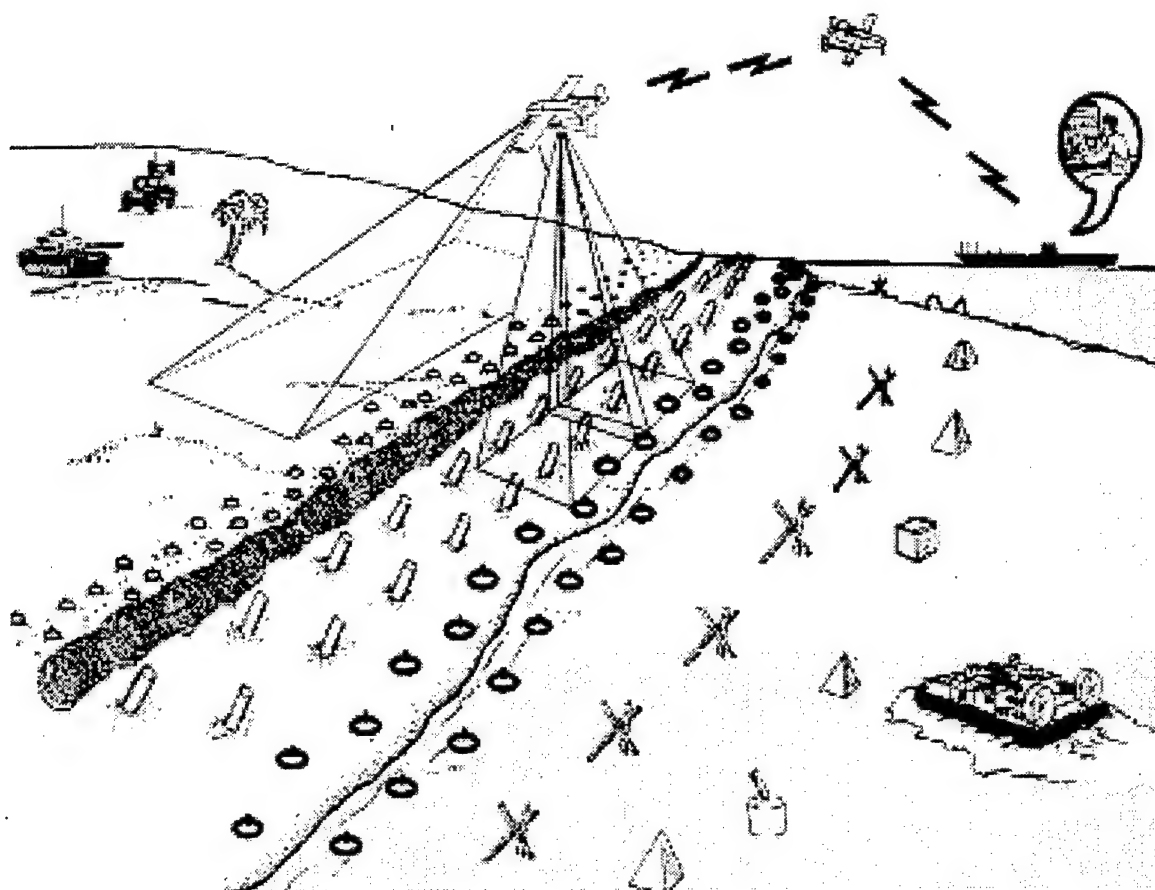


Figure 1.3. Overview of the COBRA sonar system [Ref. 5]

The concept of a seismo-acoustic sonar, as shown in Figure 1.4, offers promise as a practical method to detect buried ordnance both in the beach and the seafloor. A seismo-acoustic sonar would complement current and emerging minehunting methods and technologies, as well as provide an additional sensor for multi-sensor data fusion.

Like other systems, the seismo-acoustic sonar is highly dependent on the propagating characteristics of the medium, which may require the application of relatively complex signal processing methods to identify the target signal in the seismic sound field. This requirement will be addressed later.

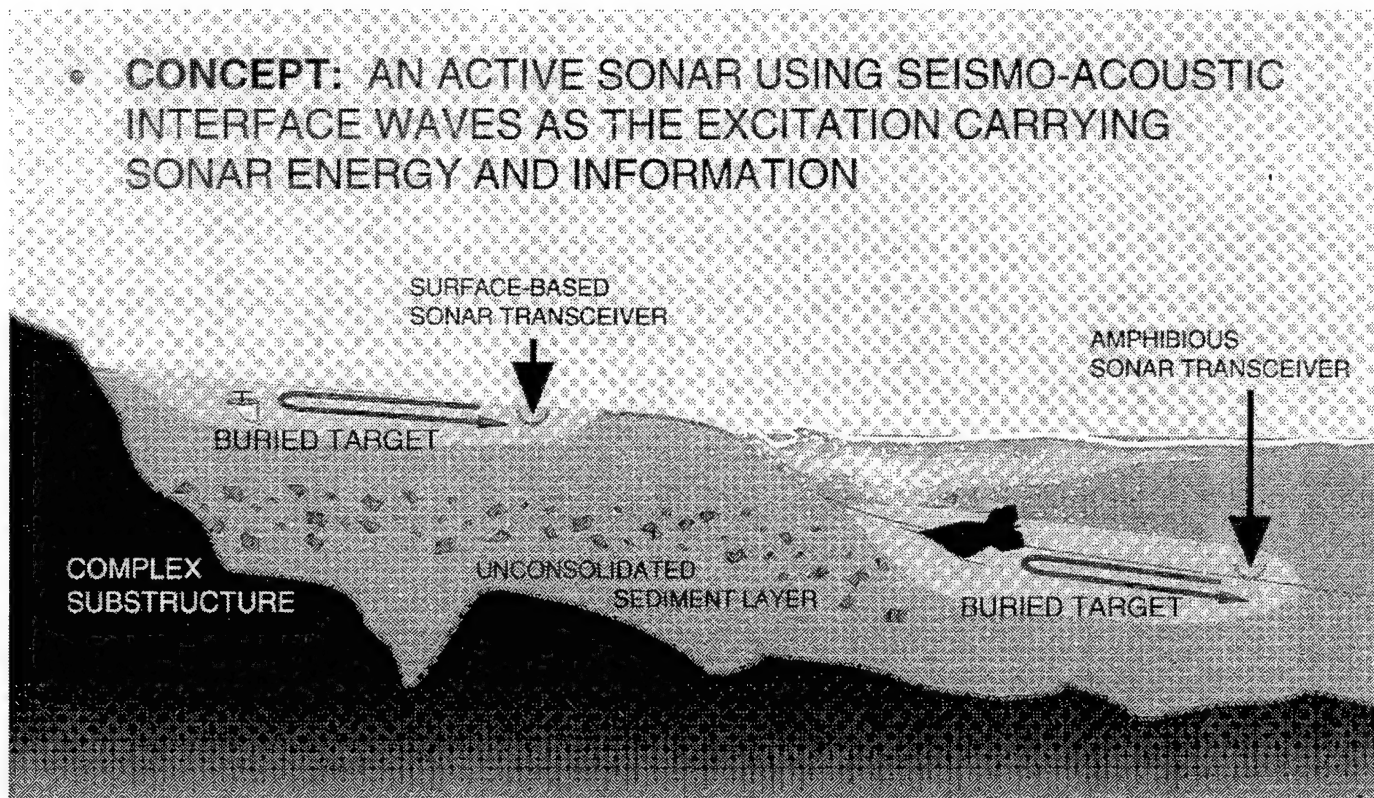


Figure 1.4. Design concept for a seismo-acoustic sonar to detect buried mines in the shallow water surf zone and in the beach [Ref. 6]



## **II. PREVIOUS RESEARCH**

There has been a long-standing effort to detect buried mines in the beach and surf zone. The Naval Coastal Systems Station in Panama City, Florida has long been working on the development of a synthetic aperture sonar that can be "sensor-fused" with magnetic sensors for detecting buried mines from the surf zone seaward. Two excellent articles on these sensor approaches, one by G.S. Sammelman, et. al. (synthetic aperture sonar) and another by T.R. Clem (magnetics), recently appeared in an Office of [Naval Research publication Naval Research Review, D. Toderoff, Vol XLIX, b. 3, 1997].

Similarly, it is scientifically feasible that seismic interface waves could be used to detect and locate shallow, buried, mine-like objects. While there have been many studies on seismic waves, there are two recent research studies of particular interest. The first study was conducted at the Applied Research Laboratories of the University of Texas at Austin (ARL:UT), where field tests were conducted to evaluate the use of seismo-acoustic waves to detect a buried mine-like object in a natural beach. The second study, conducted at the Naval Postgraduate School, initiated development of a discrete-mode, seismo-acoustic source, suitable for detecting buried, mine-like objects in the beach. These two research projects laid the foundation for the research reported in this thesis.

### **A. ARL:UT (1996)**

Feasibility tests were conducted by ARL:UT to study the possibility of using seismic interface waves to detected buried mine-like objects in a natural beach. The seismic source consisted of a six-inch by eight-inch exciter foot with protruding nails, driven by an electro-mechanical transducer, as shown in Figure 2.1. A three-element array of three-axis seismometers was used to receive the seismic signals. [Ref. 7]

Test results showed that various signal processing techniques were required to isolate the target signal in the relatively complex, seismic wavefield. [Ref. 7] These signal processing methods included coherent averaging, background subtraction, and vector polarization filtering, which will be discussed later.

The research at ARL:UT validated the proof-of-concept use of seismo-acoustic interface waves to detect buried mine-like objects. However, there was observed a significant amount of reverberation in the seismic signal. The excessive reverberation required the coherent subtraction of the reverberant background to detect the target. These results suggested one obvious method of improving the seismo-acoustic sonar: reduce the amount of the reverberant background in the seismic, target signals. A logical step to reduce the amount of reverberant background noise was to consider a different seismo-acoustic source, one that discretely generates only one type of seismic, interface wave.

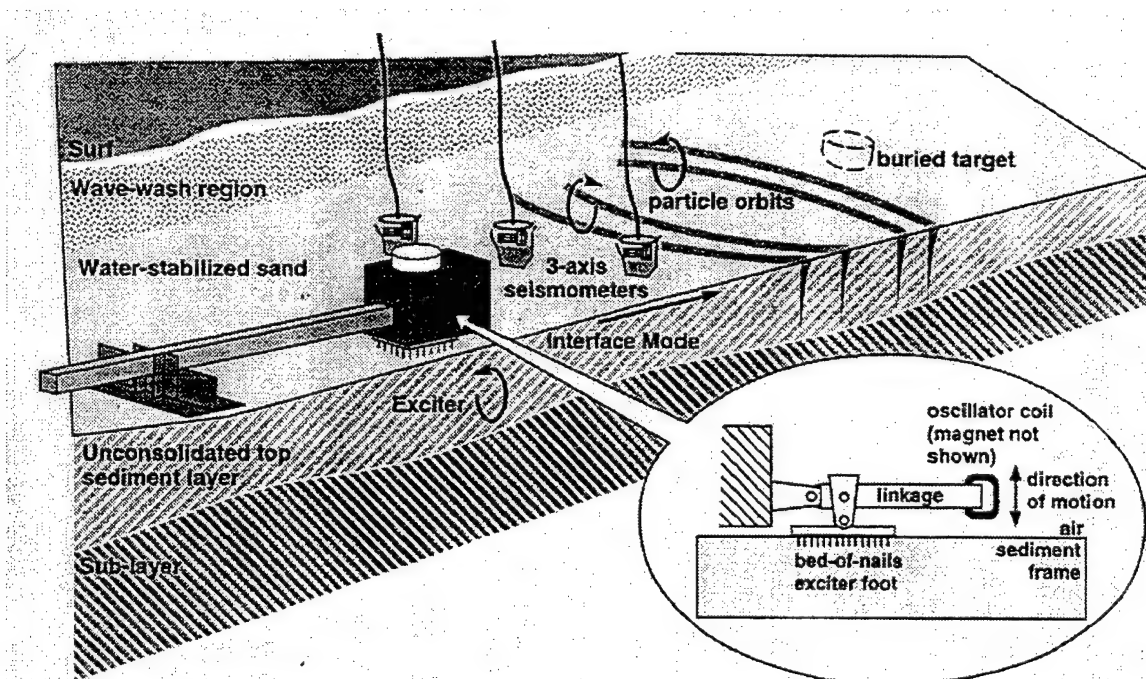


Figure 2.1. ARL:UT seismic target detection beach setup [Ref. 7]

## B. NAVAL POSTGRADUATE SCHOOL (1997)

Based on the ARL:UT research results, LT Frederick Gaghan studied a discrete-mode seismic source designed to selectively excite and generate seismic surface waves. [Ref. 8] He developed two discrete-mode seismic sources, the second being a larger scale version of the first. The final, field-tested seismic source is shown in Figure 2.2. It consists of two, off-the-shelf, 10 pound-force, moving magnet inertial reaction force

transducers (bass shakers), mounted at 45 degree angles with respect to an aluminum base support. Test results showed that, due to medium anisotropy, a drive feedback system or different type of seismic source needed to be developed to suppress unwanted wave modes. At relatively short ranges, less than about 15 meters (45 feet), it was found that multiple body and interface waves were present, resulting in a relatively complex seismic wave field. At longer ranges, greater than about 25 meters (75 feet), it was found that the propagating medium naturally filtered the seismic waves so that the wave was predominantly a single-mode wave. The most important conclusion relevant to this work was that stronger, more linear sources were needed along with refined field testing procedures.

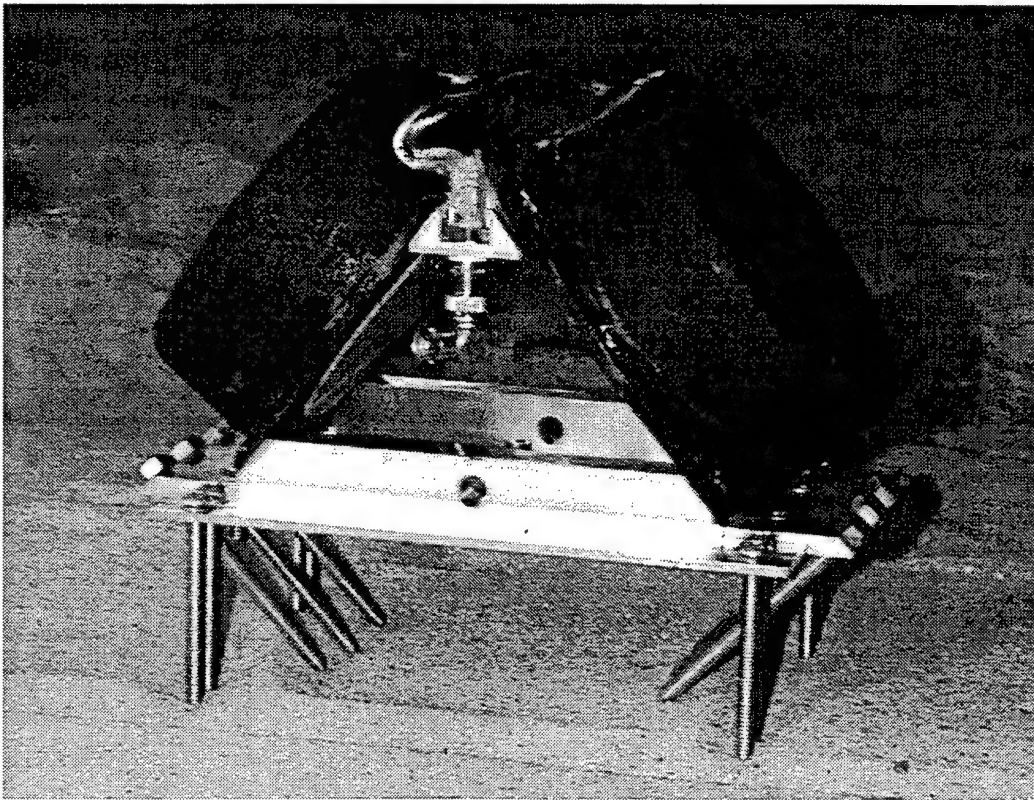


Figure 2.2. NPS discrete-mode seismic sonar design [Ref. 8]

Based on the conclusions and recommendations from the two previous research efforts, the present research focused on the development of a seismic source capable of being used to detect and locate buried mine-like objects. Significant efforts were made to

refine field-testing procedures and successfully detect a buried, mine-like target to support ongoing target strength studies.

### III. THEORY OF SEISMIC WAVES

Seismic waves have been used for geological surveying of petroleum and mineral deposits for many years. While there are actually many different types of seismic waves, the most common are those generated by an earthquake, which travel through the body of the earth and along the earth's surface. As a result, seismic waves are generally divided into two categories, body waves and surface waves. The theory of elasticity predicts two basic categories of mechanical body waves for an infinite medium, compressional waves and shear waves. In addition to these body waves, there exist many different types of surface waves, of which three are of particular interest: the Rayleigh wave, the Scholte wave, and the Love wave. Rayleigh waves are surface waves, with both radial (direction of propagation) and vertical motion, that exist on the interface boundary between a solid and a gas. Scholte waves are similar to Rayleigh waves except that they occur on the interface boundary between a solid and a liquid. Love waves are "ducted" waves, existing in the layer between three different media or near the interface, where there is an increasing shear velocity with depth, and have purely shear motion. This chapter gives a brief overview of the basic theory of seismic body waves and surface waves, and describes the advantages of using Rayleigh or Scholte waves for detecting buried ordnance.

#### A. ELASTIC BODY WAVES

The stress relations for elastic body waves are found by modeling the propagating medium as an infinite, homogenous, isotropic and elastic body, and are given by,

$$\begin{aligned} \sigma_{xx} &= \lambda\theta + 2\mu\epsilon_{xx}, & \sigma_{yy} &= \lambda\theta + 2\mu\epsilon_{yy}, & \sigma_{zz} &= \lambda\theta + 2\mu\epsilon_{zz}, \\ \sigma_{xy} &= \mu\epsilon_{xy}, & \sigma_{yz} &= \mu\epsilon_{yz}, & \sigma_{zx} &= \mu\epsilon_{zx} \end{aligned}, \quad (3.1)$$

where  $\sigma$  and  $\epsilon$  are the stress and strain, respectively,  $\lambda$  and  $\mu$  are the Lamé constants, and  $\theta$  is the dilatation, or volume strain. The stress and strain indices in (3.1) represent the direction of the stress or strain and the plane over which it is applied. [Ref. 9]

Neglecting body forces, the equations of motion are given by,

$$\rho \frac{\partial^2 \vec{u}}{\partial t^2} = (\lambda + \mu) \nabla \theta + \mu \nabla^2 \vec{u}, \quad (3.2)$$

where  $\rho$  is the density of the propagating medium,  $\vec{u}$  represents the particle displacement in vector notation,  $\lambda$  and  $\mu$  are the Lamé constants, and  $\theta$  is the dilatation or volume strain. [Ref. 9]

The solutions to the elastic wave equations of motion in (3.2) lead to two types of mechanical body waves, a compression wave, known as a Primary or P-wave, and a shear wave, known as a Secondary or S-wave. The P-wave is the fastest travelling wave, producing particle motion that is co-linear with the direction of propagation. P-waves can propagate in almost any kind of medium, including rock and water, and travel with a longitudinal speed given by

$$c_l = \sqrt{\frac{B + \frac{4}{3}\mu}{\rho}}, \quad (3.3)$$

where  $B$  is the adiabatic bulk modulus,  $\mu$  is the shear modulus, and  $\rho$  is the density (note that the Lamé constant  $\lambda$  and the shear modulus  $\mu$  are one and the same) [Ref. 9]. Contrary to P-waves, S-waves do not propagate in water, due to the fact that liquids cannot support static shear stresses. Bulk S-waves produce particle motion perpendicular to the direction of propagation and travel with a speed given by

$$c_s = \sqrt{\frac{\mu}{\rho}}, \quad (3.4)$$

where  $\mu$  is the shear modulus, and  $\rho$  is the density. [Ref. 9] In general, both P-waves and S-waves are produced when an external force disturbs an elastic medium or when an elastic surface wave interacts with an interface or a boundary.

## B. ELASTIC SURFACE WAVES

While there are actually many different types of surface waves, three specific wave types were considered in this research: Rayleigh, Scholte, and Love waves. As will be shown later, the Love wave was found to result in excessive background reverberation, and was not considered further. Rayleigh waves, on the other hand, were found to be ideal for detecting shallow, buried ordnance in the beach. While not specifically tested, Scholte waves, similar to Rayleigh waves, can also be considered as ideal wave types for detecting shallow, buried ordnance in the seafloor and surf zone.

### 1. Rayleigh Waves

In 1885, the “great” English scientist, Lord Rayleigh, demonstrated the existence of a surface wave that traveled over the interface between a semi-infinite, elastic half space and a gas; hence these waves became known as Rayleigh waves. [Ref. 10] The Rayleigh wave equations, obtained by applying the conditions for a stress-free boundary to the bulk wave equations in (3.2), are given by

$$\frac{\partial^2 \phi}{dt^2} = c_l^2 \nabla^2 \phi, \quad \frac{\partial^2 \psi}{dt^2} = c_s^2 \nabla^2 \psi, \quad (3.5)$$

where  $\phi$  and  $\psi$  are potential functions representing compression and rotation wave effects respectively. [Ref. 9] The finite solutions to (3.5) result in a propagating wave along the boundary that is attenuated with increasing depth provided the following condition is met [Ref. 9],

$$\kappa^6 - 8\kappa^4 + (24 - 16\gamma^2)\kappa^2 + (16\gamma^2 - 16) = 0. \quad (3.6)$$

The dimensionless variables  $\kappa$  and  $\gamma$  in (3.6) are velocity ratios, given by

$$\kappa = \frac{c_r}{c_s} \text{ and } \gamma^2 = \frac{c_s}{c_l} = \frac{\mu}{\lambda + 2\mu} = \frac{1 - 2\nu}{2 - 2\nu}, \quad (3.7)$$

where  $c_r$  is the Rayleigh wavespeed,  $c_s$  is the shear wavespeed given by (3.4),  $c_l$  is the longitudinal wavespeed, given by (3.3),  $\lambda$  and  $\mu$  are the Lamé constants, and  $\nu$  is Poisson's ratio. [Ref. 9] The solution to (3.6) is found for a single, real, positive root on the interval  $\kappa = (0, 1)$ , corresponding to a value of Poisson's ratio on the interval  $\nu = (0, 0.5)$ . [Ref. 11] For most solid/fluid boundaries, the ratio of Rayleigh wavespeed to shear wavespeed is typically about  $\kappa \approx 0.9$ . [Ref. 11]

As a result of the conditions described by (3.6) and (3.7), Rayleigh waves have distinctive features that make them more readily identifiable in a complex, seismo-acoustic wavefield. Probably the most obvious feature of Rayleigh waves is the elliptical particle motion produced by their passage. This unique characteristic allows Rayleigh waves to be distinguished from other wave types by identifying those waves that have a  $90^\circ$  phase shift (quarter period delay) between their horizontal and vertical components. The phase relationship between the horizontal and vertical components resulting in elliptical motion is shown in Figure 3.1, which shows an idealized seismic wavetrain generated by a single vertical impulse source. [Ref. 12]

The first two waves (outermost) shown in Figure 3.1a and 3.1b, are the relatively fast P-wave and slower S-wave, known also as the "Minor Tremor" in seismic earthquake activity. [Ref. 12] The Rayleigh wave closely follows the S-wave and is known as the "Major Tremor". In the Rayleigh wave, the horizontal and vertical components differ in phase by about  $90^\circ$ . Near the surface, this results in motion that is counterclockwise elliptical, or "retrograde", with respect to the direction of wave propagation, as shown in Figure 3.1c. Note also that, of the three wave types, for a semi-infinite, elastic medium with a free boundary, the Rayleigh wave typically has the largest amplitude or displacement, particularly the vertical component, which is of importance and will be discussed later.

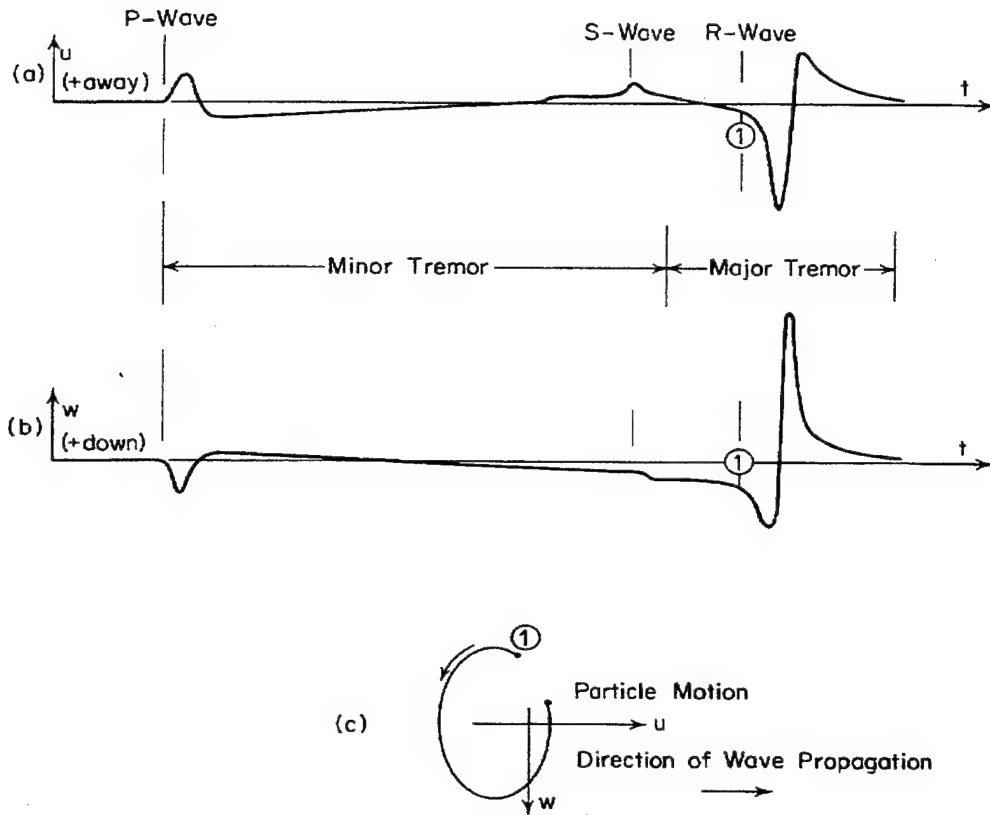


Figure 3.1. Seismic wavetrain resulting from a single vertical impulse source [Ref. 12]

Another important and distinctive feature of Rayleigh waves is that the sense of their elliptical motion changes with depth. This is further illustrated by modeling the propagating medium, a medium-grain natural beach, as a semi-infinite, uniform (non-layered) solid with elastic properties. While this model is not perfectly accurate, it will nevertheless illustrate some of the major features of Rayleigh waves. For this present project, tests were conducted on a medium-grain, natural beach with a typical Poisson's ratio of about  $\nu \approx 0.25$ , and a measured shear wavespeed of about 90m/s. The seismo-acoustic sonar was typically operated at frequencies on the order of about 100Hz. Substituting these values into the required condition (3.6), the resulting horizontal and vertical Rayleigh wave displacements were determined as a function of depth (see Figure 3.2) with the MATLAB program in Appendix D23.

For depths less than about one-tenth of a wavelength ( $0.2\lambda_r$ ), where  $\lambda_r$  represents the Rayleigh wavelength, the horizontal displacement is positive, as shown in Figure 3.2,

and the sense of the motion is retrograde with respect to the direction of propagation, as seen in Figure 3.1c. At a depth of about  $0.2\lambda_r$ , the horizontal motion is zero, resulting in purely vertical motion. At depths greater than  $0.2\lambda_r$ , the relative horizontal displacement changes direction, becoming negative, and the sense of the motion changes to clockwise or “prograde” motion with respect to the direction of wave propagation. [Ref. 11] Note also that the relative amplitudes of the horizontal and vertical displacements decrease or are attenuated with increasing depth into the propagating medium. At a depth of about two wavelengths, the amplitude of the displacement is less than 1% of the maximum displacement at the surface and for all practical purposes the Rayleigh wave can be considered to be localized to within a layer of about two wavelengths deep.

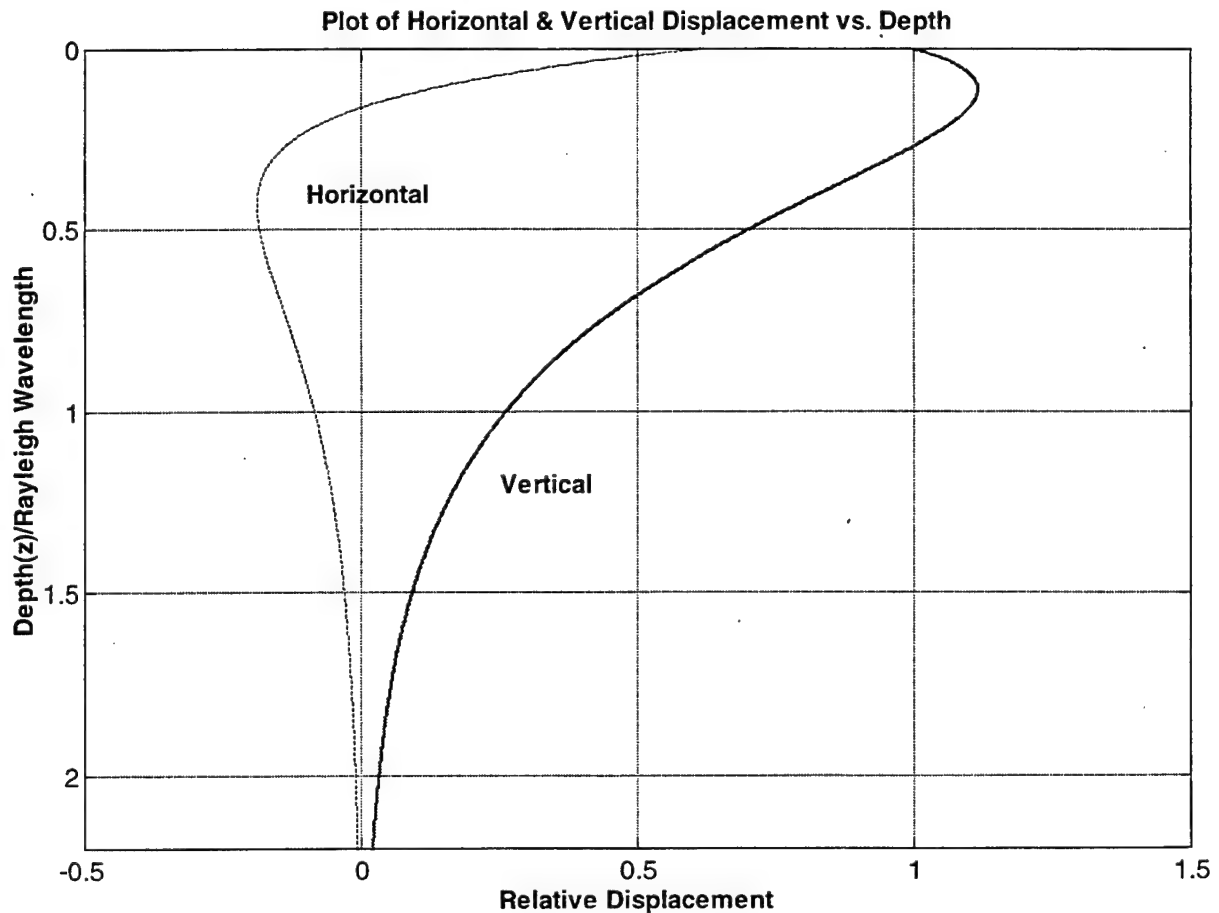
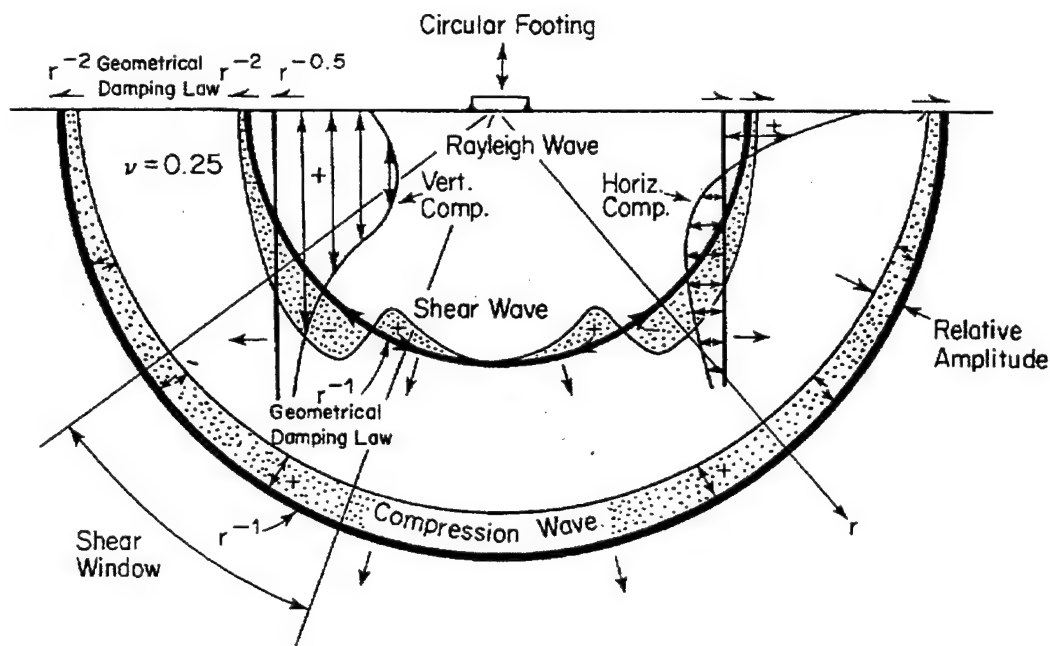


Figure 3.2. Typical Rayleigh wave displacements in a natural beach as a function of depth (see Appendix D23 for the program listing)

As shown in Figure 3.1, Rayleigh waves are the largest disturbance in a seismic wavetrain generated by a vertical impulse. Additionally, since Rayleigh waves are localized near the surface, they attenuate due to geometrical spreading less severely than do other wave types. Neglecting absorption and frictional effects, Rayleigh waves attenuate approximately as the inverse of the square root of the range ( $1/\sqrt{r}$ ) from the source or scattering center, whereas body waves attenuate approximately as  $1/r$ , due to spherical spreading. As a result, Rayleigh waves contain a significant amount of the total seismic wave energy, as illustrated in Figure 3.3, which shows the relative energy partitions for the Rayleigh, shear, and compression wave components resulting from a vertically oscillating circular plate at the surface of a semi-infinite, uniform, elastic medium. [Ref. 11]



| Wave Type   | Per Cent of Total Energy |
|-------------|--------------------------|
| Rayleigh    | 67                       |
| Shear       | 26                       |
| Compression | 7                        |

Figure 3.3. Wavefield from a vertically oscillating circular plate at the surface of an ideal, semi-infinite, uniform, elastic medium [Ref. 11]

Note that Figure 3.3 illustrates many of the Rayleigh wave features that have been discussed, namely, that for an idealized, semi-infinite, uniform, elastic medium, Rayleigh waves travel along the interface boundary, and contain a significant amount of seismic wave energy. Rayleigh waves also result in elliptical particle motion near the surface and have a significant vertical displacement component. These distinctive characteristics make Rayleigh waves well suited for use in a seismo-acoustic sonar to detect shallow, buried ordnance.

## 2. Scholte Waves

Scholte waves are essentially identical to Rayleigh waves except that the interface boundary is between a solid and a liquid. Scholte waves contain the same essential features as Rayleigh waves, as shown in Figure 3.4. [Ref. 13] Note that Scholte waves in the sea floor, similar to Rayleigh waves, are localized near the bottom-water boundary. The motion is also depth dependent, changing from retrograde elliptical at the surface to purely vertical at a depth of about one-tenth of a wavelength and then to prograde elliptical at greater depths. These distinctive characteristics of Scholte waves also make them well suited for detecting buried naval ordnance in the seafloor and shallow water surf zone sediments.

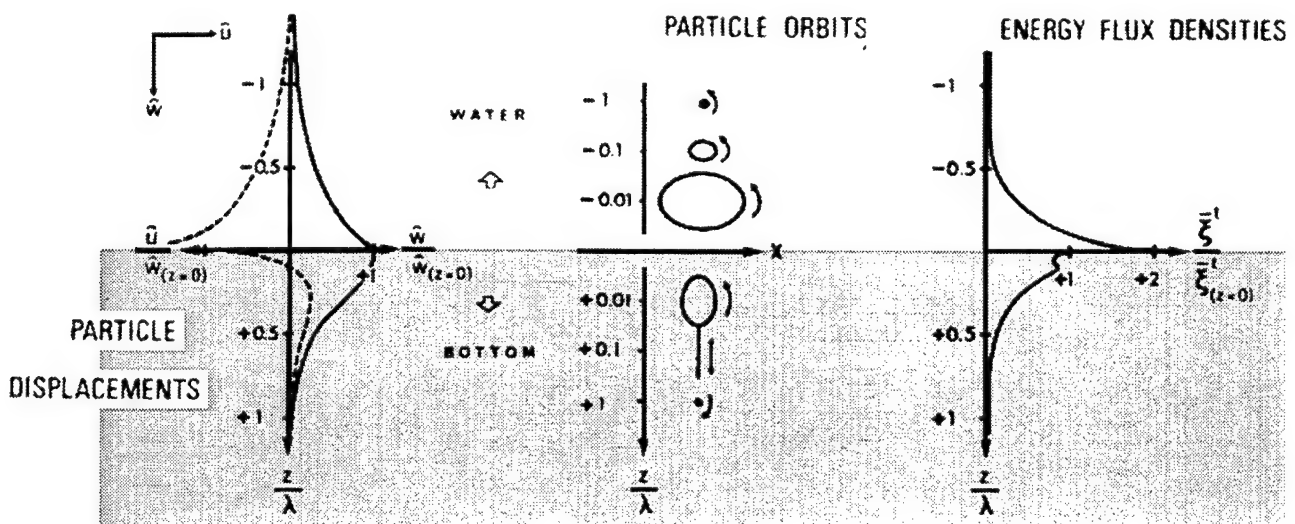


Figure 3.4. Scholte wave characteristics in the seafloor [Ref. 13]

#### IV. DESCRIPTION OF EXPERIMENTAL EQUIPMENT

The most important part of this research were the research tools, particularly the seismo-acoustic sonar. The experimental apparatus is functionally divided into four major groups, as illustrated in Figure 4.1: (1) Seismic source(s), (2) Seismic sensor(s), (3) Data acquisition, and (4) Signal processing. This chapter describes in further detail the system components that were used in this research, including the modifications that were made to the seismo-acoustic source, the sensors, and the data acquisition system.

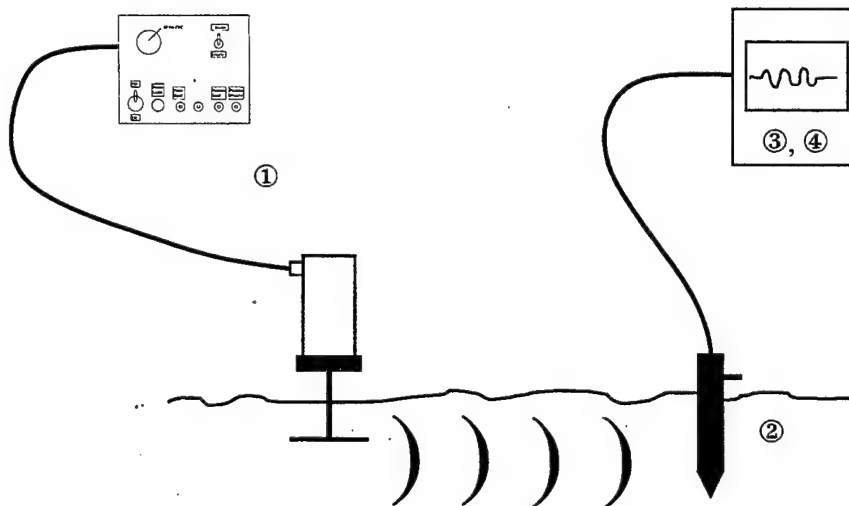


Figure 4.1. Simplified representation of the seismo-acoustic sonar system

##### A. SEISMIC SOURCE

The seismo-acoustic sonar source was based on two, commercial, off-the-shelf linear actuator systems, made by Aura Systems Inc, (see Appendix A1 for specifications). [Ref. 14] Depending on the configuration, these actuators are capable of operating as either positioners or shakers. For this research, the linear actuators were factory-configured to deliver a voltage-controlled force, capable of generating 10lbf-rms and 25lbf-peak output, with 0.5-inches of total stroke. The actuators have a relatively flat (force) frequency response from 0Hz to 250Hz. The actuators are designed without belts or gears so that the only moving part is a moving magnet within a solenoid. The result is a simple, sturdy, direct-drive, linear system, without backlash or hysteresis effects.

The actuators are individually controlled by an Electronic Control Unit (ECU), which converts a user-input voltage to a shaft output force. The ECU converts the input low-level analog voltage, to a current that is output to the actuator, typically 1.0-amp output per 1.0-volt input (1.0-amp/volt). The actuator output force is linearly proportional to the ECU-supplied current. As a result, the force applied at the output shaft follows the voltage applied to the ECU, regardless of shaft position. The force constants for both actuators used are listed in Appendix A2 and are nominally about 1.29-lbf/amp and 1.49-lbf/amp. The linear actuator system configuration is shown in Figure 4.2.

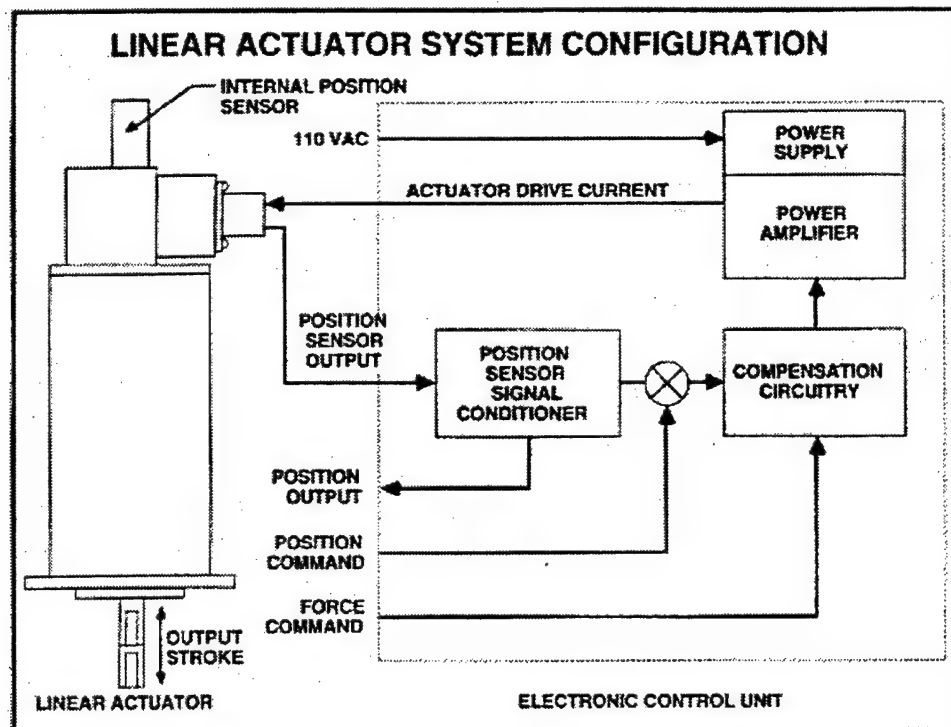


Figure 4.2. The linear actuator system configuration [Ref. 15]

The actuators can simultaneously generate both DC (static) and AC (dynamic) shaft output forces. In addition, there is an internal position sensor, connected to the ECU, that allows for automatic centering of the output shaft with up to a 10-pound static loading force. The output from the position sensor, which is linearly proportional to the shaft position, is available via a BNC connector (Position Monitor) on the ECU front panel, as shown in Figure 4.3. Tests showed that the position monitor was limited to

tracking output shaft movements at frequencies on the order of about 20Hz and below. Since the typical operating frequencies used were about 70Hz to 100Hz, a separate accelerometer was mounted to the output shaft to track output movements, as shown in Figure 4.6.

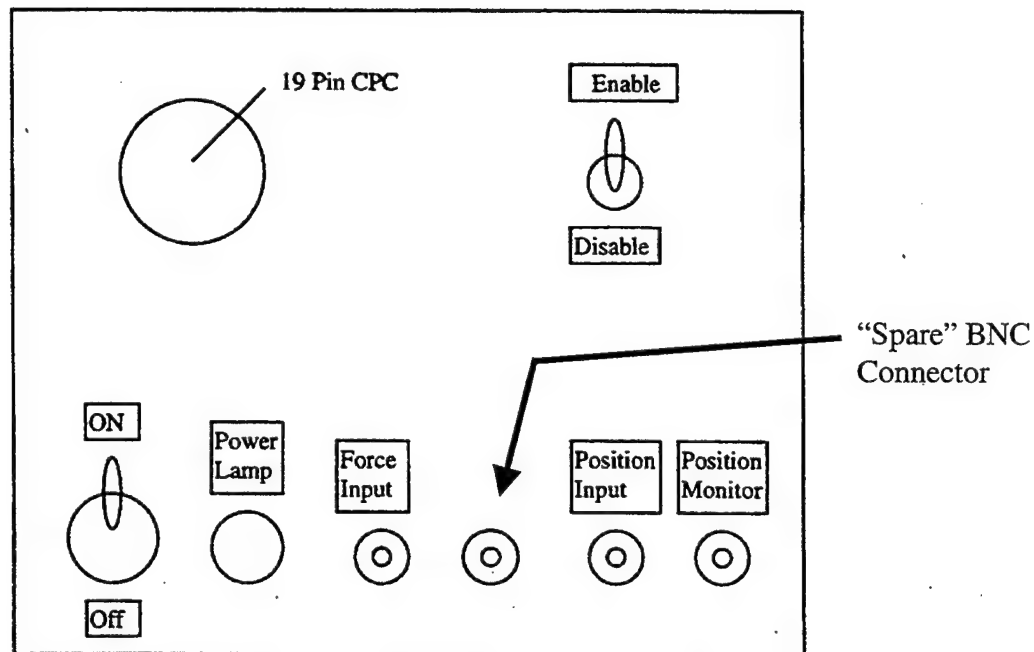


Figure 4.3. Electronic control unit (ECU) front panel

The ECU requires up to 15 Amps of 110VAC, 60Hz electrical power for normal operation. The actuator was connected to a 19-pin connector (9-pins actually used) on the ECU front panel, using a 300-foot underwater cable that was constructed for this research (see Appendix B). The underwater cable allowed remote deployment of the actuator from the ECU.

The following CAUTION is of particular importance and should be heeded:

**Do not disconnect the ECU-actuator cable connection without first setting the ECU Enable/Disable switch to the “DISABLE” position!**

This lesson was learned first-hand. Disconnecting either the actuator or ECU connection, without first turning the enable/disable switch to “DISABLE”, will cause an arc that will fuse the cable to the connector.

## 1. Actuator Modifications

Numerous modifications were made to protect the actuators from salt-water intrusion and improve their operation as a seismo-acoustic sonar source. Many of the modifications were made based on lessons-learned during field tests and by trial and error. An external view of the linear actuator, before modification, is shown in Figure 4.4.

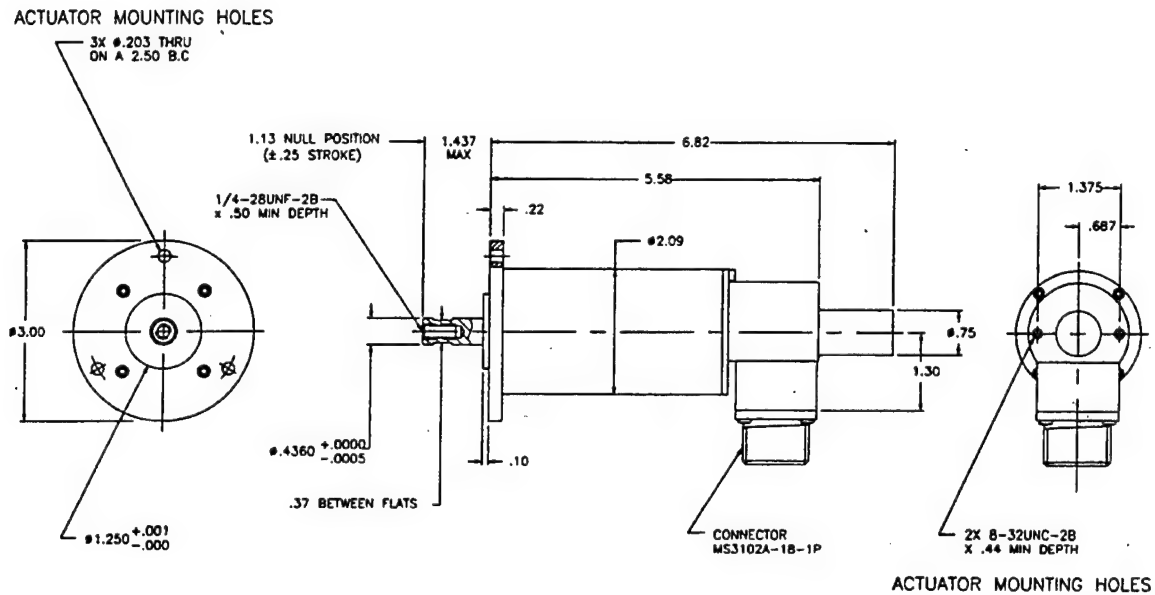


Figure 4.4. Schematic of an unmodified linear actuator [Ref. 14]

One of the first modifications was to attach a nylon cylinder and 5-inch square plate assembly to the output shaft, similar to the aluminum rod and plate shown in Figure 4.7. The actuators were typically placed in an upright position on the beach sand and driven with a 5-cycle, 100Hz input signal to the ECU. It was found that for ECU-input voltages greater than about 2.5-volts, the actuator-plate assembly literally “hopped” on the sand, producing a complex, inconsistent seismic wave at the seismometer, 5-feet distant. The cylinder-plate assembly was then buried, in the same sediment conditions, about 3-inches below the sand surface. A noticeable improvement was seen in the magnitude and the consistency of the seismic wavetrain as seen at the seismometer, 5-feet distant. The following week, under similar conditions, a 2-kg inertial mass was fastened to the actuator housing (shown in Figure 4.6), which resulted in yet an additional increase

in the amplitude of the seismic wave as measured by the seismometer. In this configuration, the actuator was operated as an inertial reaction force shaker, with the moving mass consisting of the actuator housing plus the added mass fastened to the top of the housing. The vertical amplitude of the seismic wave as measured by the seismometer, 5-feet distant, is shown in Figure 4.5 for the three modifications.

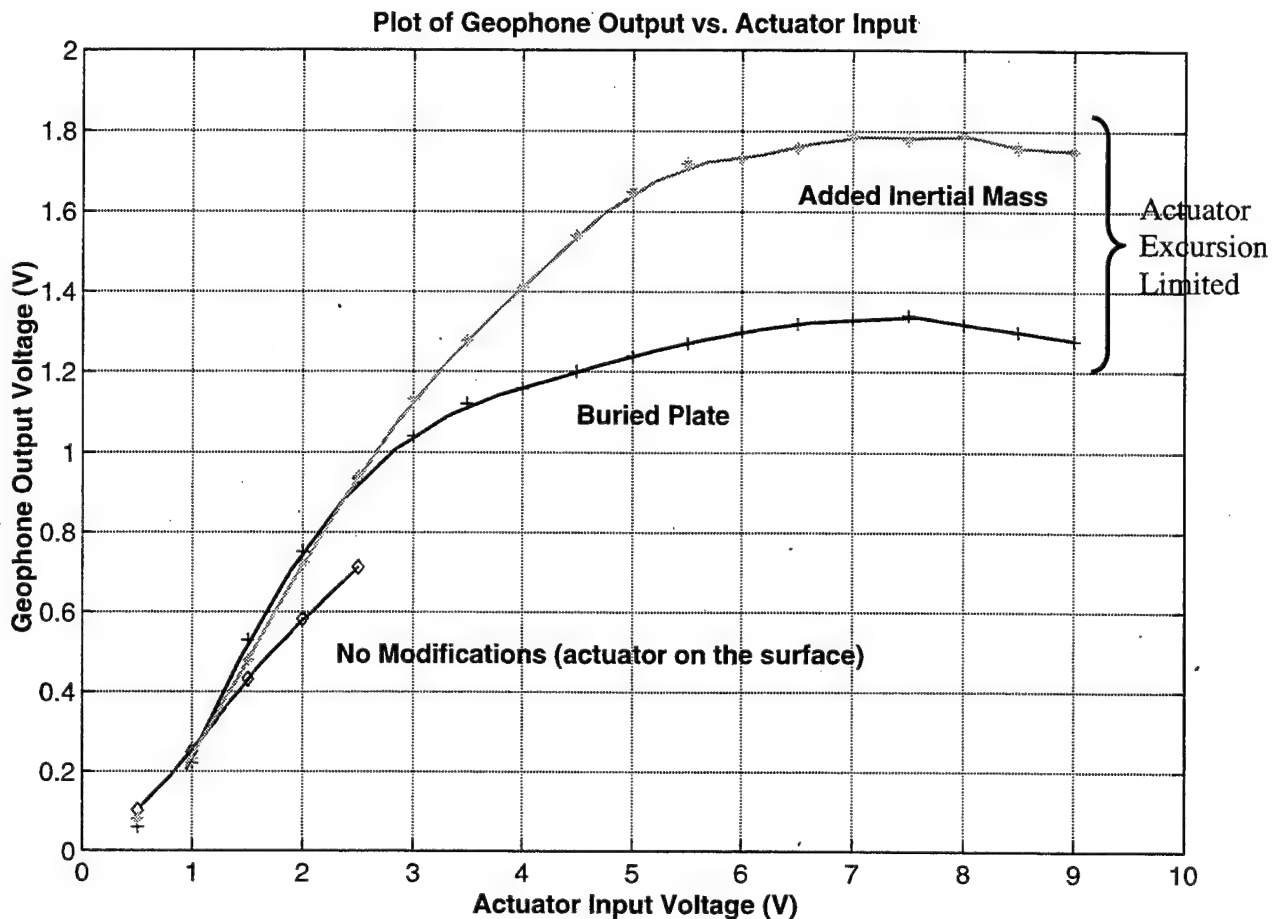


Figure 4.5. Plot of the vertical geophone output voltage vs. ECU input voltage

As can be seen from Figure 4.5, the addition of an inertial mass combined with improved ground coupling by burying the actuator-plate assembly, resulted in an approximate gain of 4-dB in maximum achievable seismic wave amplitude. The apparent amplitude “rolloff” for the buried plate and mass modifications in Figure 4.5 is a result of the actuator reaching its excursion limit. Note also that the pressure exerted by the 25-lbf actuator and 5-inch square plate is on the order of about 1-psi, much less than

the liquefaction pressure for medium-grained sands, which is typically greater than about 50-psi. [Ref. 16]

The next series of actuator modifications are shown in Figure 4.6, some of which allowed the placement and operation of the actuator inside a watertight, 6-inch diameter PVC pipe, shown in Figure 4.7. The modifications were designed to protect the actuator from salt-water immersion and allow operation of the actuator system underwater.

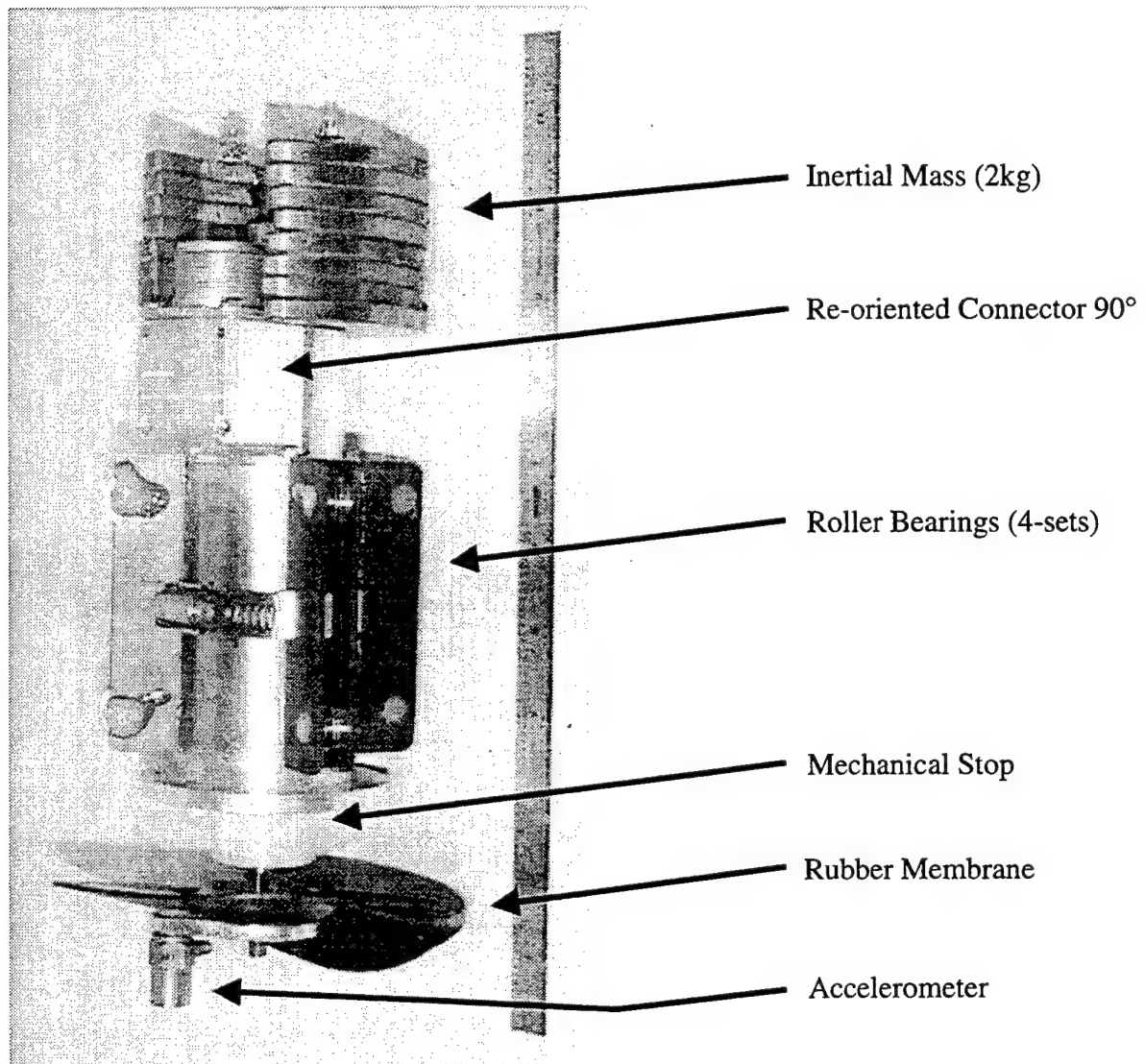


Figure 4.6. Actuator modifications

The electrical connector was replaced with an aluminum block that re-oriented the connector 90° toward the back of the actuator and allowed placement of the actuator

inside the watertight PVC pipe. A watertight, bulkhead connector (see Appendix B3) was mated to the PVC housing via a nylon block. Additionally, 4-sets of roller bearings, 2-rollers each, were attached to the actuator body allowing it to roll relatively freely inside the PVC housing. To protect the actuator from internal damage, a hollowed, nylon cylinder was mated to the base of the body, over the output shaft, which prevented excessive force against internal stops when turning the self-centering actuator off.

To seal the output shaft end, a nylon ring was mated to the end of the PVC housing and 8-holes were tapped into it. Two aluminum plates, with machine screws for attaching to the actuator output shaft and ground coupling assembly, were mounted to a black, rubber membrane which was then firmly mated via a metal ring to the end of the PVC housing. A uniaxial accelerometer (see Appendix A3) was mounted, via a machine screw, to the external, aluminum plate, as shown in Figure 4.6.

To reduce the "head" mass at the actuator output shaft, the nylon cylinder-plate assembly, weighting about 1.8-pounds was replaced by a 6-inch long, 0.5-inch diameter aluminum shaft and 6-inch aluminum square plate assembly, weighing about 0.8-pounds. The fully assembled, watertight, seismo-acoustic sonar source is shown in Figure 4.7.

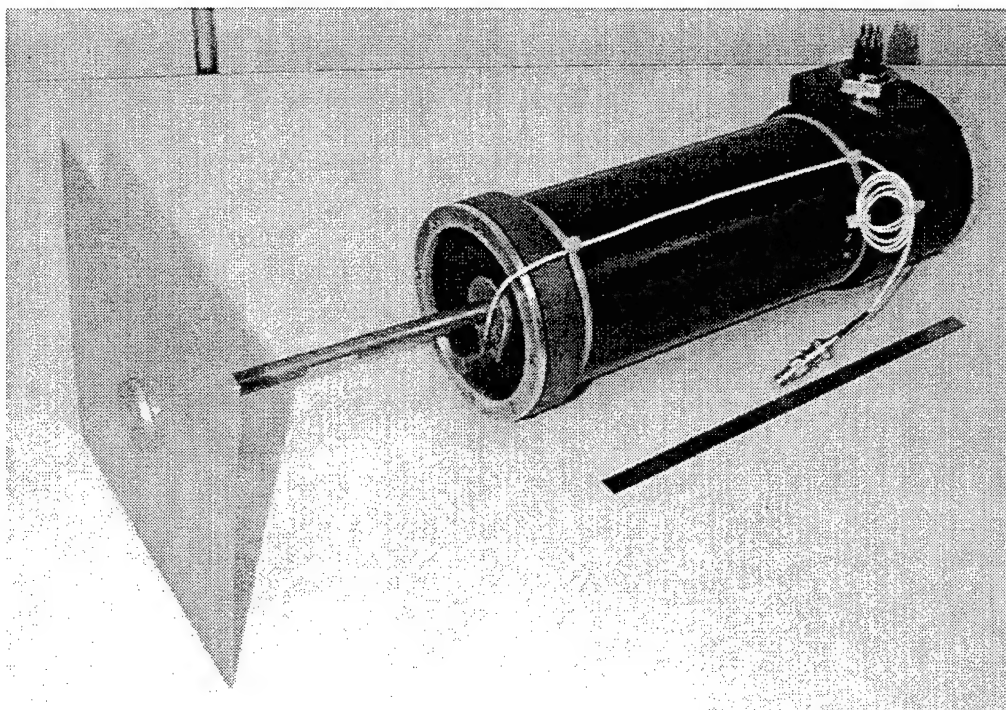


Figure 4.7. The fully assembled watertight seismo-acoustic sonar source

## 2. Electronic Control Unit (ECU) Modifications

After a number of field trips, it was noted that the source continued to “ring” after the electrical signal to the ECU was terminated. Laboratory tests showed that the actuator continued to oscillate for a few hundred milliseconds at the completion of an input pulse train. After consulting with engineers from Aura Systems Inc., it was found that the RC time constant and slewing rate of the automatic shaft centering feature had been altered by the replacement of the 6-foot, factory-supplied cable with the 300-foot, underwater cable. The result was an undesirable oscillation until the actuator settled-down to the static, centered position. The solution was to re-adjust the time constant by adding a capacitor, in parallel, across the R5 resistor on the main control board. A speaker-type push connector was hardwired to the R5 resistor and mounted on the back of the ECU as shown in Figure 4.8, enabling external capacitor loading. Trial and error lab tests showed that a 2 $\mu$ F capacitor seemed to work best in reducing the oscillations to an acceptable level.



Figure 4.8. ECU rear cover with an added speaker-type push connector

The second modification to the ECU included the addition of an extra pin to the 19-pin cable connector and tying it to the "spare" BNC connector on the ECU front panel, as shown in Figure 4.3. The ECU is factory-delivered with only 8-pins installed in the 19-pin connector, which are all that is necessary to control the actuator. As shown in the ECU/Actuator Interconnect Diagram in Appendix A4, the conductors for pins D and E on the actuator-side are tied together on the ECU-side before connecting to the ECU. After consulting with Aura engineers, pins D and E were tied together at the actuator-side, which made one of the 9-conductors in the 300-foot cable available for other uses and actually resulted in better grounding and shielding properties.

Originally, the "extra" conductor, made available from this modification, was intended to be used to route the actuator accelerometer signal, which was originally installed on the waterproof inside of the PVC housing, back to the ECU and from there to the data acquisition computer. Unfortunately, the electrical interference generated by the actuator-ECU system added an excessively large 120Hz component to the accelerometer signal when using this wire, making it virtually unusable, since typical operating frequencies were on the order of 70-100Hz. As a result, a separate coaxial cable was used for the accelerometer signal and there is an extra conductor available from the actuator to the ECU, which may be used for other purposes, i.e. a thermocouple.

It was found that the actuators tended to overheat when constantly operated in the vertical position. The overheating was caused by the constant ECU current that was required to maintain the statically centered position with the relatively heavy inertial mass loaded on top. Therefore the ECU switch was set to "Disable" between experimental runs.

### **3. Relative Source Gain**

Comparing the vertically operated, linear actuator system with the previous, discrete-mode, seismo-acoustic sonar source [Ref. 8], both operating at their maximum capability, the actuator produces a much greater seismic interface wave intensity (see Figure 4.9). For a source-receiver separation of 70-feet, the actuator source produced a

vertical seismometer signal of about 60db greater than the discrete-mode source. Based on these results, it seems that the linear actuator system looks promising for a seismo-acoustic sonar with a reasonable standoff range capability.

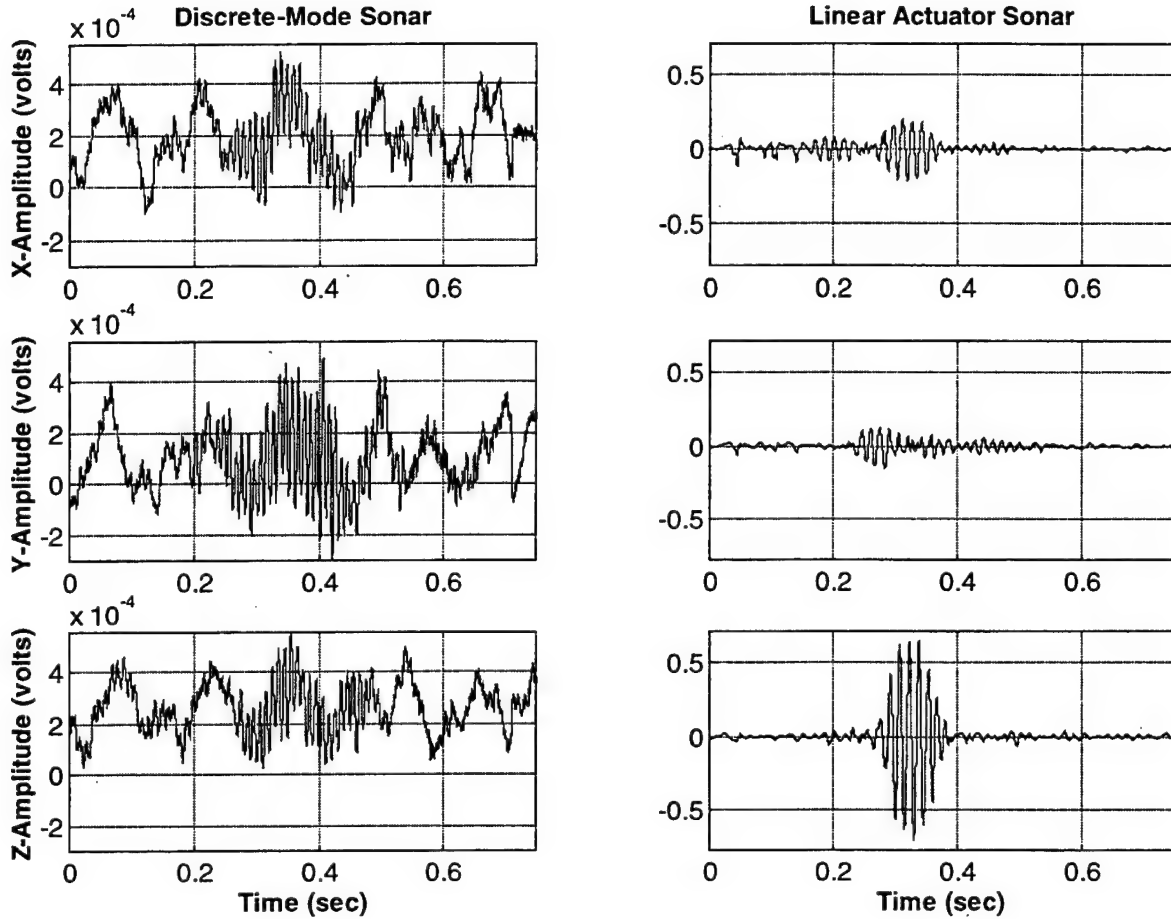


Figure 4.9. Comparison of the seismic interface waves for the discrete-mode and modified linear actuator sonar at a source-receiver distance of 70-feet

## B. SEISMIC SENSORS

For this research, two three-axis seismometers, consisting of three orthogonally-oriented geophone sensors, were used as receiving elements (see Appendix A5 for specifications). Each seismic sensor consists of three geophones, mounted in a cylinder of urethane (see Figure 4.10) to form a triaxial velocimeter. The geophone converts the velocity of the particle motion caused by the propagating wave into an output voltage.

The output voltage is linearly proportional to the particle velocity, which can then be used to further analyze the seismic wavefield, as will be discussed later. The geophones have the following dimensions: height-23 cm, diameter-5 cm.

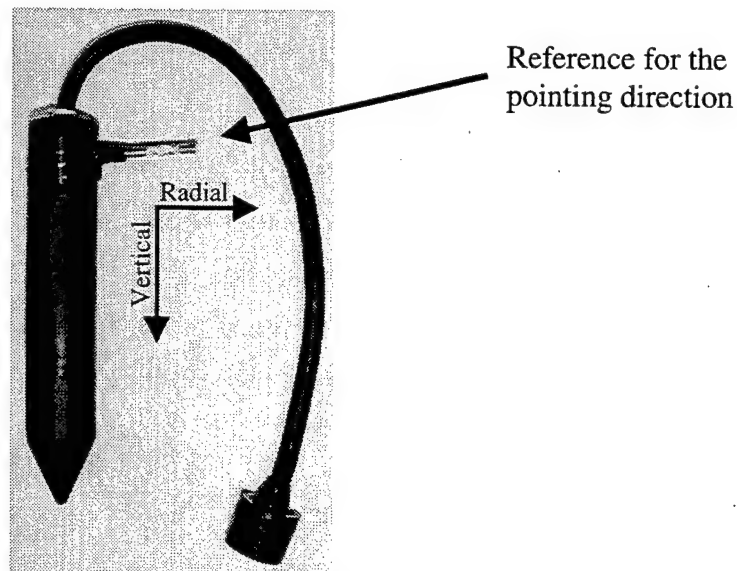


Figure 4.10. Triaxial geophone seismic sensor

During field tests there were noticeable frequency components in the seismometer signals on the order of about 150Hz to 175Hz, which could not initially be accounted for or explained. Similar, unexplainable frequency components were seen during previous research studies, using the same geophones. [Ref. 17] Closer examination of the geophone specification sheets in Appendix A5 revealed that the geophones have an undesirable, "typical spurious frequency" of about 150Hz to 190Hz. Fortunately, for this research, typical operating frequencies were below these spurious frequencies, typically 70Hz to 100Hz.

The geophone signals are amplified in the deployed unit with a selectable 10dB or 40dB (typically 40dB selected) amplifier, typically powered by two, 12-volt, rechargeable batteries, wired in series to provide  $\pm 12$ -volts. During field tests it was noticed that the batteries would typically drain to about 10-volts by the end of the day. In order to provide more consistent seismic measurements, the batteries were replaced by an ac/dc power converter which continuously supplied the required  $\pm 12$ -volts.

During lab tests it was noticed the actuator-ECU system produced a moderate 20kHz component in the geophone signal. Using the ac/dc power converter had an added benefit in that it appeared to reduce the 20kHz interference by about 10%. The most effective reduction in the 20kHz noise interference was found by placing the ECUs in a separate equipment rack, effectively isolating the receiving elements from the transmit elements.

### C. DATA ACQUISITION

Data acquisition was accomplished with Signal Processing System's SPS390 Signal Analyzer, shown in Figure 4.11. The SPS390 is a 16-bit, 0-40kHz analyzer, capable of recording up to eight channels of data.

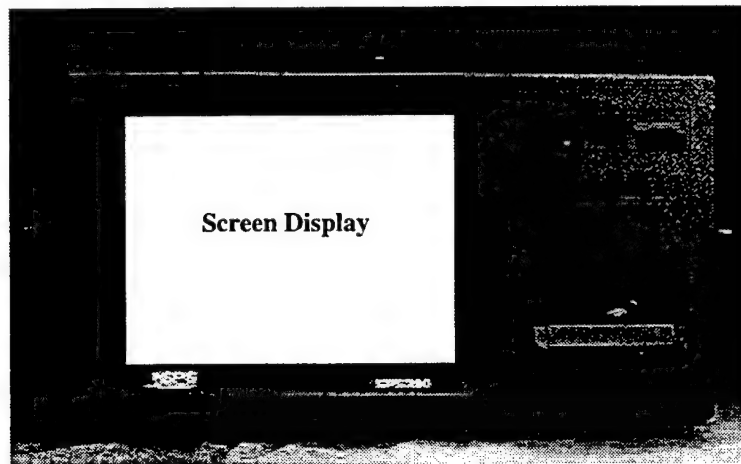


Figure 4.11. Signal Processing Systems (SPS390) signal analyzer used for data acquisition

For this research, the SPS390 was upgraded to a 32-bit operating system and the Random Access Memory (RAM) was increased to 128MB. These upgrades provided more a more reliable data acquisition system and allowed data file transfers to another computer for signal processing without terminating the SPS390 signal processing program. The result was a relatively quick turn-around time (2-3 minutes) from data acquisition to signal processing and data analysis. To support follow-on research, the configuration, menu settings, and 8-channel inputs (standardized throughout the research) are included in Appendix A6.

#### D. SIGNAL PROCESSING

The signal processing of the recorded seismic data during this research has been an evolutionary process. At the start of this research, seismic data were recorded and stored in the field, then processed in the lab 2 to 3 days later. This method was found to be excessively inefficient, considering that it would take a week or more to analyze the data. As a result, equipment and signal processing capabilities were developed to allow near real-time (2-3 minutes delayed) signal analysis in the field. This capability allowed an on-site assessment of the effectiveness of sonar placement and test configurations, significantly improving testing procedures and results.

Twenty two signal processing subroutines (see Appendix D) were written using Matlab's Signal Processing Toolbox. [Ref. 18] The data analysis and signal processing methods that were developed are summarized in 4 basic steps, shown in Table 4.1.

| STEP | COMPUTER           | OPERATION   |
|------|--------------------|---|
| 1    | SPS390             | Record accelerometer and seismic geophone signals   |
| 2    | SPS390-to-Portable | Download the recorded data (via a null-model cable) |
| 3    | Portable           | Convert the data to Matlab 4.1 format               |
| 4    | Portable           | Signal Analysis (MATLAB Subroutines)                |

Table 4:1. Summary of data acquisition and signal processing steps

The MATLAB subroutines, listed in Appendix D, are sufficiently commented and do not require further explanation at this point. One particular signal processing method, vector polarization filtering, deserves further discussion. As discussed in Chapter III, Rayleigh waves, by their very nature, have radial and vertical components that differ in phase, resulting in *polarized* elliptical particle motion. This feature provides a method for discriminating between different wave types to identify those interface waves with a relative phase difference between the radial and vertical components. This method is known as "Vector Polarization Filtering". [Ref. 7]

In this research, polarization filtering is the process of extracting from a radial-vertical signal pair, the component of the crossed signal power that comes from the elliptical particle motion of the interface wave. [Ref. 7] This is accomplished by applying the Hilbert Transform to the radial-vertical signal pair (see Ref. 7 for further discussion) and calculating the time domain, crossed power function as given by,

$$P_{rv} \equiv r_{hilbert}^* \times v_{hilbert} , \quad (4.1)$$

where  $P_{rv}$  is the crossed power function,  $r_{hilbert}^*$  is the complex conjugate of the hilbert transform of the radial component of motion, and  $v_{hilbert}$  is the hilbert transform of the vertical component of motion, consistent with the notation used in Ref. 7. The in-phase radial and vertical components are contained in the real parts of  $P_{rv}$  while the out-of-phase components are contained in the imaginary parts. [Ref. 7] As a result, the imaginary part of  $P_{rv}$  is approximately proportional to the power of the Rayleigh wave and deflects positively or negatively for polarized signals, depending on whether the motion is prograde or retrograde, respectively. [Ref. 7] This technique is used to reject other signals, particularly the bulk P and S waves, and will be illustrated later.

## E. TRANSPORTATION

During this research a John Deere, 4x6 "TrailGator" (see Appendix A7) was acquired to move and position naval mine-like targets in the beach, see Figure 4.12. Additionally, since part of the focus of this research was to refine testing procedures, considerable efforts were made to minimize and simplify equipment requirements. As a result, the transmit, receive, and signal processing equipment components described previously were condensed down to two equipment racks that were transported and staged from the bed of the TrailGator, as shown in Figure 4.13. The TrailGator proved to be an invaluable addition to the research project and presents opportunities for expanded development (i.e. deploying a combination seismo-acoustic sonar and sensor array), which will be discussed later.



Figure 4.12. Front view of the TrailGator and beach equipment

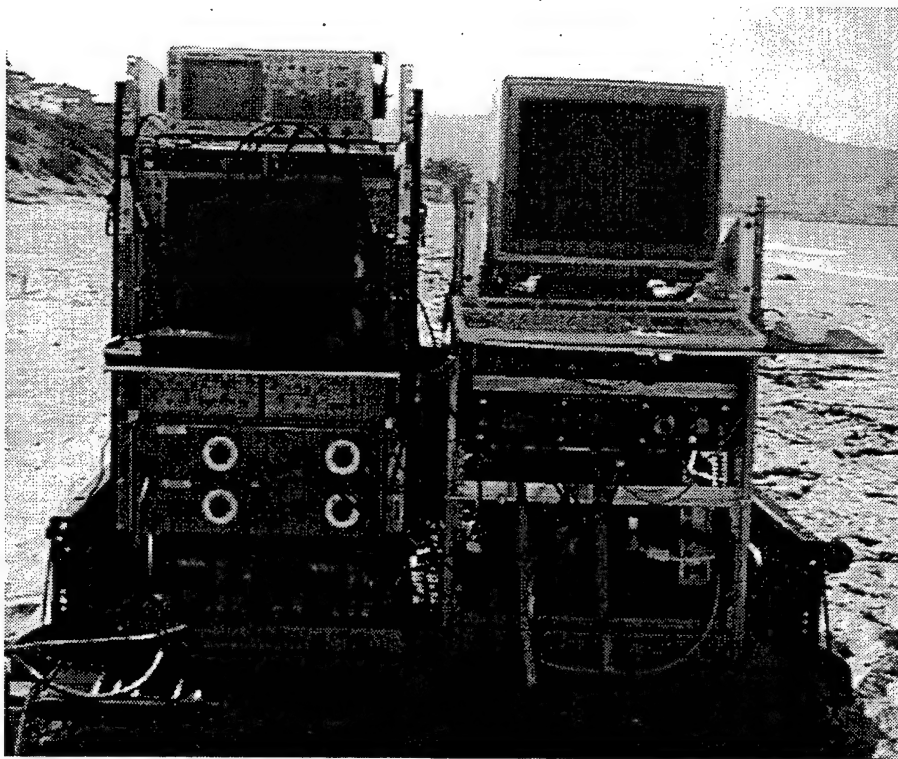


Figure 4.13. Transmit and receive equipment racks in the TrailGator bed



## V. TESTING PROCEDURES

One of the major goals of this research was to refine field-testing procedures for the seismo-acoustic sonar development. As a result, a significant amount of time and effort, more than seven months, was put into developing streamlined and efficient beach setup and testing procedures. Rather than describing the evolution of the developing test procedures, this chapter will outline the procedures that were developed and successfully used at the later latter part of this research. Before describing the testing procedures, this chapter begins with a brief description of the beach test site, characterization of the beach sand, and a spectral analysis of the ambient ground vibration.

### A. BEACH TEST SITE

The beach test site was located on the Monterey Bay coastline, adjacent to the Naval Postgraduate School, at the NPS Beach Research Facilities. See Figure 5.1.

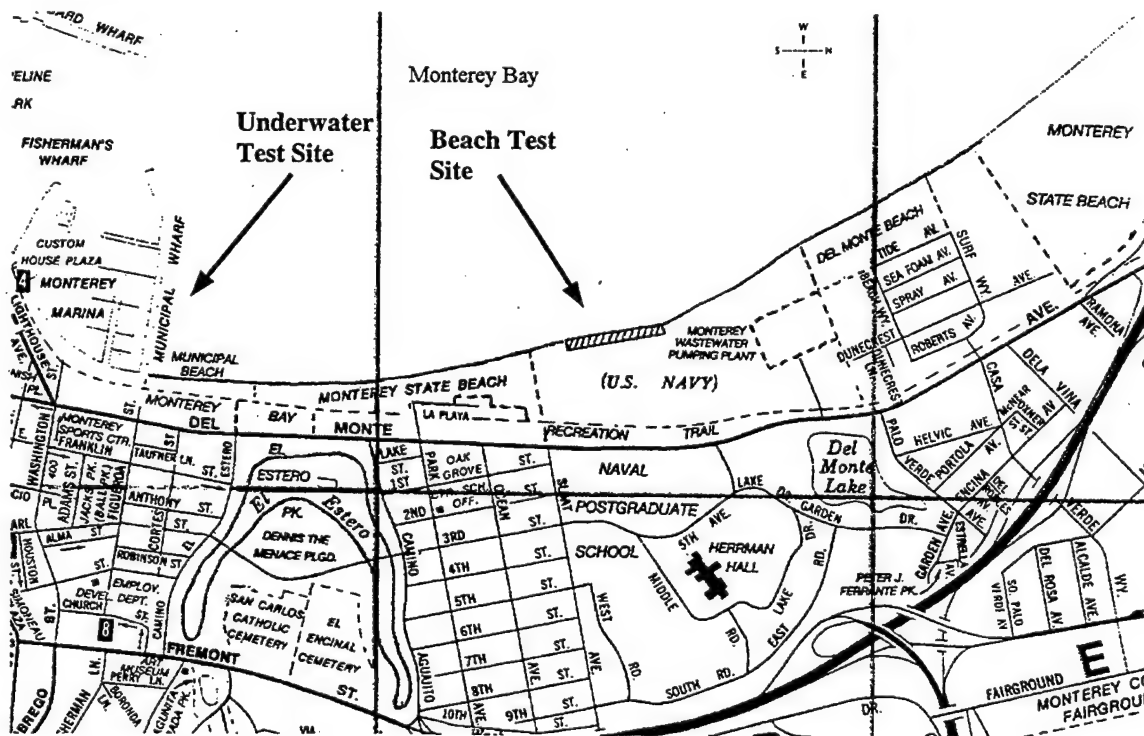


Figure 5.1. Beach and underwater test sites

Map copyrighted 1994 by the California State Automobile Association. Reproduced by permission.

The beach site proved to be well suited for this research, with easy access to the beach via a 20-foot wide, dirt road. The width of the beach and available test area varied with the tides, ranging from a width of about 120-feet at low tide to less than 10-feet at high tide. See Figure 5.2.



Figure 5.2. Beach test site at high tide

## **B. SEDIMENT CHARACTERIZATION**

In general, beach sand is composed of a variety of elements, including minerals, rocks, organic and inorganic compounds, water, and air. The relative amounts of these different elements vary, depending on the geographical location and the depth of the sediment. [Ref. 8] In addition to its composition, sand is characterized by a variety of features, including grain size, density, and moisture content. Each of these characteristics affects the propagation of elastic wave energy along the beach-air interface. While the relationship between sand characteristics and interface wave propagation are relatively

complex, it is generally accepted that interface wave energy is less attenuated in high moisture content and densely compacted soil environments. [Ref. 16]

Although the Rayleigh wave equations, for a uniform, semi-infinite, elastic half space (3.5), are frequency-independent (dispersionless), real beach sediments are not uniform, meaning that they are not necessarily dispersionless. Hence the speed of Rayleigh waves may depend on the frequency. In a natural beach or seafloor sediment, the overburden weight of the surface sediments causes an increase in shear modulus with increasing depth into the medium. Consequently, longer wavelength, lower frequency acoustic waves propagate deeper into the sediment, where the shear velocity is greater. As a result, long wavelength, low frequency signals travel faster than short wavelength, high frequency signals. At relatively higher frequencies, greater than 100Hz, there is little dispersion because the wave remains near the surface, where the sediment is relatively uniform. To complicate matters further, a core sample of the beach sediment revealed, unsurprisingly, that the moisture content of the sand varied with depth. At a depth of about 1-meter, it was found that the sand was completely saturated, corresponding to the depth of the tide water table at that time.

### **C. AMBIENT NOISE SPECTRA**

Using the geophones as receivers, a measurement of the ambient ground vibration at the beach test site was made. The measurement allowed an assessment of the influence that the ambient noise would have on identifying the target signal, and provided qualitative information on which operational frequencies to avoid. See Figure 5.3. The test setup is outlined in Appendix C1 and the MATLAB program used for the spectral analysis is outlined in Appendix D16.

Note that the spectral content of the ambient background noise is greatest from about 10Hz to 40Hz, consistent with previous measurements made at this site. [Ref. 8] The predominant source of the ambient noise is undoubtedly the breaking of waves similar to those shown in Figure 5.2. The measurement was useful in providing guidance on selecting the high-pass filtering frequency and allowed a relative sense of confidence

that the sonar operational frequencies, typically 70Hz to 100Hz, are not within the strong ambient noise band.

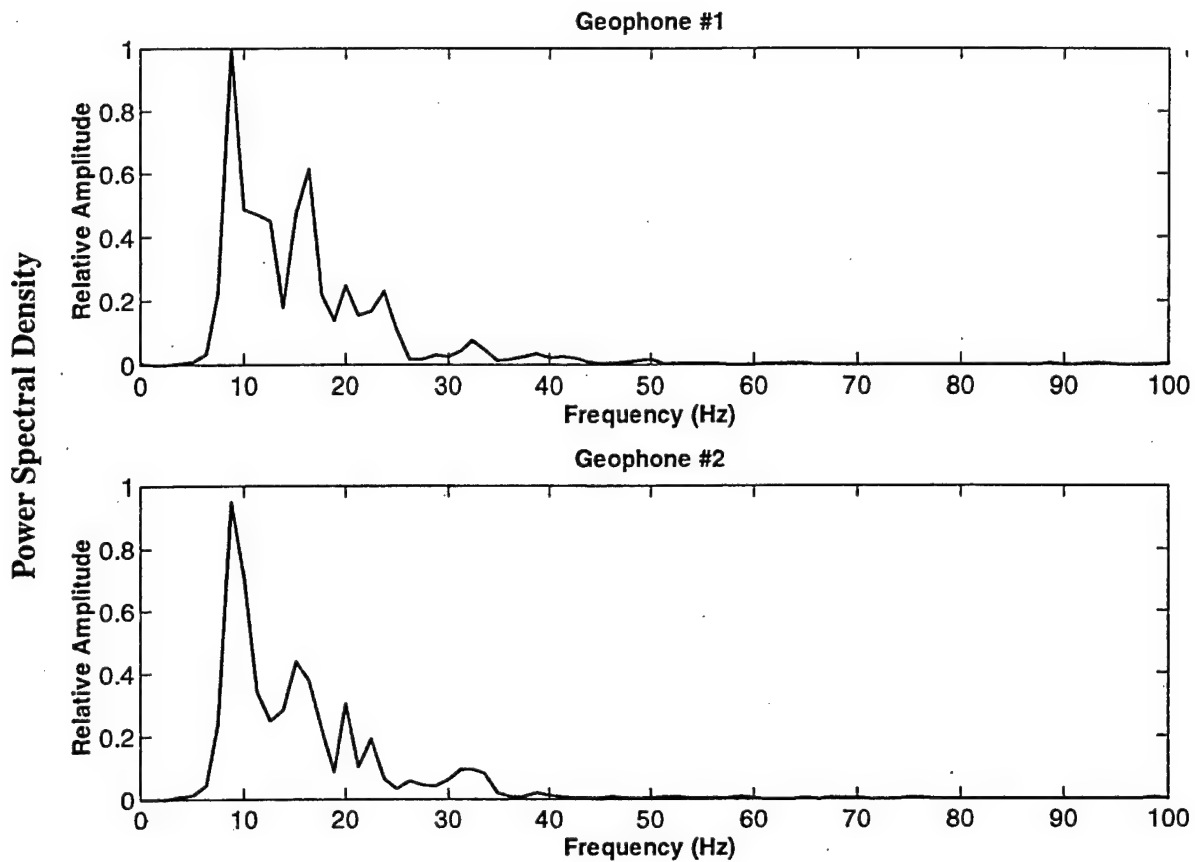


Figure 5.3. Omnidirectional velocity power spectral density for the ambient ground vibrations at the beach test site (see Appendix C1 for the test setup)

#### D. SOURCE EMPLOYMENT

Two seismic sources were developed to independently generate horizontal and vertical motion. The versatility of the sources allowed for creative testing of many different actuator orientations and operating combinations. More than 100 different tests were conducted over 21 days of field testing, each with different drive signals, actuator orientations, geophone locations and target positions. The seismic interface waves resulting from these many tests were closely studied and evaluated for further use in buried target detection.

The placement and operation of the actuators can be categorized into two different configurations. In the first configuration, the actuators are operated either horizontally or vertically, while in the second, they are operated simultaneously, one horizontal and one vertical, with a  $90^\circ$  relative phase difference between their drive signals. With the reader as the receiver, Figure 5.4 shows a typical vertical and horizontal actuator placement, resulting in vertical and shear wave excitation, respectively.

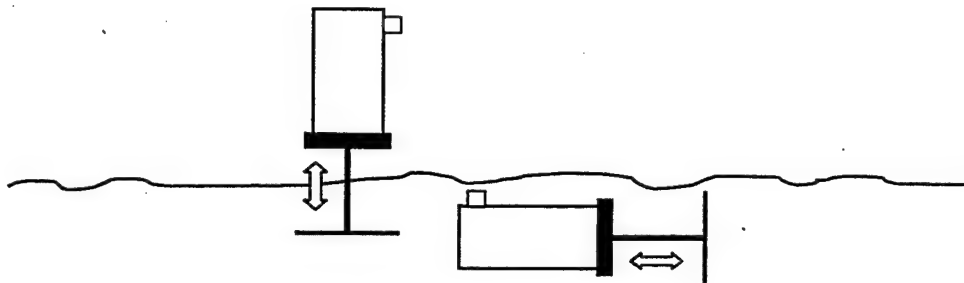


Figure 5.4. Typical actuator placement for vertical and shear wave excitation.

### 1. Placement and Orientation

Different actuator orientations and operating combinations resulted in the generation of various seismic interface waves, each with distinctive features and characteristics. These waves were evaluated for their suitability for use in detecting buried targets. Based on previous research [Refs. 7 & 8], the evaluation centered on finding seismic waves that had both a single-mode polarization and minimal reverberation.

The first, and simplest, actuator placement that was tested was to orient the source vertically, as shown in Figure 5.4. The test setup is shown in Appendix C2, which shows two actuators separated by 46-cm (18-inches) and 1.8-meters (6-feet) from the receiver. The actuators are driven with a single cycle, 10-volt, 90Hz signal. The geophone signals for the relative x, y, and z-motion are shown in Figure 5.5, which was generated using the MATLAB program in Appendix D4. The vertical line at about 0.01-seconds indicates the start time for the input actuator pulse. Note that the x-radial and z-vertical motions

are the dominant wave components and that the reverberant wavefield has decayed to less than 5% of the maximum amplitude at about 0.1-seconds.

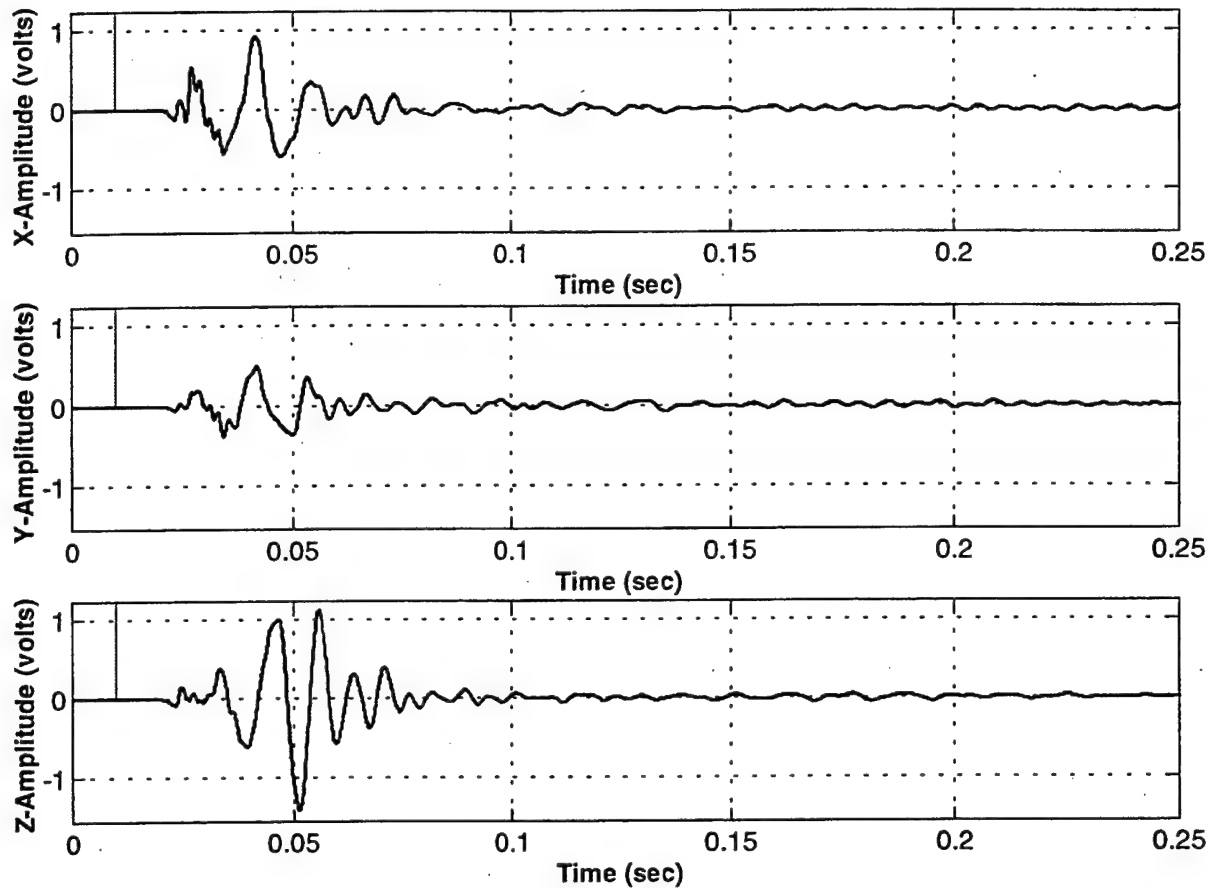


Figure 5.5. Relative seismic motion (velocity) from a vertically-oriented source

As discussed in Chapter III, computation of the crossed power function (4.1) is a practical means of separating the Rayleigh wave signal and rejecting the bulk P and S waves. A plot of the imaginary component of the crossed power function provides an indication of the polarization, or direction, of the elliptical wave motion, prograde or retrograde. With the seismometer reference post (see Figure 4.10) pointing in the direction of the incident wave, a positive deflection of the crossed power from (4.1) indicates that the motion of the Rayleigh wave is prograde, whereas a negative deflection indicates a retrograde wave. The observed imaginary crossed power for a vertically-oriented source is shown in Figure 5.6, which was generated using the MATLAB

program in Appendix D12. Note that the deflection is negative, corresponding to an interface wave with prograde motion for a geophone that is pointed away from the incident wave source as shown in the test setup in Appendix C2.

Similar tests were conducted for a horizontally-oriented actuator first pointing directly at the receiver at a  $0^\circ$  angle, resulting in a P-wave, and then transversely at a  $90^\circ$  angle, resulting in a Love wave. In both cases it was found that reverberations were excessively large and that there were at least two excited modes, as the polarization of the elliptical particle motion was observed to change from one sense to the other within the pulse train. These two actuator orientations were not considered further for use in detecting buried targets.

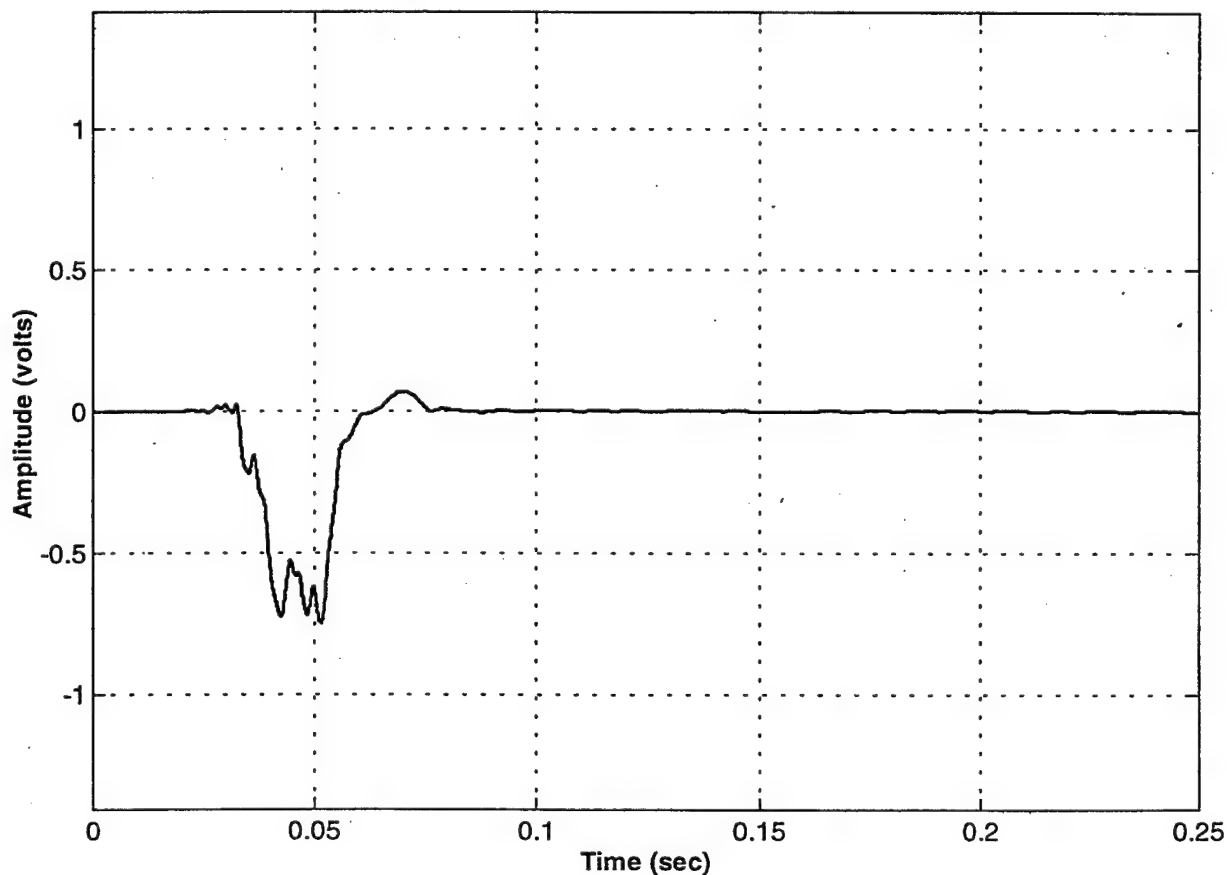


Figure 5.6. A plot of the imaginary crossed power for a vertically-oriented source with the receiver directed away from the source

## 2. Phasing

In the second type of configuration, the actuators were oriented side-by-side, one horizontal and the other vertical. The actuators were driven with a relative  $90^\circ$  phase difference to simulate and excite either retrograde or prograde Rayleigh wave motion. The results were ambiguous; in all of the tests the polarization of the elliptical particle motion changed during the pulse wavetrain. Similar phenomena had also been observed during previous studies [Ref. 8]. It is unclear whether there were actually two different modes, one prograde and one retrograde wave, or whether the same wave was being reflected from the saturated layer about 1-meter in depth. It seems unlikely that the change in polarization was due to reflection from the underlying layer, as the wave polarization for the vertically oriented source should have been just as likely to generate waves that were reflected from the underlying layer.

The test configuration for generating retrograde and prograde motion with the actuators is shown in Appendix C3. The test configuration shows two actuators, one horizontal and the other vertical, separated by 46-cm (18-inches) and driven with a two cycle, 6-volt, 100Hz signal with a relative phase difference between the two, for simulating retrograde or prograde elliptical motion. Figure 5.7 shows the crossed power calculated from (4.1), which indicates the polarization or direction of motion for a retrograde input and a source-receiver distance of 5-feet (1.5-meters) and 10-feet (3.0-meters). Note that the polarization initially starts out as prograde at 5-feet (1.5-meters) and changes to a mixed retrograde/prograde wave at 10-feet (3.0-meters).

Using the same geometry and configuration as for the retrograde test, the phase of the input signal was changed to simulate and excite prograde motion. The resulting motion is indicated in the plot of the imaginary crossed power in Figure 5.8. Note that the polarization is a mixed retrograde-prograde motion at 5-feet and changes to purely prograde at 10-feet. Although there appears to be a single-mode, prograde polarization at 10-feet, similar to the polarization for the vertically oriented source, this type of wave was not used because of the desire for a short-range sonar system and the fact that the mechanism for mixed polarization was not fully understood.

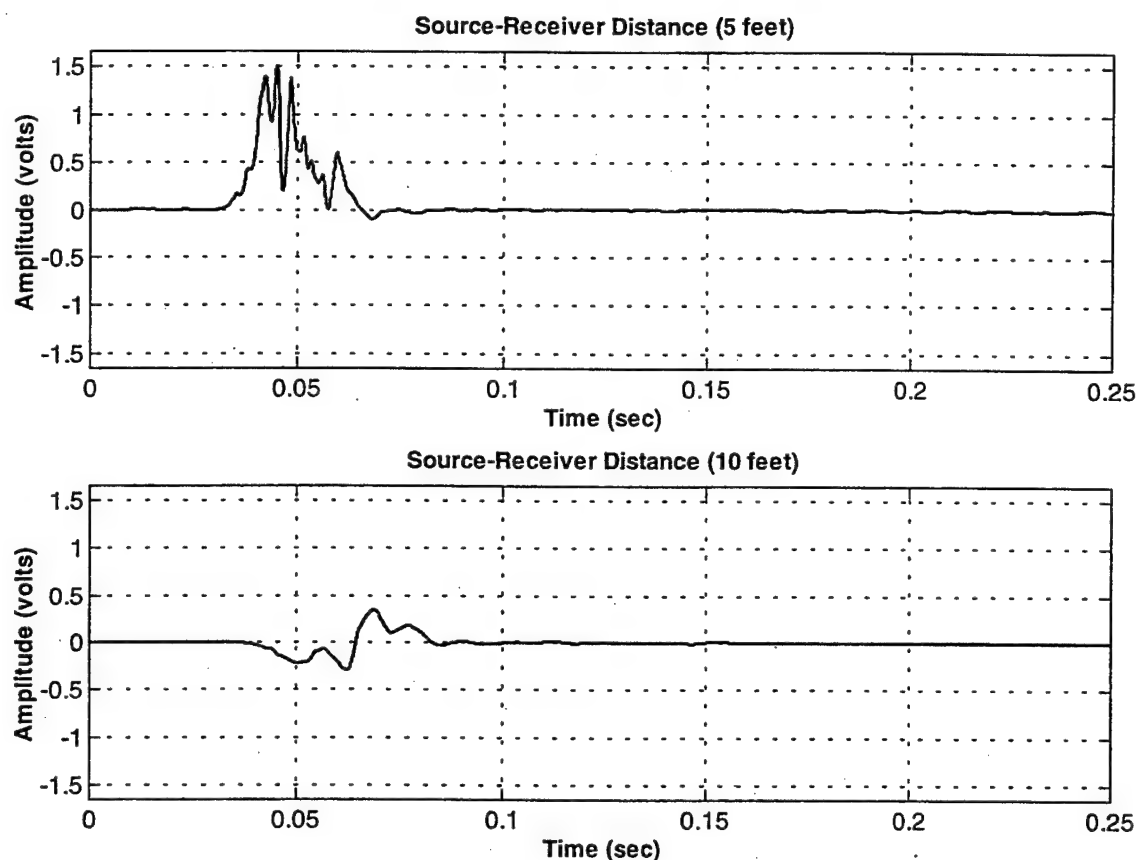


Figure 5.7. The imaginary crossed power resulting from a retrograde-phased actuator pair with the receiver oriented towards the source

In all tests of this type, orienting the two actuators, one horizontal and one vertical, and driving them with a relative phase lag resulted in a combination of modes or wave types that included both retrograde and prograde motion. After extensive testing, it was determined that the vertically oriented source resulted in a simpler, single-mode wave that was more suitable for detecting buried targets. Compared with other wave types, the vertical source produced waves that had relatively less reverberation and a consistent, single mode or polarization. The following testing procedures are based on operating the seismo-acoustic sonar as a vertical source.

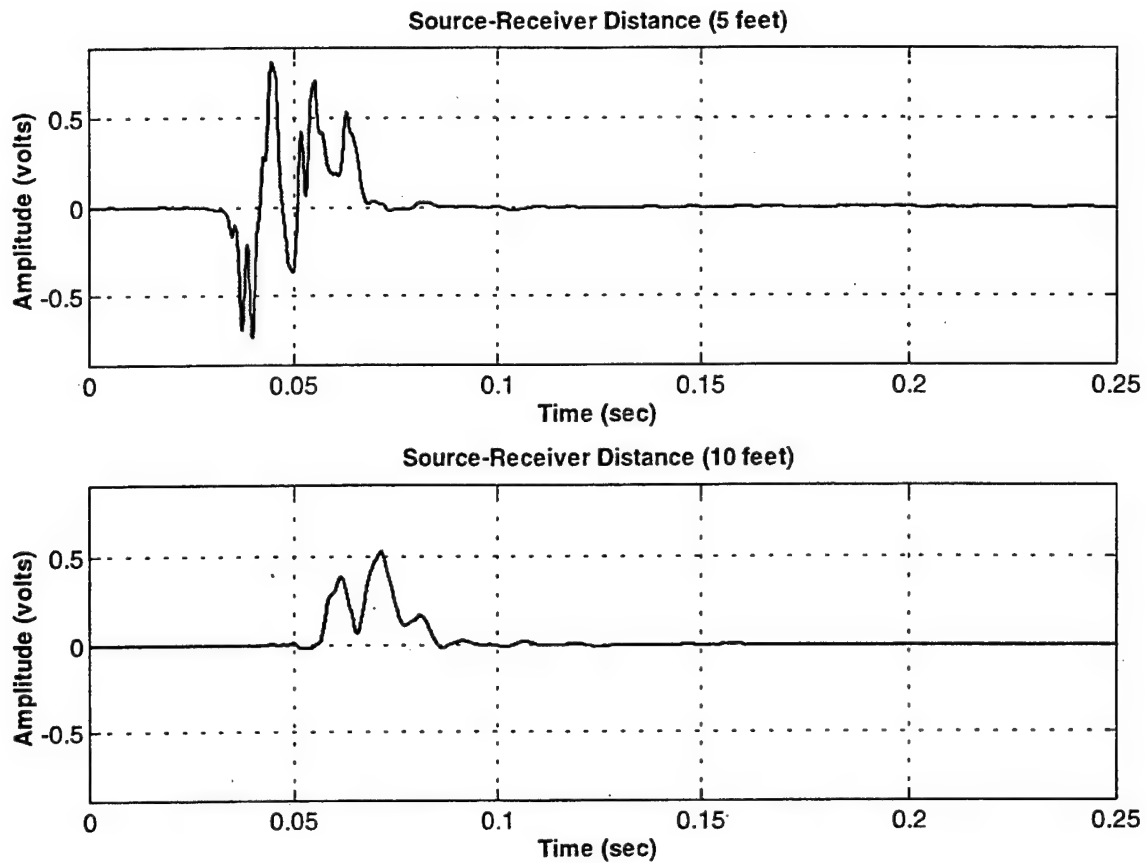


Figure 5.8. The imaginary crossed power resulting from a prograde-phased actuator pair with the receiver oriented towards the source

## E. TESTING CHRONOLOGY

The bulk of the equipment was transported from NPS to the beach site in a large, unfurnished mobile home. The mobile home was stationed on the bluff overlooking the beach and served as a staging area as well as supplying electrical power for the beach equipment. The equipment, including mine-like targets, was transported from the bluff to the beach using the TrailGator 4x6 utility vehicle. Once on the beach, the equipment was unloaded and set up according to pre-planned test configurations as shown in Figure 5.9. After the initial equipment setup, optimization measurements were made to find the best operating frequency and the associated wavespeed at that frequency.

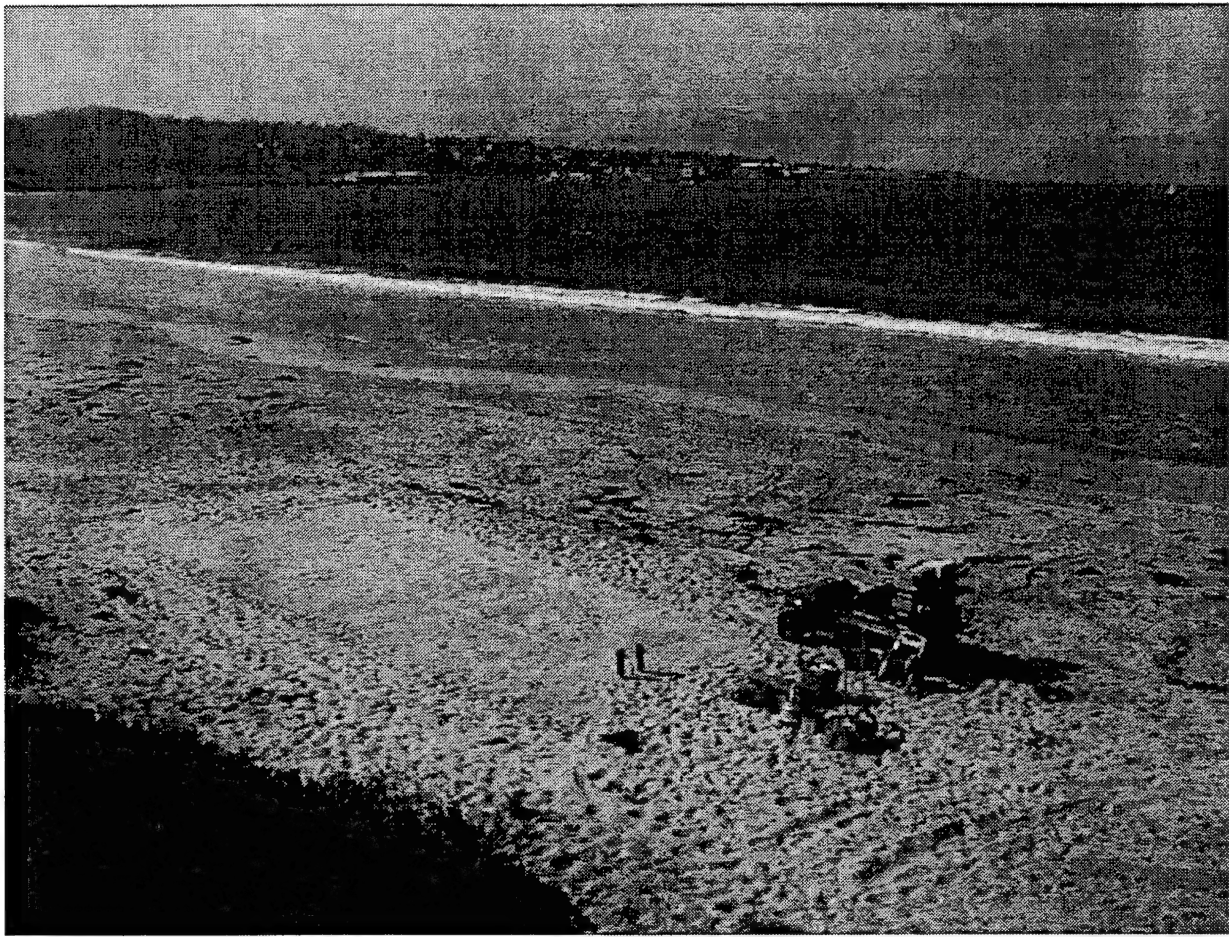


Figure 5.9. Equipment setup at the NPS beach research site

## 1. Frequency

Based on previous research, the driving frequency for the source was initially set at 100Hz. Typical velocities for this frequency were found to be on the order of about 80 m/s  $\pm 10$ , resulting in a wavelength of about 0.8 m. After many unsuccessful target detection attempts at this frequency, consideration was given to testing other frequencies. In general, it was found that frequencies below 100Hz worked best, consistent with previous “ground truthing” measurements made to determine the frequencies and wavespeeds of the dominant interface wave modes. [Ref. 8]

Generally, it was found that at frequencies of about 55Hz and below, the motion of the drive plate, as measured by the accelerometer, became noticeably different from the drive waveform. The cause of this apparent non-linearity is not known. At higher frequencies, greater than about 150Hz, the interface wave was found to quickly attenuate with range. Based on trial and error, various frequencies, starting from about 60Hz and increasing in 10Hz increments, were tested on-site to determine the frequency that resulted in the wave with the largest vertical component.

The evolving waveform as a function of distance for two, different operating frequencies, 100Hz and 70Hz, are shown in Figures 5.10 and 5.11, respectively. Note that the wavespeed for the 70Hz wave is slightly higher, as it penetrates deeper into the sediment, where the shear velocity is higher. More importantly, the 70Hz wave is attenuated less than the 100Hz wave, making 70Hz the optimal source drive frequency for the sediment on this particular day. In general, the optimal frequency was determined by placing the geophones at a fixed distance from the source, typically 40 feet (see Appendix C4), and adjusting the frequency to find the wave with the largest vertical amplitude.

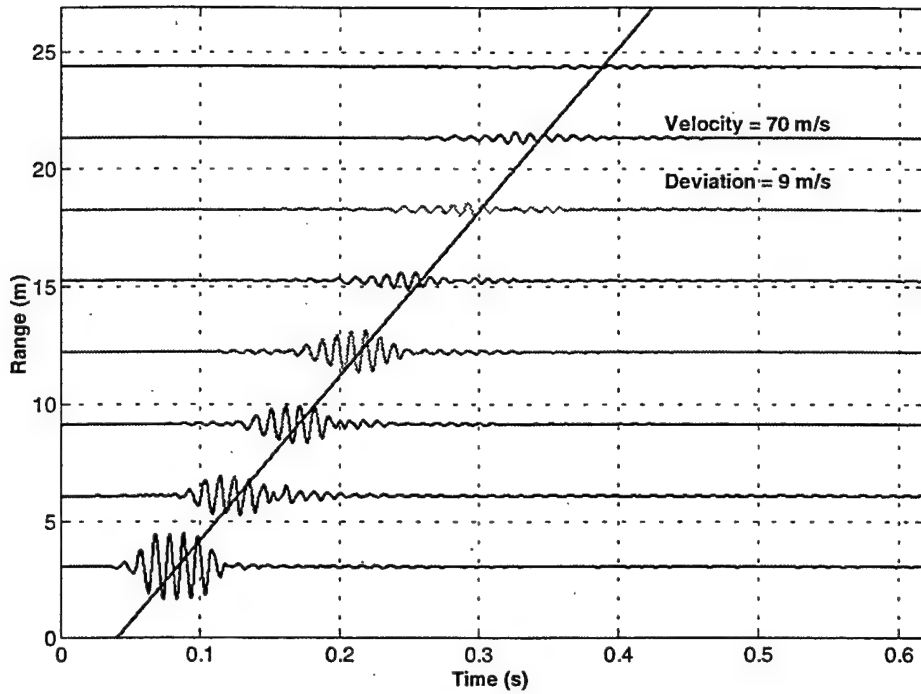


Figure 5.10. Surface wave evolution for a 100Hz input drive signal

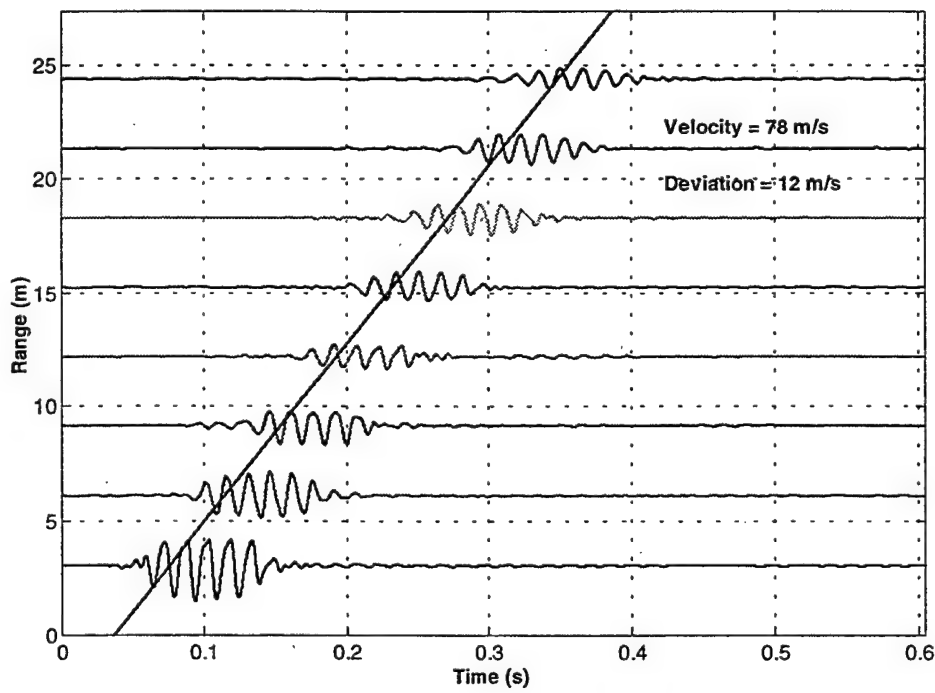


Figure 5.11. Surface wave evolution for a 70Hz input drive signal

## **2. Wavespeed**

After determining the optimal operating frequency (test setup in Appendix C4), the wavespeed was measured by cross correlating the vertical geophone signal with the source accelerometer signal (see the MATLAB program listing in Appendix D7). The cross correlation provided the time delay for maximum correlation between the two signals, providing the time that it took for the wave to travel from the source to the receiver. Based on the known source-receiver distance and the measured time delay, the wavespeed was quickly determined, within 2-3 minutes. The measured wavespeed was then used for echo-ranging in subsequent background measurement and target detection tests.

## **3. Background Data**

After determining the optimal drive frequency and its associated wavespeed, the geophones were repositioned at an appropriate distance from the source, typically 6 to 10 feet (1.8 to 3.0 meters), as shown in Appendix C5. A series of 10 background (i.e. no target) measurements were made using a single cycle drive cycle at the optimal frequency, and the geophone signals coherently averaged. This averaged "background" data was then analyzed using the vector polarization filtering algorithm in Appendix D12 to determine the time that the wavefield, as seen at the geophones, had decayed back to a nearly quiescent state. Based on the known wavespeed, the minimum range at which a buried target might be detected was estimated. Using this information, the target was buried at an appropriate distance from the receiving geophones.

## **4. Target Data**

Two differently shaped and sized targets were tested in this research. The mass of these two targets was varied, and will be discussed later. The target data collection test phase was conducted by burying a target, typically 5 cm below the surface, at an

appropriate distance, and collecting 10 data sets, using the same drive conditions as for the background data. As necessary, the data were coherently averaged and vector polarization filtered (see Appendices D2 and D12 for MATLAB subroutines) for study and target detection analysis.

## **5. Signal Processing**

Numerous signal processing routines, more than 23 total, were developed, using MATLAB's signal processing toolbox. [Ref. 18] These subroutines were invaluable in allowing near real-time analysis of the measured seismic signals. As previously discussed, the background and target signals were coherently averaged and polarization filtered. Also available for target signal analysis was a coherent subtraction subroutine (see Appendix D19), which coherently subtracted the background, reverberation field data from the target signal. This capability allowed a comparison of before and after seismic wavefield characteristics to determine and assess the detection of the target signal. Also available was an incoherent subtraction subroutine (see Appendix D18) which subtracted the background imaginary power from the target imaginary power. Similar to the coherent background subtraction, this method offered an additional capability to assess detection of the target signal.



## VI. TEST RESULTS (VERTICAL SOURCE)

Summarized in this chapter are some of the important test results from a vertically oriented seismic source. As previously mentioned, because of the versatility of the seismo-acoustic actuator source, it was possible to conduct numerous tests studying seismic interface wave generation and propagation. The results presented in this chapter include wave attenuation, source velocity, energy, and displacement measurements, target detection, and underwater testing.

### A. ATTENUATION

Although it was not studied in depth, limited attenuation measurements were made to help evaluate the types of seismic waves that were being generated. Based on the theoretical results presented in Chapter III, neglecting absorption, Rayleigh interface waves can be expected to attenuate due to cylindrical spreading. As a result, the acoustical power of the cylindrically spreading interface wave can be expected to decrease as the inverse ( $1/r$ ) of the radial distance from the source. Since the complex power (4.1) gives the relative power of the seismic pulse [Ref. 7], determining the attenuation of the seismic wave is relatively straightforward. Using the 70Hz seismic source and evolving seismic pulse shown in Figure 5.11, the cross power function was calculated and the maximum observed values were plotted as a function of range in Figure 6.1. Curves for cylindrical ( $1/r$ ) and spherical spreading ( $1/r^2$ ) are also included for comparison.

The measured attenuation curve in Figure 6.1 indicates that the seismic wave is attenuated less severely than for spherical spreading. In addition to spreading effects, absorption from the friction of the sand grains rubbing together results in wave attenuation. The results shown in Figure 6.1 qualitatively suggest that the vertical source, operating at 70Hz, is generating an interface wave that attenuates due to cylindrical spreading.

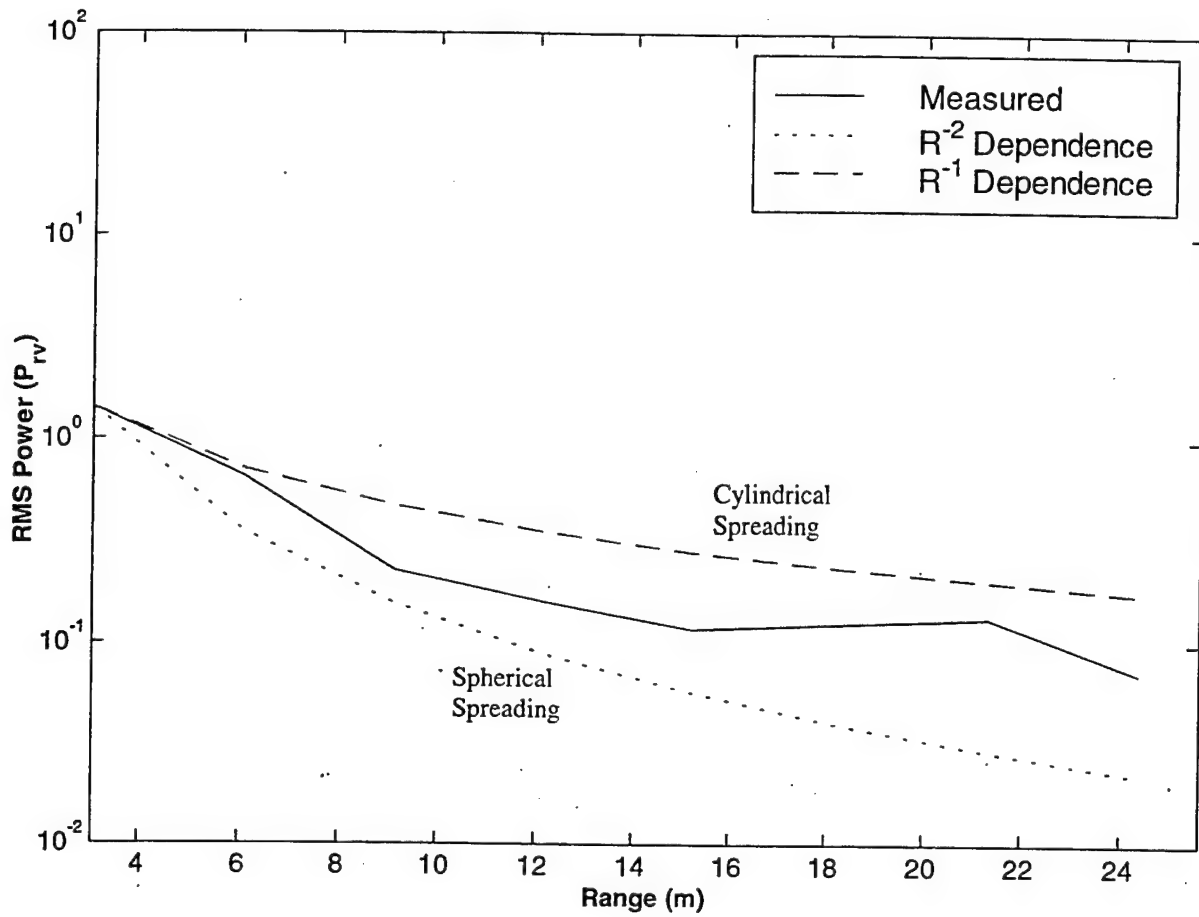


Figure 6.1. Seismic wave attenuation using two vertical actuators operating at 70Hz.

## B. VELOCITY AND DISPLACEMENT

The velocities and displacements of the motion produced by the vertically oriented seismic source were determined for the test setup shown in Appendix C2. The recorded geophone signals are shown in Figure 5.5. The geophone velocities are given directly by the output signal and the source velocity was found by integrating the actuator accelerometer signal. The displacements were obtained by integrating the velocities. The relative velocities and displacements for the seismic source and geophone (computed using the MATLAB subroutines in Appendices D20 and D8, respectively), 6-feet (1.8-meters) distant, are shown in Figures 6.2 and 6.3, respectively.

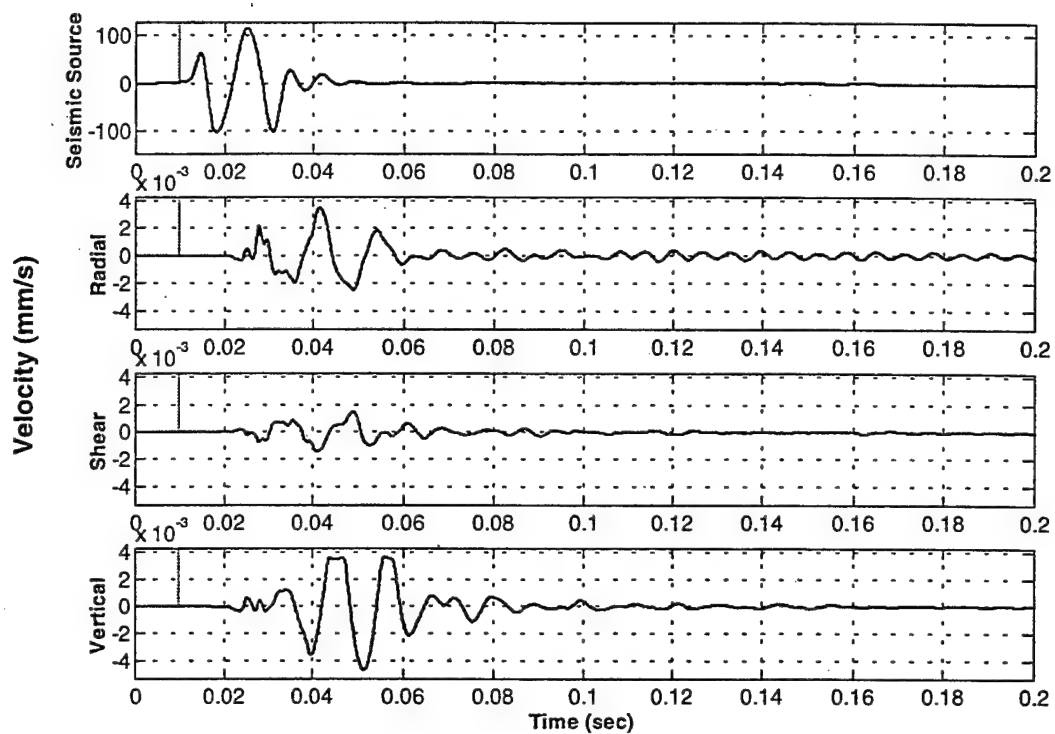


Figure 6.2. Relative velocities of the linear actuator shaft and geophones

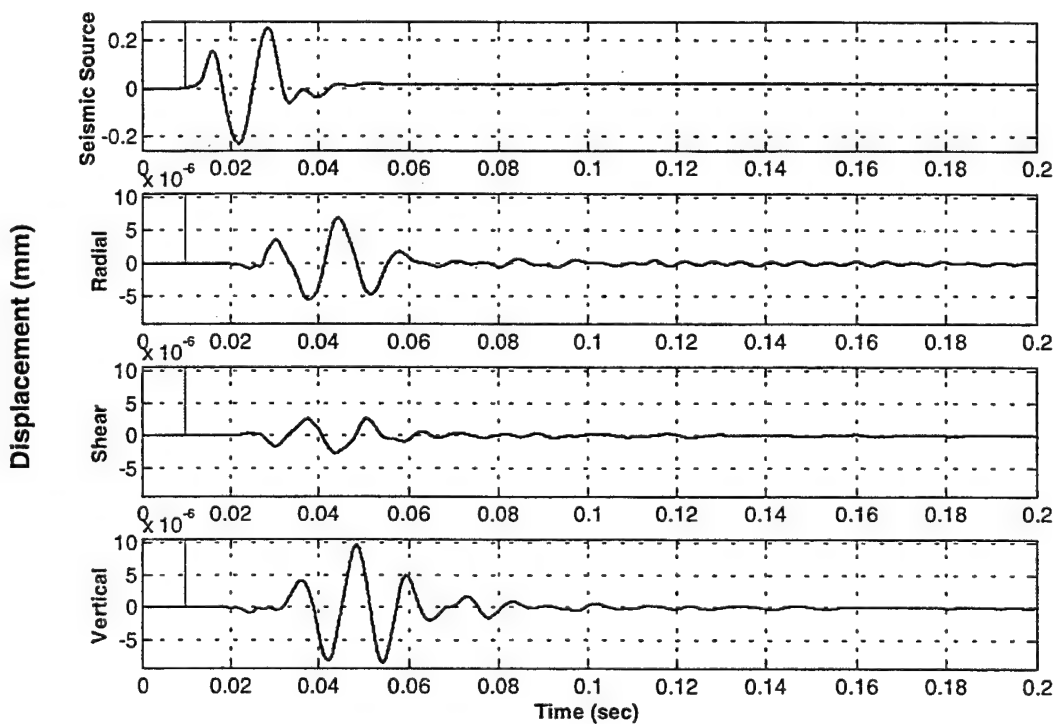


Figure 6.3. Relative displacements of the linear actuator shaft and geophones

The average power transmitted from the actuator to the sediment was estimated by calculating the product of the actuator force times the drive shaft velocity. It was determined that approximately 0.6-watts of seismic power was generated at the drive plate of a single, linear actuator system.

### C. TARGET DETECTION

After months of testing and equipment modifications, two buried mine-like targets were unambiguously detected using the linear actuator seismo-acoustic sonar system. The first target was a 156-lb (71-kg) helium gas tank, shown in Figure 6.4. The gas tank was modified so that the top could be removed to allow for the placement of 26-lb (11.8-kg) lead blocks inside, thus increasing its mass.



Figure 6.4. Buried helium gas tank target

The second target, shown in Figure 6.5, was a 1.5-foot (0.68-meter) diameter, 1-foot (0.45-meter) height gunpowder keg weighing about 16-lbs (7-kg) empty. The removable lid allowed placement of 26-lb blocks inside, shown in Figure 6.5.

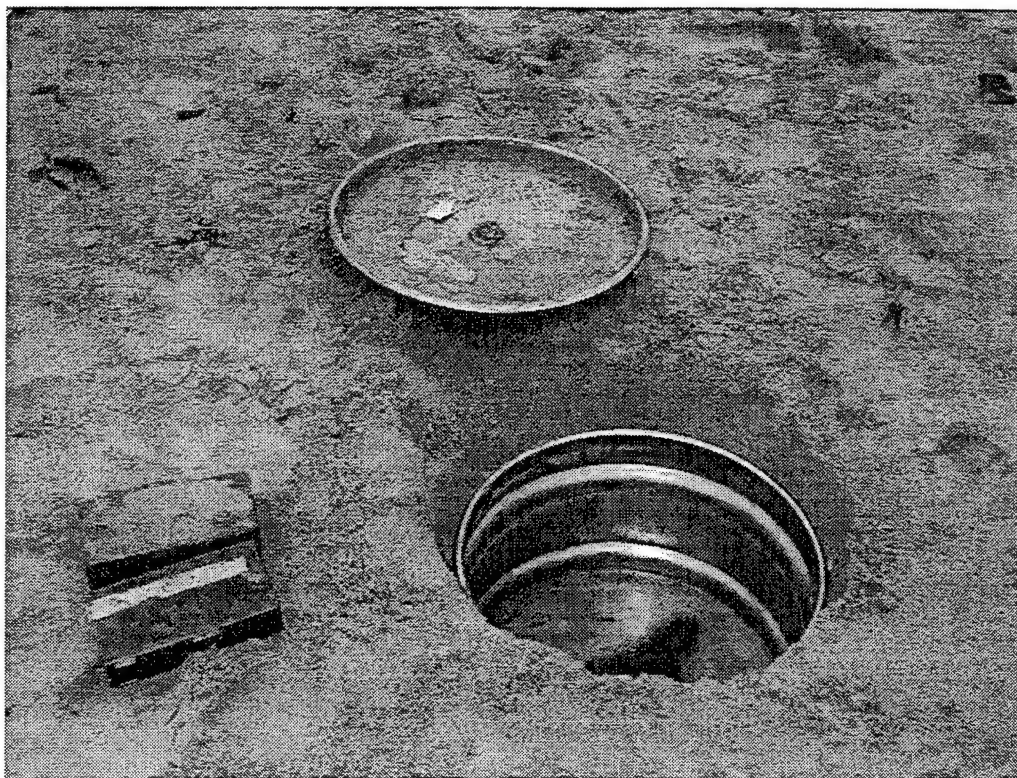


Figure 6.5. Buried gunpowder keg target with 25-lb lead blocks alongside

A test was conducted to detect the buried helium tank in Figure 6.4. The test setup, outlined in Appendix C5, consisted of two linear actuators, oriented vertically, and driven with a single cycle pulse at 70Hz. The geophones are 5-feet (1.5-meters) from the source and the target is buried 11-feet (3.35-meters) from the source. The wavespeed was determined to be about 290-ft/s (88-m/s). The background and target signals, using 10 coherently averaged records (subroutine in Appendix D2), for the source, and the relative the radial, shear, and vertical components of the geophone motion are shown in Figure 6.6. Note that the target signal, which should be seen at about 0.08 seconds, is not readily identifiable in the raw, recorded data.

The crossed power for the background data, target data, and target data with background coherently subtracted out was calculated using (4.1) and the results are presented in Figure 6.7. The measured wavespeed of the day (67m/s) was used to transform the time-based record to a range-based record.

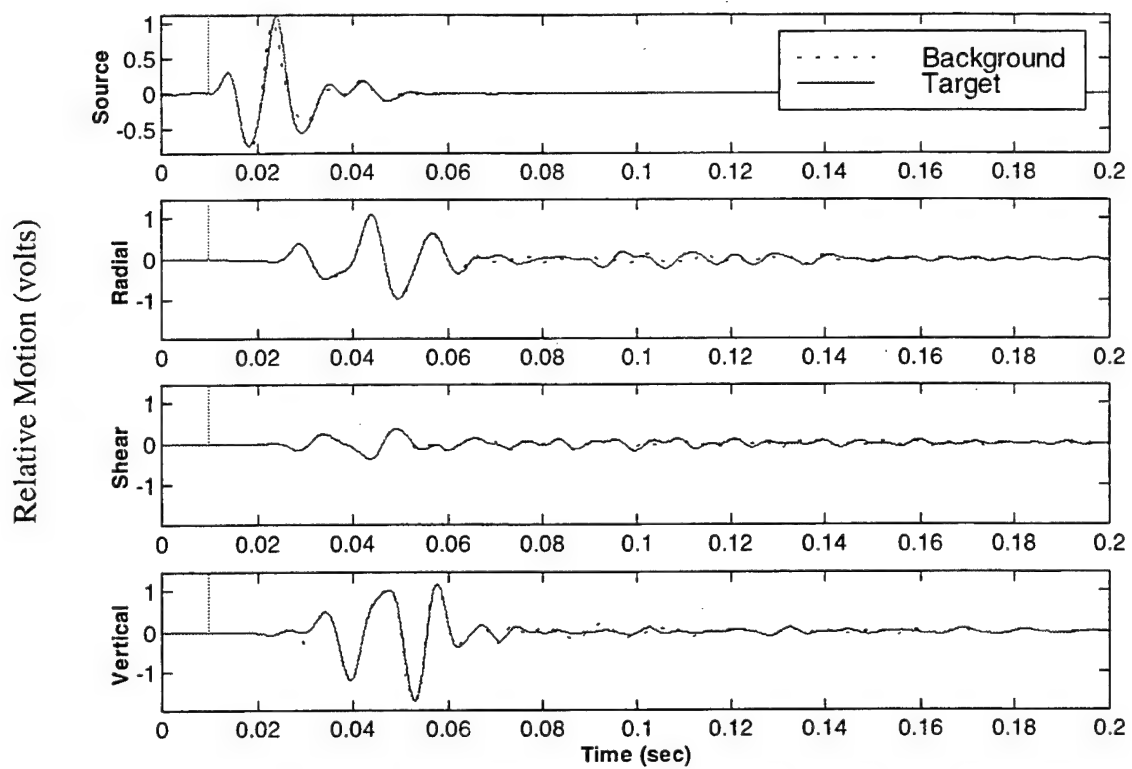


Figure 6.6. Relative source and geophone motions for the background and target data.

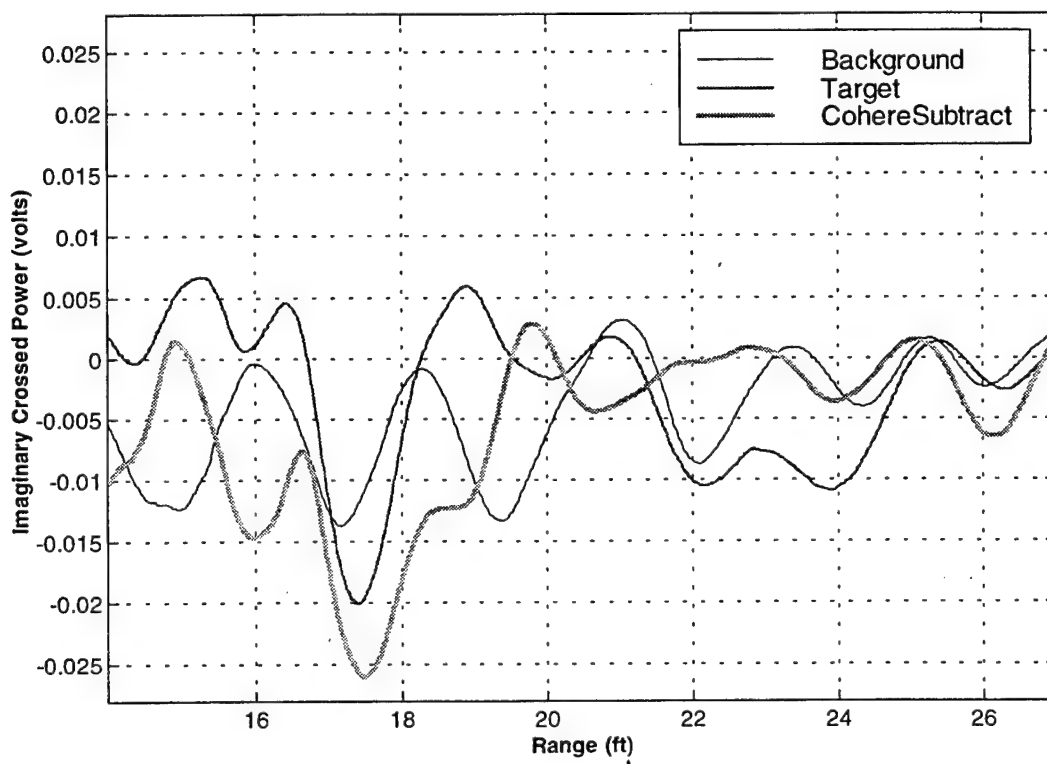


Figure 6.7. Imaginary crossed power for the background and target data.

Note that the imaginary crossed power gives a clear indication of the presence of the buried tank at about 17-feet (5.2-meters), as expected for a round trip range of 11-feet (3.3-meters) to the target and 6-feet (1.8-meters) back to the geophone. The negative deflection of the imaginary power indicates that the motion of the target echo is retrograde.

Similar tests were conducted two weeks later. The tests used both the helium tank and the gunpowder keg, which were buried a few days prior to the tests. In these tests, the geophones were positioned at 10-feet (3.0-meters) and the targets at 16-feet (4.9-meters). The test setup is outlined in Appendix C6. The mass of the targets was also increased in 104-lb (47-kg) increments using the lead blocks shown in Figure 6.5. The RMS values of the relative motion for the buried, 572lb gas tank are shown in Figure 6.8. Note the apparent evidence of the target at about 23-feet (7-meters).

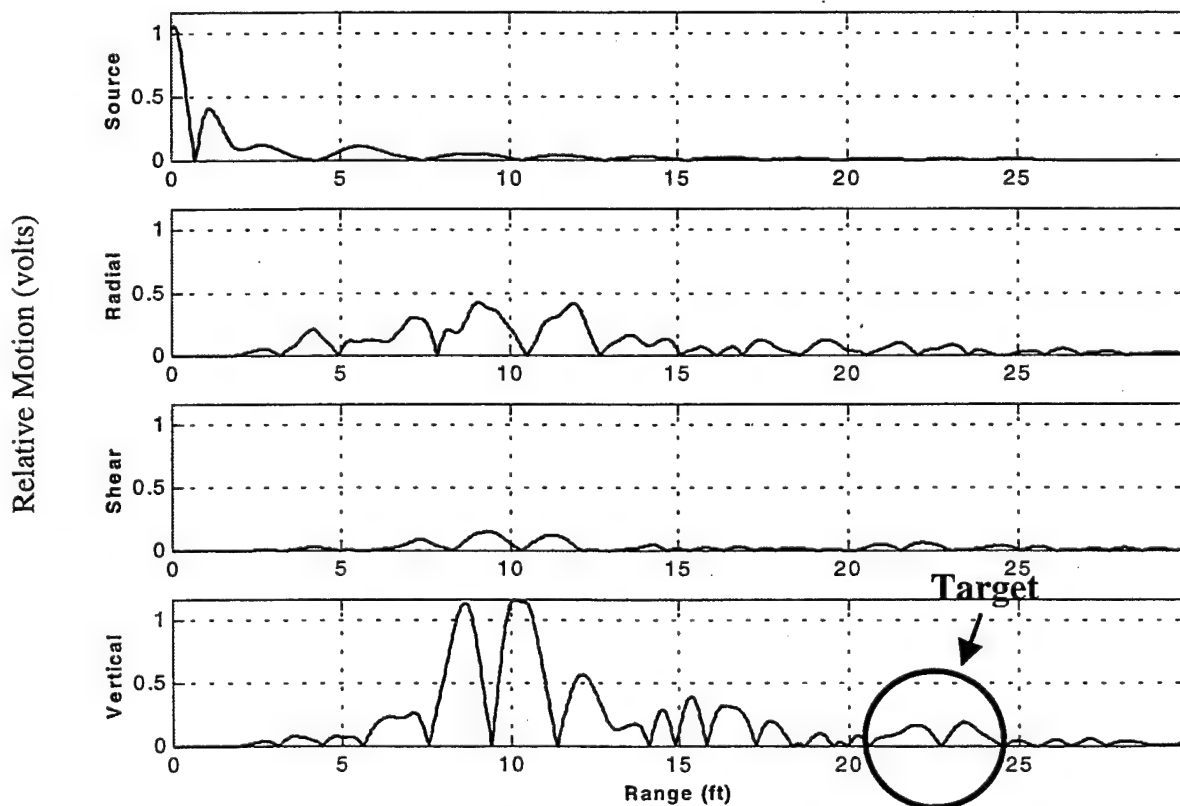


Figure 6.8. Relative RMS source and geophone motions for the buried 572lb gas tank.

The crossed power for the gas tank with increasing mass loading was calculated using (4.1) and the results are presented in Figure 6.9. Note that the imaginary crossed power gives a clear indication of the presence of the buried tank at about 23-feet (7-meters) as expected for a round trip range of 16-feet (3.3-meters) to the target and 6-feet (1.8-meters) back to the geophone. The relative target strength appears to be related to the target mass, as seen by the increasing imaginary power amplitude with increasing target mass. The positive deflection of the crossed power indicates that the motion of the target signal is prograde, which is surprising. It should be noted that, both targets had scoured themselves to a depth of about 0.5-feet (0.15-meters) due to water action from relatively high tides. It may be that this results in target scattered signal motion that is prograde.

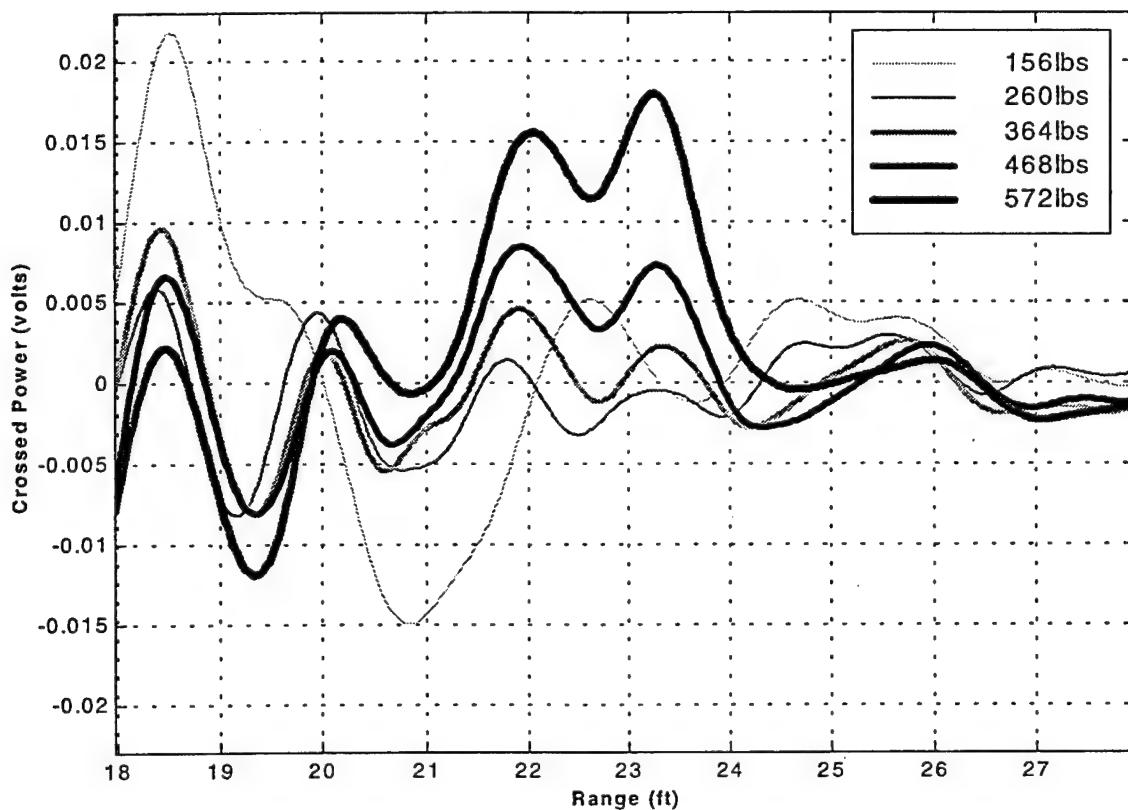


Figure 6.9. Imaginary crossed power for the helium gas tank target

Similar results were seen for the gunpowder keg, which was left buried in the beach for 4-days after the helium gas tank measurements. The crossed power for the

gunpowder keg with increasing mass loading was calculated and the results are presented in Figure 6.10. The results are similar to the buried gas tank, which was detected four days earlier. The presence of the keg is clearly indicated by the positive deflection of the crossed power at a range of about 24 feet (7.3-meters). As with the gas tank, the relative target strength increases with increasing target mass.

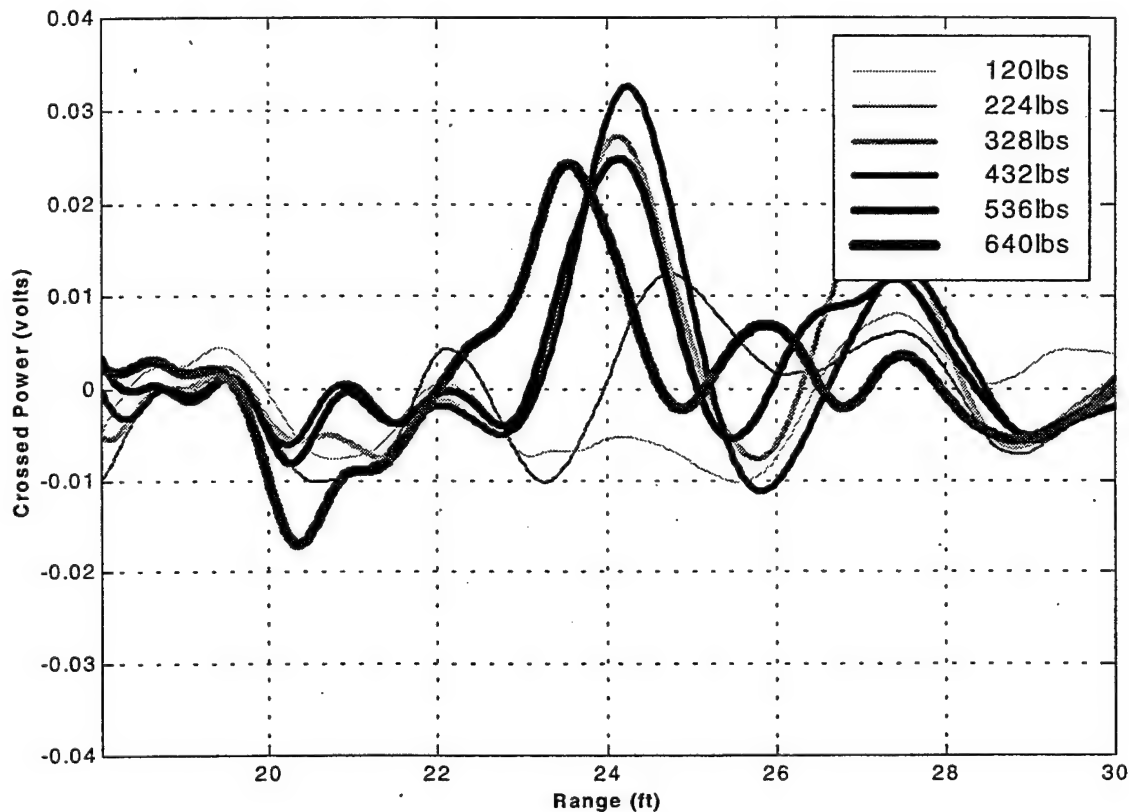


Figure 6.10. Imaginary crossed power for the gunpowder keg target

Relatively unambiguous target detection using the vertically oriented seismo-acoustic source was seen for both the helium gas tank and the gunpowder keg.

#### D. UNDERWATER TEST

Near the completion of this study, a single field trip was made to test the seismo-acoustic sonar system underwater. Unfortunately, high tides and storm surge prevented

successful deployment and underwater testing. The lessons learned from the test are included to help support further testing in this area.

The underwater testing initially started at the beach site. It was found that the 300-foot underwater actuator and geophone cables were not long enough to allow deployment just beyond the surf zone. Although not available for that particular day, a small boat would allow deployment of the system near the surf zone, from the water side.

Since deployment from the beach was not possible, the equipment was loaded into the mobile home and transported to the municipal wharf at the Monterey Marina. See Figure 5.1. Unfortunately, the relatively strong storm surge did not allow underwater placement of the actuators or geophones. Typically, this site would be ideal for underwater tests, as it is known for its relatively good visibility and flat, sandy beach bottom. The location is also ideal because it allows use of the mobile home to stage the electrical equipment and has easy beach access for water entry, as shown in Figure 6.11.



Figure 6.11. Underwater test site showing easy water access (the author and his spouse)

## **VII. CONCLUSIONS AND RECOMMENDATIONS**

### **A. CONCLUSIONS**

A uniaxial seismo-acoustic sonar source based on a linear force actuator was developed for this research. This source resulted in an impressive 60db improvement over the previous seismic source that was developed at NPS. [Ref. 8] Previous efforts at ARL:UT resulted in the detection of a buried object at a range of 3-meters after coherently subtracting the reverberant background data from the target data. [Ref. 7] Clearly it is not practical to rely on background measurements to detect buried mines in an operational environment. This source detected buried mine-like targets at ranges up to 5-meters and did not require coherent background subtraction.

The linear force actuators worked exceptionally well to generate seismic interface waves with minimal reverberation. The complexity of the seismic wavefield was reduced and buried target detection was enhanced. The results of this thesis support the use of seismic interface waves to detect ordnance.

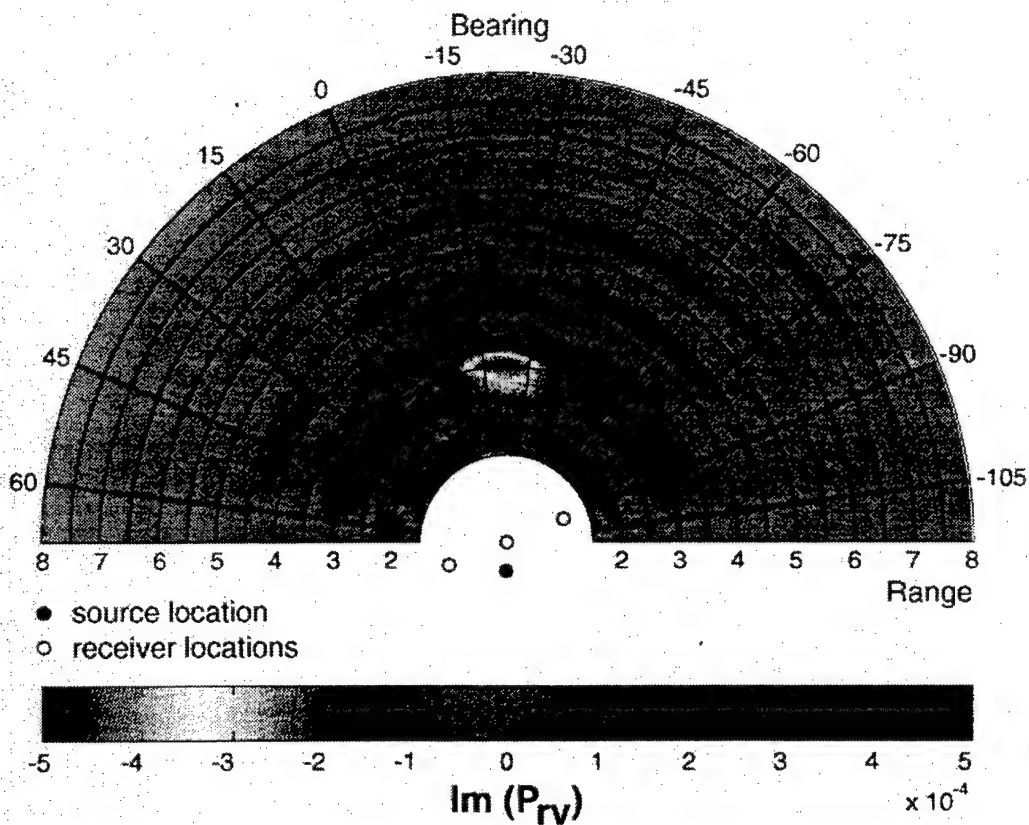
### **B. RECOMMENDATIONS**

While the linear force actuator source resulted in successful target detection, it is limited in the amount of force that it can apply to the sediment (25-lb peak force). Therefore, the intensity of the seismic interface wave and the effective operating range of seismo-acoustic sonar system is limited by the force capability of the actuator-based system. To increase the intensity and range of the system, a single, waterproof actuator, capable of 100+lb peak force should be acquired and used in subsequent studies.

In addition to a more intense source, an array of receivers should be developed to determine the azimuth or bearing to the target. The combination of an intense seismic source combined with an array of geophone sensors will allow for bearing and range to target measurements at greater standoff ranges.

Along with the development of a seismic receiver array, a MATLAB or other appropriate subroutine should be written to make practical use of the range and azimuth data provided by the array. Conceivably, within 2-3 minutes after recording the data, a polar plot display, similar to the display presented in Figure 7.1, would allow for a near real-time assessment of buried mine-like objects in the seismic wavefield. The display could also be updated as more data was collected and processed.

Figure 7.1. Polar plot display showing bearing and range to a buried target [Ref. 7]



The SPS390 Data Acquisition and Signal Processing System has the capability to store and average data based on an external trigger signal. To support increased and more effective data collection, the averaging feature available with the SPS390 should be used. The SPS390 owners manual [Ref. 19] contains an "Averager" conversion program that would allow for the conversion of the .avg file format into an ASCII file format compatible for analysis using MATLAB's Signal Processing tools.

Finally, underwater tests should be initiated as soon as possible. In theory, underwater Scholte waves are nearly identical to Rayleigh waves. The seismo-acoustic source developed in this research should work equally as well underwater as it did on the beach. However, this needs confirmation. In fact, since naval mines are typically more massive (500lbs to 2000lbs) than land-based mines, it should be relatively easier to detect them using a seismic-based sonar. Conceivably, an autonomous underwater vehicle could be used as the supporting platform for a seismo-acoustic sonar system to detect buried naval mines in the shallow water near the surf zone and seaward.



## **APPENDIX A. EQUIPMENT SPECIFICATIONS AND SPS390 SETTINGS**

This appendix contains the equipment specification sheets and SPS390 data acquisition settings that were used during this research.

- Appendix A1 – Aura linear actuator and ECU specifications
- Appendix A2 – Linear actuator force constants
- Appendix A3 – Actuator accelerometer specifications
- Appendix A4 – ECU/Actuator interconnect diagram
- Appendix A5 – Geophone specifications
- Appendix A6 – SPS390 setup and menu settings
- Appendix A7 – John Deere TrailGator specifications

## HIGH FIDELITY ACTUATOR PERFORMANCE SUMMARY

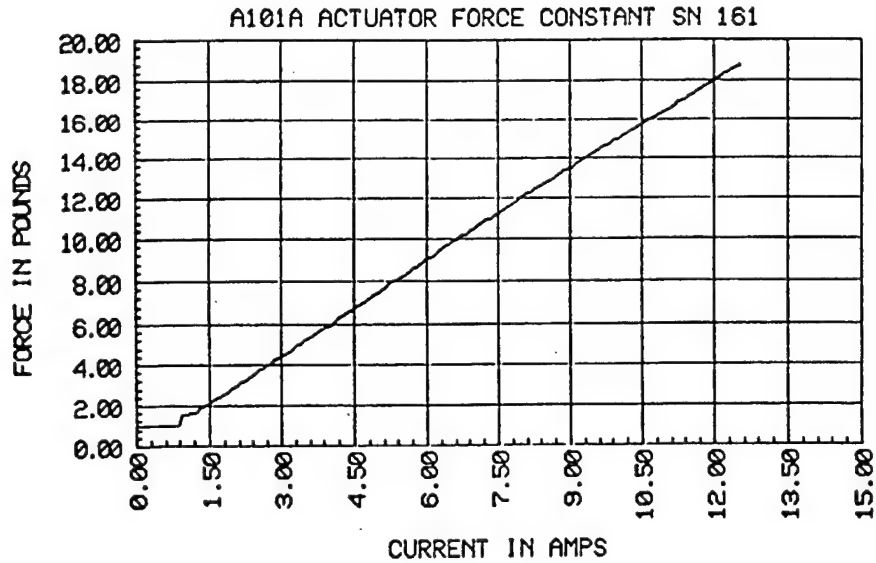
### APPENDIX A1. LINEAR ACTUATOR AND ECU SPECIFICATIONS

| MODEL NUMBER                                 | 10/0.5 - P | 10/1 - P | 10/2 - P | 10/2.2-P | 100/6 - P | 300/6 -P | 1600/32 - P | 10/0.5 - S | 20/0.5- U           | 50/0.6- S | 50/0.6- U | 350/3.2-U |
|--|------------|----------|----------|----------|-----------|----------|-------------|------------|---------------------|-----------|-----------|-----------|
| <b>Performance</b>                           |            |          |          |          |           |          |             |            |                     |           |           |           |
| Peak Force at 50% duty cycle( Pounds Force)  | 15         | 10       | 10       | 10       | 200       | 300      | 1000        | 15         | 15                  | 30        | 60        | 320       |
| Peak Force rated at 1% Duty Cycle.           | 30         | 50       | 30       | 30       | 450       | 450      | 1960        | 26         | 25                  | 80        | 80        | 350       |
| Rated Continuous Force (Pounds force).       | 10         | 8        | 7        | 7        | 100       | 277      | 850         | 10         | 20(sub),<br>10(air) | 25        | 50        | 300       |
| Stroke (Inches)                              | 0.62       | 1.0      | 2.0      | 2.25     | 6.2       | 6.2      | 32          | 0.5        | 0.6                 | 0.6       | 0.6       | 3.25      |
| Force Constant (Pounds Force Per Amp)        | 1.5        | 1.4      | 1.38     | 1.2      | 7.5       | 7.53     | 16.5        | 1.4        | 1.4                 | 4.8       | 6.8       | 15.2      |
| Force Non-Linearity Over Rated Stroke (%)    | <5         | <5       | <5       | <5       | <5        | <5       | <5          | <5         | <5                  | <5        | <5        | <5        |
| Maximum Acceleration (G's)                   | 25         | 40       | 15.2     | 15.2     | 12.6      | 12.6     | 12.25       | 32         | 32                  | 12        | 12        | (40)      |
| ( ) Indicates Current Limit Used (Amps)      | (16)       | (35)     | (18)     | (18)     | (55)      | (55)     | (119)       | (16)       | (16)                | (25)      | (25)      | (25)      |
| Maximum Force Slew Rate (Lb/I/S)             | 45,000     | 30,000   | 20,000   | 20,000   | 205,000   | 205,000  | 218,000     | 52,000     | 52,000              | 88,000    | 88,000    | 274,000   |
| ( ) Indicates Voltage Buss Used (VDC)        | (170)      | (170)    | (170)    | (170)    | (330)     | (330)    | (330)       | (170)      | (170)               | (170)     | (170)     | (300)     |
| Life Time (Number of 1Hz, 1/2 Stroke Cycles) | 5X10e8     | >5X10e7  | 1X10e8   | 1x10e8   | 3X10e7    | 3X10e7   | 6X10e6      | 5X10e8     | 5X10e8              | 5X10e8    | 2X10e8    | 1X10e7    |
| <b>Characteristics</b>                       |            |          |          |          |           |          |             |            |                     |           |           |           |
| Stiction Level (Pounds Force)                | <0.5       | <0.2     | <0.4     | <0.4     | <7.0      | <7.0     | <20         | <0.25      | <0.25               | <0.5      | <0.5      | <1.0      |
| Moving Mass (Pounds Mass)                    | 1.0        | 1.2      | 1.65     | 2.0      | 26.7      | 28.0     | 180         | .78        | 1.0                 | 6.6       | 6.6       | 91.5      |
| Actuator Weight (Pounds)                     | 3.24       | 8.0      | 8.0      | 7.1      | 82.8      | 115.0    | 680         | 3.5        | 4.6                 | 22.6      | 22.6      | 241.5     |
| Maximum Side Load (Pounds At Full Extension) | 5          | 5        | 5        | 5        | 40        | 40       | 300         | N/A        | N/A                 | N/A       | N/A       | N/A       |
| DC Coil Resistance (Ohms)                    | 0.75       | 1.0      | 1.6      | 1.5      | 1.16      | 1.16     | 1.2         | 0.77       | 0.77                | 1.70      | 1.70      | 1.2       |
| <b>Operating Environment</b>                 |            |          |          |          |           |          |             |            |                     |           |           |           |
| Rated Operating Temperature (°F)             | 70         | 70       | 70       | 70       | 70        | 70       | 70          | 70         | 70                  | 70        | 70        | 70        |
| Maximum Operating Case Temperature (°F)      | 160        | 160      | 160      | 160      | 160       | 160      | 160         | 160        | 160                 | 160       | 160       | 160       |
| Relative Humidity (%) At 70°F                | 30         | 30       | 30       | 30       | 30        | 30       | 30          | 30         | 100                 | 30        | 100       | 100       |
| <b>Misc.</b>                                 |            |          |          |          |           |          |             |            |                     |           |           |           |
| Sensor Type                                  | LVDT       | LVDT     | LVDT     | LVDT     | MLDT      | MLDT     | MLDT        | LVDT       | LVDT                | LVDT      | LVDT      | LVDT      |
| Commutation Type                             | NONE       | NONE     | NONE     | NONE     | BRUSHED   | BRUSHED  | BRUSHED     | NONE       | NONE                | NONE      | NONE      | NONE      |
| Device Type (Actuator Or Shaker)             | ACTUATOR   | ACTUATOR | ACTUATOR | ACTUATOR | ACTUATOR  | ACTUATOR | ACTUATOR    | SHAKER     | SHAKER              | SHAKER    | SHAKER    | SHAKER    |
| Maximum Shock, Half Sine, 11 msec (G's)      | 30         | 30       | 30       | 30       | 15        | 15       | 15          | 30         | 30                  | 30        | 30        | 15        |
| Maximum Submersion Pressure , psi            | N/A        | N/A      | N/A      | N/A      | N/A       | N/A      | N/A         | N/A        | 250                 | N/A       | 250       | 250       |

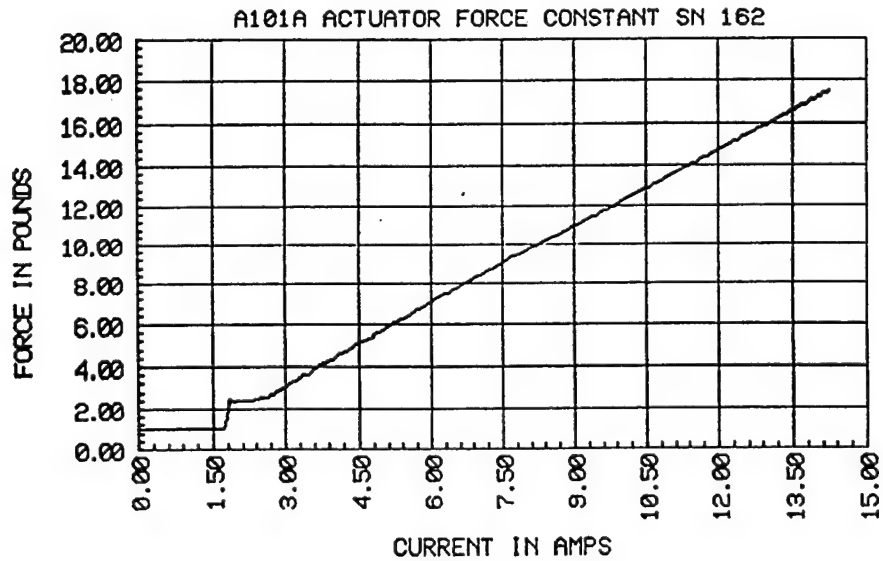
## ELECTRONIC CONTROL UNIT PERFORMANCE SUMMARY

| MODEL NUMBER  | ECU 8/110 - A | ECU 25/110 - S | ECU 25/110 - SD | ECU 25/208 - 1 | ECU 45/208 - 1 | D-ECU 50/208-3 | ECU 90/208 - 3 | ECU 120/208 - 3 |
|---|---------------|----------------|-----------------|----------------|----------------|----------------|----------------|-----------------|
| <b>Performance</b>  |               |                |                 |                |                |                |                |                 |
| Peak Supplied Current (Amps)  | 16            | 16             | 45              | 45             | 90             | 120            | 120            | 150             |
| Maximum Continuous Current (Amps)                                     | 8             | 8              | 25              | 25             | 45             | 90             | 90             | 120             |
| Supply Buss Voltage (Volts)   | 170           | 170            | 170             | 300            | 300            | 300            | 300            | 300             |
| AC Power Supply Voltage (Volts AC/Number Of Phases)                   | 110/1         | 110/1          | 110/1           | 208/1          | 208/1          | 208/3          | 208/3          | 208/3           |
| AC Power Supply Current (Amps)  | 7             | 10             | 10              | 15             | 30             | 30             | 30             | 30              |
| <b>Control Interface</b>  |               |                |                 |                |                |                |                |                 |
| Position Input Voltage Range (Volts)<br>(Full Scale Stroke Command)   | +/- 10        | +/- 10         | +/- 10          | +/- 10         | +/- 10         | +/- 10         | +/- 10         | +/- 10          |
| Position Output Voltage Range (Volts)<br>(Measured Full Scale Stroke) | +/- 10        | +/- 10         | +/- 10          | +/- 10         | +/- 10         | +/- 10         | +/- 10         | +/- 10          |
| Force Input Voltage Range (Volts)<br>(Full Scale Force Command)       | +/- 10        | +/- 10         | +/- 10          | +/- 10         | +/- 10         | +/- 10         | +/- 10         | +/- 10          |
| Force Output Voltage Range (Volts)<br>(Full Scale Force Response)     | +/- 10        | +/- 10         | +/- 10          | +/- 10         | +/- 10         | +/- 10         | +/- 10         | +/- 10          |
| Position Input Gain (Volts Per Inch)                                  | 20/stroke     | 20/stroke      | 20/stroke       | 3.22           | 20/stroke      | 20/stroke      | 20/stroke      | 0.62            |
| Position Output Gain (Volts Per Inch)                                 | 20/stroke     | 20/stroke      | 20/stroke       | 3.22           | 20/stroke      | 20/stroke      | 20/stroke      | 0.62            |
| Current Monitor Gain (Amps Per Volt)                                  | 2.0           | 10             | 8.0             | 8.0            | 10             | 10             | 10             | 10              |
| Controller type   | Analog        | Analog         | Analog          | Analog         | Analog         | Digital        | Analog         | Analog          |
| <b>Operating Environment</b>  |               |                |                 |                |                |                |                |                 |
| Rated Operating Temperature (°F)                                      | 70            | 70             | 70              | 70             | 70             | 10             | 70             | 70              |
| Relative Humidity (%) At 70°F   | 30            | 30             | 30              | 30             | 30             | 30             | 30             | 30              |
| <b>Cables</b>   |               |                |                 |                |                |                |                |                 |
| AC Supply Power   | X             | X              | X               | X              | X              | X              | X              | X               |
| Motor Power   | X             | X              | X               | X              | X              | X              | X              | X               |
| Sensor  |               |                |                 | X              | X              | X              | X              | X               |
| Heavy Duty Ground   |               |                |                 |                |                | X              | X              | X               |

## APPENDIX A2. LINEAR ACTUATOR FORCE CONSTANTS



FORCE CONSTANT:  $4 \text{ to } 16 + 0 = 1.49$   
 COMMENT: UUT MOUNTED VERT 1.7H ADDED TO Y AXIS, MID-STROKE  
 FILE: A101F161.DAT    SETUP: A129-FC.DSU    10-24-1997    11:03



FORCE CONSTANT:  $4 \text{ to } 16 + 0 = 1.2$   
 COMMENT: UUT MOUNTED VERT 1.7H ADDED TO Y AXIS, MID-STROKE  
 FILE: A101F162.DAT    SETUP: A129-FC.DSU    10-24-1997    10:54

## APPENDIX A3. ACTUATOR ACCELEROMETER SPECIFICATIONS

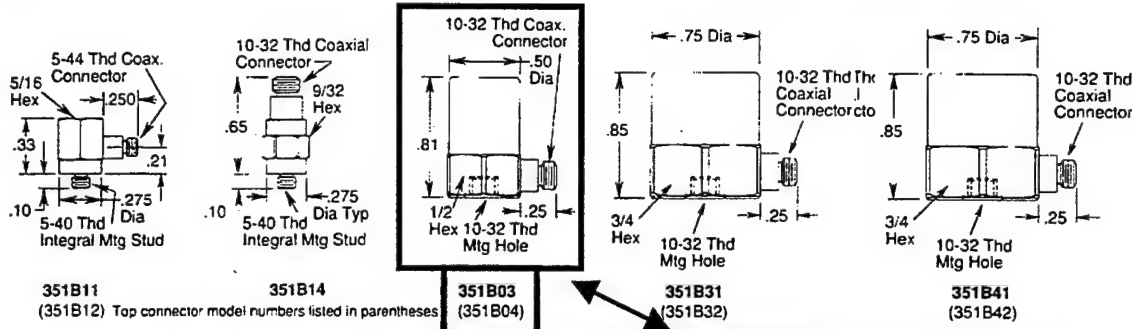
with built-in electronics

CRYOGENIC - QUARTZ SHEAR ICP®

11

Dimensions shown in inches except where noted.

English Selection Guide



351B11  
(351B12) Top connector model numbers listed in parentheses

351B14

351B03  
(351B04)

351B31  
(351B32)

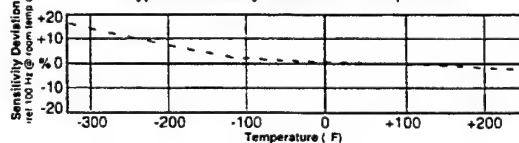
351B41  
(351B42)

| MODEL NUMBER                         | Unit             | HIGH FREQUENCY / LOW MASS |               | GENERAL       | HIGH SENSITIVITY |               |
|--------------------------------------|------------------|---------------------------|---------------|---------------|------------------|---------------|
|                                      |                  | 351B11                    | 351B14        | 351B03        | 351B31           | 351B41        |
| Voltage Sensitivity (@ 4 mA); (1, 2) | mV/g             | 5                         | 5             | 10            | 50               | 100           |
| Frequency Range ( $\pm 5\%$ )        | Hz               | 1 to 10 000               | 1 to 8 000    | 1 to 6 000    | 1 to 4 000       | 1 to 2 000    |
|                                      | Hz               | 0.7 to 15 000             | 0.7 to 10 000 | 0.7 to 9 000  | 0.7 to 7 000     | 0.7 to 3 500  |
| Resonant Frequency                   | kHz              | $\geq 40$                 | $\geq 40$     | $\geq 35$     | $\geq 22$        | $\geq 14$     |
| Amplitude Range (3)                  | $\pm g$ pk       | 300                       | 300           | 150           | 30               | 15            |
| Resolution (broadband)               | g pk             | 0.01                      | 0.01          | 0.005         | 0.001            | 0.0005        |
| Mechanical Shock Limits              | $\pm g$ pk       | 5 000                     | 5 000         | 5 000         | 2 000            | 1 000         |
| Temperature Range (4)                | $^{\circ}F$      | -320 to +250              | -320 to +250  | -320 to +250  | -320 to +250     | -320 to +250  |
| Temperature Coefficient (5)          | $\%/^{\circ}F$   | see graph                 | see graph     | see graph     | see graph        | see graph     |
| Amplitude Linearity                  | %                | $\pm 1$                   | $\pm 1$       | $\pm 1$       | $\pm 1$          | $\pm 1$       |
| Transverse Sensitivity               | %                | $\leq 5$                  | $\leq 5$      | $\leq 5$      | $\leq 5$         | $\leq 5$      |
| Base Strain Sensitivity              | g/ $\mu\epsilon$ | $\leq 0.002$              | $\leq 0.002$  | $\leq 0.0005$ | $\leq 0.0002$    | $\leq 0.0002$ |
| Excitation Voltage                   | VDC              | 18 to 30                  | 18 to 30      | 18 to 30      | 18 to 30         | 18 to 30      |
| Constant Current Excitation (6)      | mA               | 4                         | 4             | 4             | 4                | 4             |
| Output Impedance                     | ohm              | $\leq 1200$               | $\leq 1200$   | $\leq 1200$   | $\leq 1200$      | $\leq 1200$   |
| Output Bias Voltage                  | VDC              | 3 to 10                   | 3 to 10       | 3 to 10       | 3 to 10          | 3 to 10       |
| Discharge Time Constant              | second           | $\geq 0.5$                | $\geq 0.5$    | $\geq 0.5$    | $\geq 0.5$       | $\geq 0.5$    |
| Sensing Element                      | quartz           | tri-shear                 | tri-shear     | tri-shear     | tri-shear        | tri-shear     |
| Connector                            | type             | 5-44 coax                 | 10-32 coax    | 10-32 coax    | 10-32 coax       | 10-32 coax    |
| Sealing                              | type             | weld/herm                 | weld/herm     | weld/herm     | weld/herm        | weld/herm     |
| Mounting Thread                      | size             | 5-40                      | 5-40          | 10-32         | 10-32            | 10-32         |
| Housing                              | material         | titanium                  | titanium      | titanium      | titanium         | titanium      |
| Weight                               | gram (oz)        | 2 (0.07)                  | 1.8 (0.06)    | 10 (0.35)     | 25 (0.88)        | 32 (1.1)      |
| OPTIONAL MODELS: (7)                 |                  |                           |               |               |                  |               |
| Top Connector                        |                  | 351B12                    | standard      | 351B04        | 351B32           | 351B42        |
| Ground Isolated ( $>10^8$ ohms)      |                  | J351B11                   | J351B14       | J351B03       | J351B31          | J351B41       |
| Adhesive Mount                       |                  | A351B11                   | A351B14       | A351B03       | A351B31          | A351B41       |
| SUPPLIED ACCESSORIES: (8, 9)         |                  |                           |               |               |                  |               |
| Mounting Stud (10)                   |                  | N/A                       | N/A           | 081B05        | 081B05           | 081B05        |
| OPTIONAL ACCESSORIES: (8)            |                  |                           |               |               |                  |               |
| Adhesive Mounting Base               |                  | 080A15                    | 080A15        | 080A          | 080A12           | 080A12        |
| Magnetic Mounting Base               |                  | 080A30                    | 080A30        | 080A27        | 080A27           | 080A27        |
| Triaxial Mounting Adaptor            |                  | 080A16                    | 080A16        | 080B10        | 080A11           | 080A11        |
| CABLING: (8)                         |                  |                           |               |               |                  |               |
| Mating Cable Connectors              | type             | G                         | A             | A             | A                | A             |
| Recommended Stock Cable              | series           | 002                       | 002           | 002           | 002              | 002           |

### NOTES:

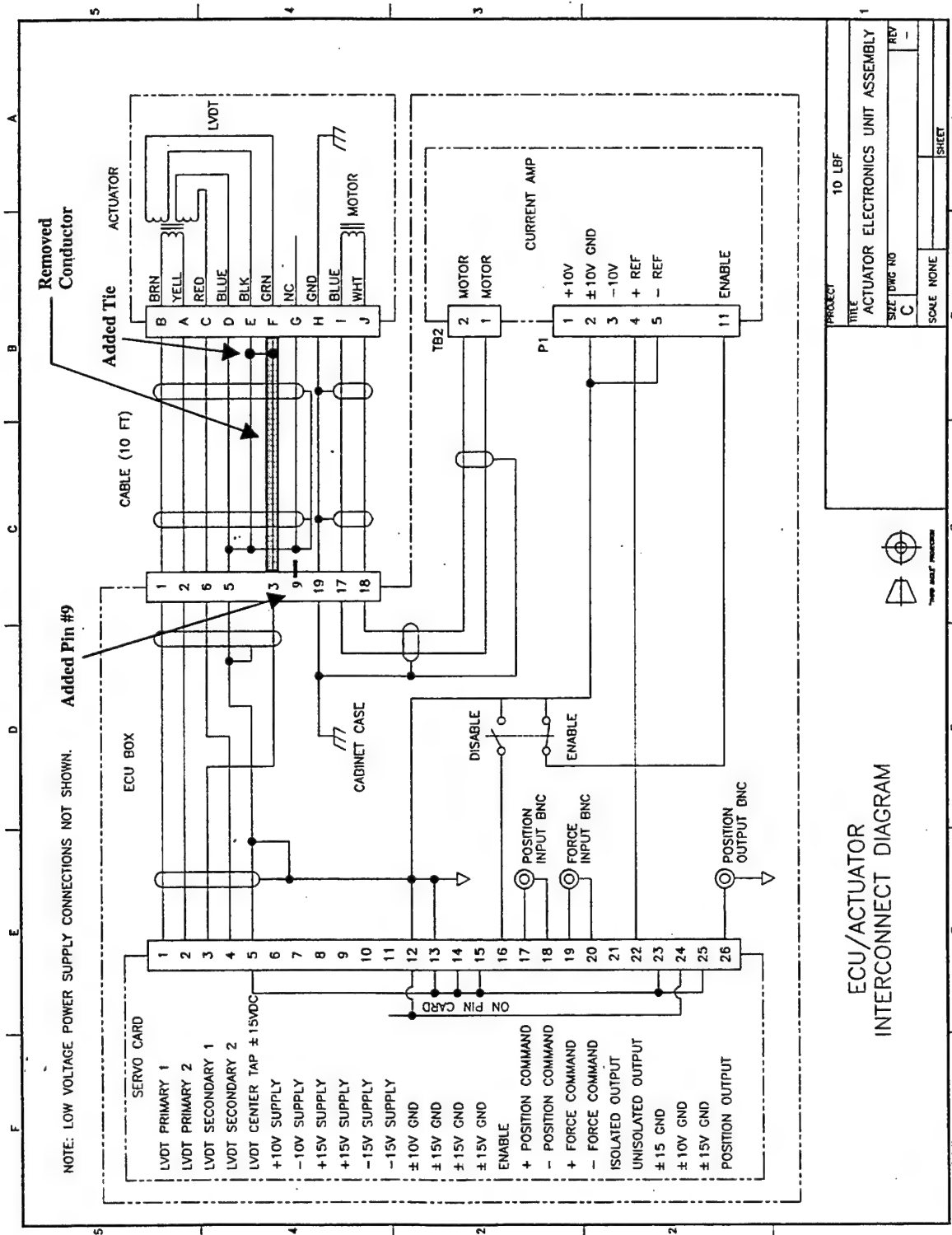
- All models have a sensitivity tolerance of  $\pm 10\%$ .
- Sensitivity determined with 4 mA constant current excitation. (Consult PCB for calibration at other current levels.)
- Amplitude range is for a  $\pm 1.5$  volt output full scale.
- In-house testing capabilities limited to  $-320^{\circ}F$  ( $-196^{\circ}C$ ). Sensors have been successfully operated in liquid helium environments.
- Within 5% of typical graph.
- Operational range: 2-12 mA. Sensitivity drops 1% for each mA increase.
- See page 8 for a description of the optional models. (Specifications may differ slightly. Consult factory before ordering.)
- See cables/accessories section beginning on page 78 for a complete description of the supplied and optional accessories.

Typical Sensitivity Deviation vs. Temperature



- NIST traceable calibration certificate from 10 Hz to  $\pm 5\%$  frequency point supplied. Exact temperature coefficient at  $-320^{\circ}F$  ( $-196^{\circ}C$ ) also provided.
- Supplied mounting stud is threaded 10-32 to 10-32.

## APPENDIX A4. ECU/ACTUATOR INTERCONNECT DIAGRAM



# **APPENDIX A5. GEOPHONE SPECIFICATIONS** (Made by Halliburton Geophysical Services, Inc.)

## **SPECIFICATIONS FOR SM-6 GEOPHONES**

| Parameters   | Symbol | Unit      | Geophone Model  |                 |                 |              |              |
|--|--------|-----------|-----------------|-----------------|-----------------|--------------|--------------|
| <b>Frequency</b><br>Natural Frequency<br>Frequency Tolerance<br>Maximum tilt angle for specified<br>Fn (vertical units only)<br>Typical spurious frequency   | Fn     |           | A               | B               | B               | B            | B            |
|  |        | Hz        | 4.5<br>± 0.5 Hz | 4.5<br>± 0.5 Hz | 8.0<br>± 0.5 Hz | 10.0<br>± 5% | 14.0<br>± 5% |
|  |        | DEG<br>Hz | -<br>-          | -<br>-          | 20<br>150       | 25<br>170    | 25<br>190    |
| <b>Distortion</b><br>Distortion with 0.7 in/s pp coil<br>to case movement<br>Distortion measured at<br>frequency of<br>Maximum tilt angle for distortion<br>specification (vertical units only)    |        |           | < 0.3%          | < 0.3%          | < 0.2%          | < 0.2%       | < 0.2%       |
|  |        | Hz        | 12              | 12              | 12              | 12           | 14           |
|  |        | DEG       | -               | -               | 15              | 20           | 20           |
| <b>Damping</b><br>Open circuit damping for<br>375 ohm coil<br>Shunt resistance used for<br>damping calibration with<br>375 ohm coil<br>Damping with shunt for<br>375 ohm coil<br>Damping tolerance | Bo     |           | 0.265           | 0.560           | 0.315           | 0.250        | 0.180        |
|  | Rs     | Ohm       | -               | -               | 2257            | 1339         | 645          |
|  | Bt     |           | -               | -               | 0.60            | 0.60         | 0.60         |
|  |        |           | ± 5%            | ± 5%            | ± 5%            | ± 5%         | ± 5%         |

|  |    |  |                                    |
|--|----|--|------------------------------------|
| <b>Standard coil resistance</b><br>(other values available)          | Rc | 375 ± 5%                               | Ohm                                |
| <b>Sensitivity for Model 'A'</b><br><b>Sensitivity for Model 'B'</b> |    | 28.0 ± 5%<br>0.71<br>28.8 ± 5%<br>0.73 | V/m/s<br>V/in/s<br>V/m/s<br>V/in/s |
| RtBcFn for Model 'A'<br>RtBcFn for Model 'B'                         |    | 3875<br>6000                           | Ohm Hz<br>Ohm Hz                   |

| Physical Specifications    | Basic unit (element) | PE-4 case         | PE-5 case         | HPE-case          |
|----------------------------|----------------------|-------------------|-------------------|-------------------|
| Length                     | -                    | 40.0 mm (1.57 in) | 40.0 mm (1.57 in) | 57 mm (2.24 in)   |
| Width                      | -                    | 35.0 mm (1.38 in) | 35.0 mm (1.38 in) | 45 mm (1.77 in)   |
| Diameter                   | 25.4 mm (1.00 in)    | -                 | -                 | -                 |
| Height                     | 36.0 mm (1.42 in)    | 56.0 mm (2.20 in) | 62.0 mm (2.44 in) | 35.0 mm (1.38 in) |
| Weight                     | 81.0 g (2.86 oz)     | 183 g (6.46 oz)   | 141 g (4.97 oz)   | 192.5 g (6.79 oz) |
| Guarantee with normal use* | 2 years              | 1½ years          | 1½ years          | 1½ years          |

\* model guaranteed for one year  
:al use excludes damage caused by high voltage and physical damage to case  
Sensor reserves the right to alter specifications to offer the best possible product.

Suspended mass Model 'A' 18.1 g  
Model 'B' 11.1 g  
Total coil to case movement 4 mm (0.16 in)  
Operating temperature range -40°C to +100°C  
(-40°F to +212°F)  
All parameters specified at 20°C

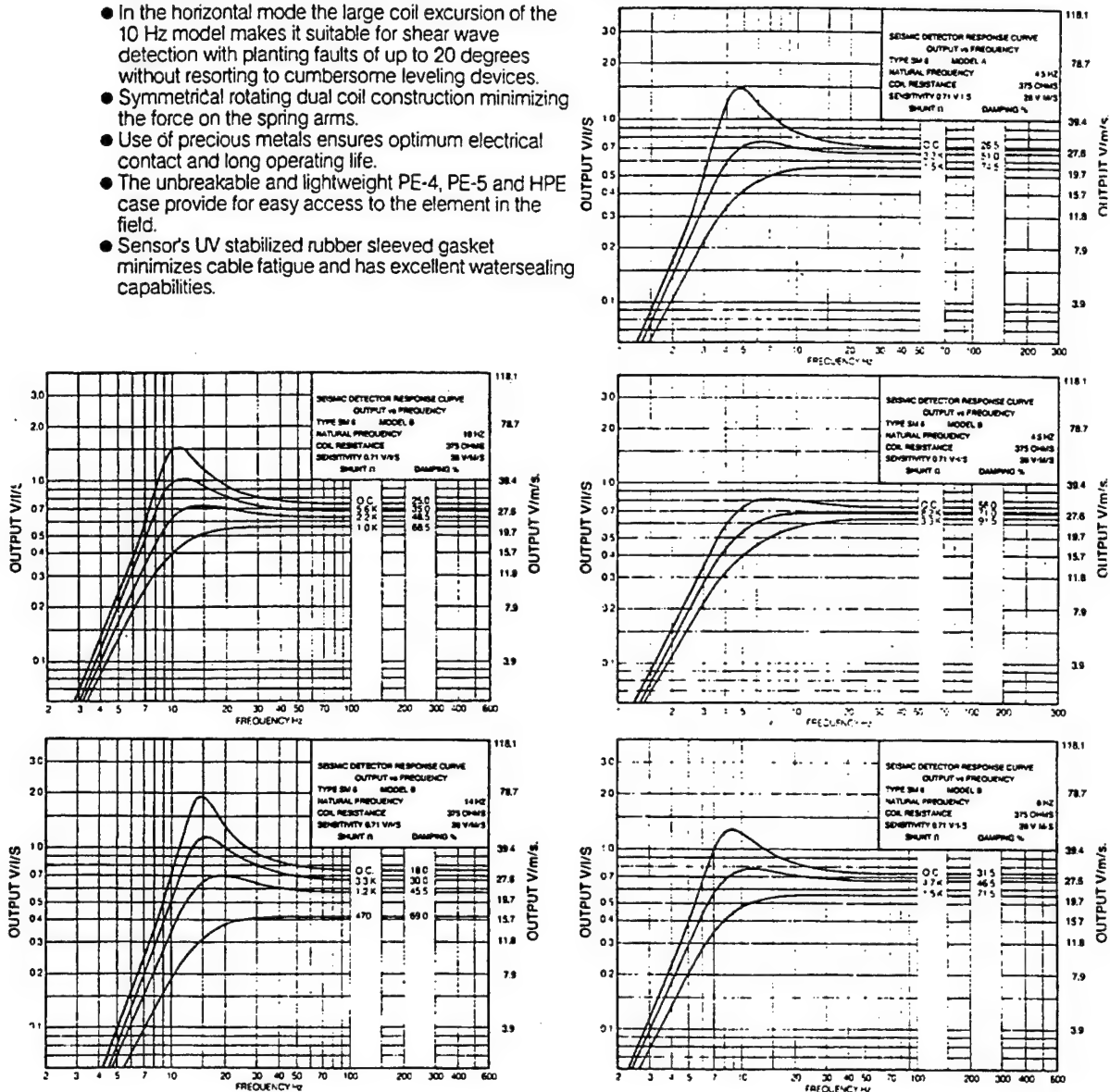
**KEY**  
Sensitivity : G  
Natural frequency : Fn  
Open Circuit Damping : Bo  
Coil Current Damping : Bc =  $\frac{RLBcFn}{(Rc + Rs)}$  ± 5%  
Coil Resistance : Rc  
Shunt Resistance : Rs  
Total Damping : Bt = Bo + Bc  
Total Resistance : Rt = Rc + Rs  
RLBcFn Model 'A' = 10.8 Rc  
Model 'B' = 18.0 Rc  
Transduction constant  
Model 'A' G = 0.0387 √ Rc V/m/sec. ± 5% 1.445 √ Rc V/m/sec. ± 5%  
Model 'B' G = 0.0377 √ Rc V/m/sec. ± 5% 1.484 √ Rc V/m/sec. ± 5%

The SM-6 is a digital grade, miniature geophone based on the popular SM-4 design. Engineered for consistent performance over a long life. Advanced computerized testing, manufacturing techniques and quality control are used in the production process to provide both the uniform parameters and the rugged qualities necessary in modern geophones.

#### Features of the SM-6

- Available coil movement of 4 mm (0.16 in) which makes it suitable in a vertical mode and high tilt for lower natural frequencies and for industrial purposes where the force of one G is exceeded.
- In the horizontal mode the large coil excursion of the 10 Hz model makes it suitable for shear wave detection with planting faults of up to 20 degrees without resorting to cumbersome leveling devices.
- Symmetrical rotating dual coil construction minimizing the force on the spring arms.
- Use of precious metals ensures optimum electrical contact and long operating life.
- The unbreakable and lightweight PE-4, PE-5 and HPE case provide for easy access to the element in the field.
- Sensor's UV stabilized rubber sleeved gasket minimizes cable fatigue and has excellent watersealing capabilities.

#### SM-6 FREQUENCY RESPONSE CURVES



ALL SALES AND DELIVERIES ARE SUBJECT TO SENSOR STANDARD TERMS AND CONDITIONS INCLUDING THE GUARANTEE PROVISION STATED THEREIN.

## APPENDIX A6. SPS390 SETUP AND MENU SETTINGS

### File Menu

**Open Configuration** → *std8chan* (configuration settings are listed below)  
**Save Extended Record** → used to save *.xrc* data files

### Setup Menu

#### Acquisition

Coupling → *AC*  
FS rms → user selectable, typically 1-5volts  
mV/EU → *100*  
EU Name → *Units*  
db Ref → *0*  
V Ref → *0*  
Source → *External*  
Repetitive → as desired  
Source Channel Delay → *-100* samples  
Sampling Method → *Internal*  
Frequency Span → *4kHz*  
RPM Readout → deselected

#### Analysis

Channel...Active → select all *8 channels*  
Channel...Reference → select *channels 1 & 2*  
Block Size → *4096 samples, 1600 lines*  
Overlap → *0%*  
Process Weighting → *Hanning*  
Memory → *8192 samples*  
Domain → *Cross Properties*  
Method → *Linear*  
Stop Criterion → *Single*

#### Preferences

DDE Server Capability → selected  
Display Buttons → selected  
Controls on Top → selected  
Overload Audio Tone → *500Hz* (as desired)  
Shorthand Notation → deselected  
Peak Interpolation → deselected

## Setup Menu(cont)

### Display

Function → *Time Trace*  
Source → *Live*  
X-Axis Units → *Seconds (Linear)*  
Y-Axis Units → *V (Linear)*  
Active Reference → *channel 2*  
Ticks → deselected  
Grids → deselected  
Shorthand Notation → deselected

## Mode Menu

Mode → *Cross Properties*  
Waterfall → deselected  
Total Input Samples → 65536

- \* It is necessary to open a compressed time trace window for one of the reference channels under the "Window" Menu for proper data formatting during save operations.

## APPENDIX A7. JOHN DEERE TRAILGATOR SPECIFICATIONS

# Specifications.

|                                | 4x2  | 6x4  |
|--------------------------------|--|--|
| <b>Engine and electrical</b>   |  |  |
| Make                           | KHI  | KHI  |
| Type                           | 4-cycle gas  | 4-cycle gas  |
| Cylinders                      | 1  | 2  |
| Valving                        | Overhead valves                                      | Overhead valves                                      |
| Displacement                   | 17.5 cu. in. (286 cc)                                | 37.7 cu. in. (617 cc)                                |
| Horsepower (SAE J1940)         | 10   | 18   |
| Maximum torque                 | 14.5 lb-ft @ 2,500 rpm                               | 32.5 lb-ft @ 2,200 rpm                               |
| Ignition                       | Capacitive discharge                                 | Transistor controlled                                |
| Lubrication                    | Full pressure  | Full pressure  |
| Oil filter                     | Replaceable (optional)                               | Replaceable (standard)                               |
| Rpm, idle (no load)            | 1,175  | 1,175  |
| Rpm, fast (no load)            | 3,750  | 3,650  |
| Cooling system                 | Air  | Liquid   |
| Air cleaner                    | Dry, replaceable, single element, with remote intake | Dry, replaceable, single element, with remote intake |
| Muffler                        | Spark arresting                                      | Spark arresting                                      |
| Battery                        | 32-amp/hr, 295 cold cranking amps                    | 32-amp/hr, 295 cold cranking amps                    |
| Alternator                     | 13-amp regulated                                     | 20-amp regulated                                     |
| Headlights                     | Two 37.5-watt Halogen                                | Two 37.5-watt Halogen                                |
| Fuel system capacity           | 5.3 U.S. gal. (20 L)                                 | 5.3 U.S. gal. (20 L)                                 |
| <b>Transmission</b>            |  |  |
| Type                           | Continuously variable transmission (CVT)             | Continuously variable transmission (CVT)             |
| Differential lock              | Standard; hand operated                              | Standard; hand operated                              |
| Drive chain                    | N/A  | No. 50 industrial roller chain                       |
| Ground speed                   | 0-15.5 mph (0-25 km/h)                               | 0-15.5 mph (0-25 km/h)                               |
| Transaxle                      | Fully enclosed; oil bath                             | Fully enclosed; oil bath                             |
| Gear selection                 | Forward, neutral, reverse                            | Forward, neutral, reverse                            |
| Overall reduction ratio:       |  |  |
| Low                            | 73.8:1   | 73.8:1   |
| High                           | 16.5:1   | 16.5:1   |
| <b>Brakes</b>                  | Wet disk in transaxle                                | Wet disk in transaxle                                |
| <b>Steering</b>                | Rack and pinion with Ackerman-type geometry          | Rack and pinion with Ackerman-type geometry          |
| <b>Ground pressure (max.)</b>  |  |  |
| With 200-lb. operator only     | 5.6 psi (.39/kg/cm <sup>2</sup> )                    | 6.9 psi (.49/kg/cm <sup>2</sup> )                    |
| Fully loaded vehicle           | 7.5 psi (.53/kg/cm <sup>2</sup> )                    | 7.1 psi (.50/kg/cm <sup>2</sup> )                    |
| <b>Dimensions</b>              |  |  |
| Length (without bumper)        | 100.5 in. (255.2 cm)                                 | 104.9 in. (266.5 cm)                                 |
| Length (with bumper)           | 101.6 in. (258 cm)                                   | 106.0 in. (269.3 cm)                                 |
| Width                          | 60.0 in. (152.5 cm)                                  | 60.0 in. (152.5 cm)                                  |
| Front-tread centers            | 50.0 in. (127 cm)                                    | 50.0 in. (127 cm)                                    |
| Rear-tread centers             | 48.0 in. (122 cm)                                    | 48.0 in. (122 cm)                                    |
| Height (overall)               | 43.6 in. (110.7 cm)                                  | 43.6 in. (110.7 cm)                                  |
| Wheelbase                      | 69.5 in. (176.6 cm)                                  | 79.0 in. (200.6 cm) front/rear                       |
| Weight (including fuel/fluids) | 879 lb. (398.6 kg)                                   | 1,057 lb. (479.4 kg)                                 |
| <b>Ground clearance:</b>       |  |  |
| Under transaxle                | 6.7 in. (170 mm)                                     | 6.7 in. (170 mm)                                     |
| Under foot platform            | 8.5 in. (215 mm)                                     | 8.5 in. (215 mm)                                     |
| Seating capacity               | 2  | 2  |
| Seat type                      | Standard medium back                                 | Professional high back                               |
| Turn clearance circle          | 22 ft. (6.7 m)                                       | 24.8 ft. (7.6 m)                                     |
| Towing capacity                | 900 lb. (408 kg)                                     | 1,200 lb. (544 kg)                                   |
| Payload capacity*              | 900 lb. (408 kg)                                     | 1,200 lb. (544 kg)                                   |
| <b>Cargo Box</b>               |  |  |
| Material                       | 16-gauge steel                                       | 16-gauge steel                                       |
| Capacity:                      |  |  |
| Volume                         | 10.1 cu. ft. (0.29 m <sup>3</sup> )                  | 11.2 cu. ft. (0.32 m <sup>3</sup> )                  |
| Weight                         | 500 lb. (227 kg)                                     | 800 lb. (364 kg)                                     |

\*Includes 200-pound operator, 200-pound passenger, and maximum box capacity (Specifications and design subject to change without notice.)



## **APPENDIX B. UNDERWATER ACTUATOR CABLES AND CONNECTORS**

This appendix contains the specifications and wiring diagrams for the underwater actuator cables and connectors that were used during this research.

Appendix B1 – Belden 9775 cable specifications

Appendix B2 – Seacon rubber-molded connector specifications

Appendix B3 – Seacon bulkhead connector specifications

Appendix B4 – Underwater cable wiring diagram

# APPENDIX B1. ACTUATOR UNDERWATER CABLE SPECIFICATIONS



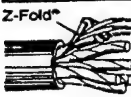
**Paired**  
Individually Shielded

## Audio and Computer Cables

| Description<br>UL AWG <sup>1</sup> Style | Trade No.<br>UL NEC Type<br>CSA Cert. | No.<br>of<br>Pairs | Standard<br>Lengths |   | Std.<br>Unit<br>Lbs.<br>ea. | Nominal D.C.R. |        | Nominal<br>O.D. |    | Nom.<br>Imp.<br>(ohms) | Nom.<br>Vel.<br>of<br>Prop. | Nominal<br>Capacitance |          |            |          |
|--|---------------------------------------|--------------------|---------------------|---|-----------------------------|----------------|--------|-----------------|----|------------------------|-----------------------------|------------------------|----------|------------|----------|
|  |                                       |                    | ft                  | m |                             | Cond           | Shield | Inch            | mm |                        |                             | pF/<br>ft.             | pF/<br>m | pF/<br>ft. | pF/<br>m |

**18 Gage**  
Stranded Conductors (19x30)  
**Polyethylene Insulated**

**Product Description**  
Tinned copper, polyethylene insulated, twisted pairs. Each pair individually shielded with Beldfoil® aluminum-polyester shield and 20 AWG stranded tinned copper drain wire. Overall chrome PVC jacket. Color code chart No. 3, Technical Information Section.

|  |  |    |                    |                        |                        |                   |                     |      |       |    |     |    |    |    |     |
|--|--|----|--------------------|------------------------|------------------------|-------------------|---------------------|------|-------|----|-----|----|----|----|-----|
| <br>Z-Fold®<br><br>Beldfoil<br>100% Shield<br>Coverage<br>75 2919<br>30V 80°C<br>See Attenuation,<br>Rise Time and<br>Bit Rate data for<br>this series on<br>page 99. | <b>9773</b><br>NEC CM<br>CSA<br>PCC FT 1 | 3  | 100<br>500<br>1000 | 30.5<br>152.4<br>304.8 | 8.4<br>48.2<br>94.3    | 6.4Ω/M'<br>21Ω/km | 8.3Ω/M'<br>27.2Ω/km | .404 | 10.26 | 50 | 66% | 30 | 98 | 55 | 180 |
|  | <b>9774</b><br>NEC CM<br>CSA<br>PCC FT 1 | 6  | 100<br>500<br>1000 | 30.5<br>152.4<br>304.8 | 19.3<br>95.6<br>192.5  | 6.4Ω/M'<br>21Ω/km | 8.3Ω/M'<br>27.2Ω/km | .560 | 14.22 | 50 | 66% | 30 | 98 | 55 | 180 |
|  | <b>9775</b><br>NEC CM<br>CSA<br>PCC FT 1 | 9  | 100<br>500<br>1000 | 30.5<br>152.4<br>304.8 | 25.7<br>131.8<br>256.6 | 6.4Ω/M'<br>21Ω/km | 8.3Ω/M'<br>27.2Ω/km | .655 | 16.64 | 50 | 66% | 30 | 98 | 55 | 180 |
|  | <b>9776</b><br>NEC CM<br>CSA<br>PCC FT 1 | 12 | 100<br>500<br>1000 | 30.5<br>152.4<br>304.8 | 32.4<br>206.4<br>420.8 | 6.4Ω/M'<br>21Ω/km | 8.3Ω/M'<br>27.2Ω/km | .735 | 18.67 | 50 | 66% | 30 | 98 | 55 | 180 |
|  | <b>9777</b><br>NEC CM<br>CSA<br>PCC FT 1 | 15 | 100<br>500<br>1000 | 30.5<br>152.4<br>304.8 | 45.0<br>213.7<br>460.0 | 6.4Ω/M'<br>21Ω/km | 8.3Ω/M'<br>27.2Ω/km | .819 | 20.8  | 50 | 66% | 30 | 98 | 55 | 180 |

Belden 9775  
Cable used

\* Capacitance between conductors.  
\*\* Capacitance between one conductor and other conductors connected to shield.



## RMK-FS AND ASSOCIATED PARTS

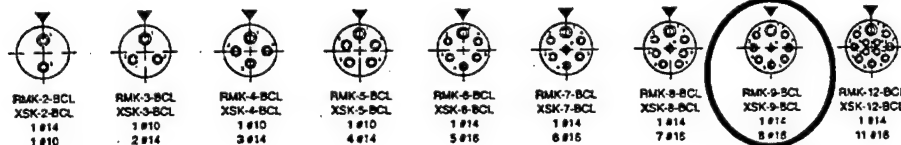
### MATEABLE BULKHEAD CONNECTORS

## (MATES TO RMK-FS &amp; RMK-FS-R/A)

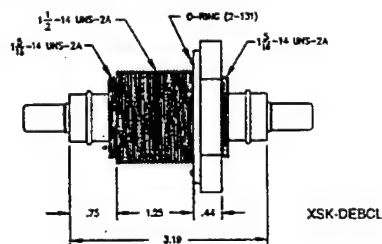
**Material:** 316 Stainless St.; **Internal Insulation:** Special Neoprene  
**Contacts:** Copper Alloy, Hard Gold Plated per MIL-G-45204  
**Pressure rating, Mated:** up to 20,000 psi

**Material:** Glass Reinforced Epoxy  
**Contacts:** Copper Alloy, Hard Gold Plated per MIL-G-45204  
**Pressure Rating, Mated:** up to 20,000 psi

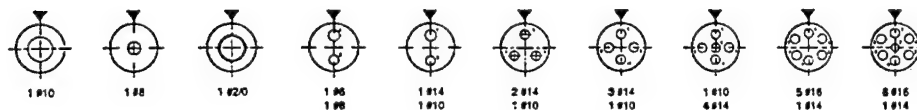
**Description:** A non-metallic connector homogeneously molded of glass reinforced epoxy (GRE). One of the oldest and most reliable connectors in our product line. For the same connector body, but with female sockets refer to the VSK (page 50-31).



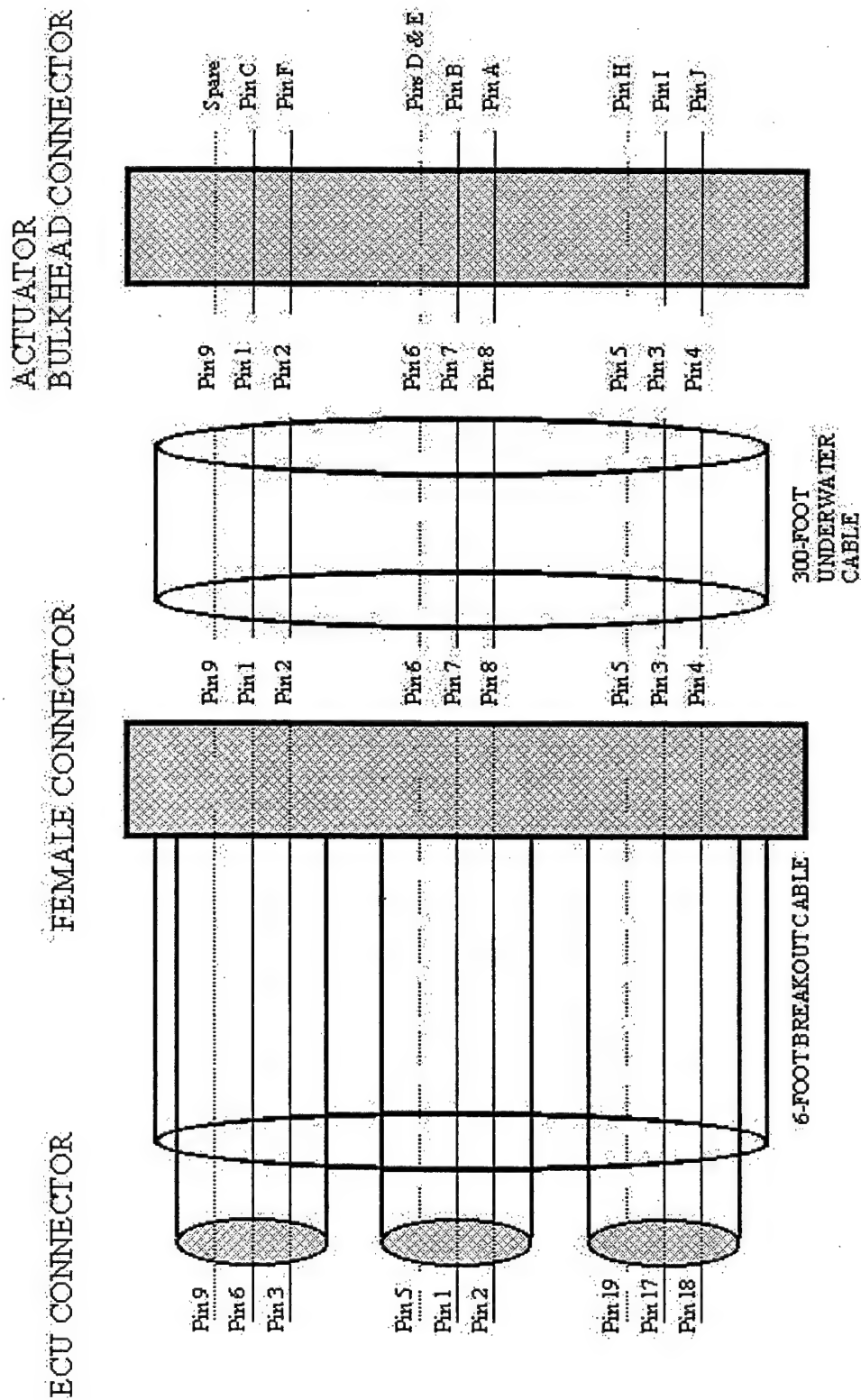
**Material:** Glass Reinforced Epoxy  
**Contacts:** Copper Alloy, Hard Gold Plated per MIL-G-45204  
**Pressure Rating, Mated:** up to 20,000 psi from front side.



RMK-9-BCL  
Connector  
Used



# APPENDIX B4. WIRING DIAGRAM FOR UNDERWATER ACTUATOR CABLES AND CONNECTORS





## APPENDIX C. EXPERIMENTAL SETUPS

This appendix contains the experimental setups for selected tests presented in this thesis.

Appendix C1 – Ambient Noise Analysis

Appendix C2 – Vertically Oriented Seismic Source Setup

Appendix C3 – Rayleigh Wave Seismic Source Setup

Appendix C4 – Frequency Optimization and Wavespeed Measurement Setup (Vertical)

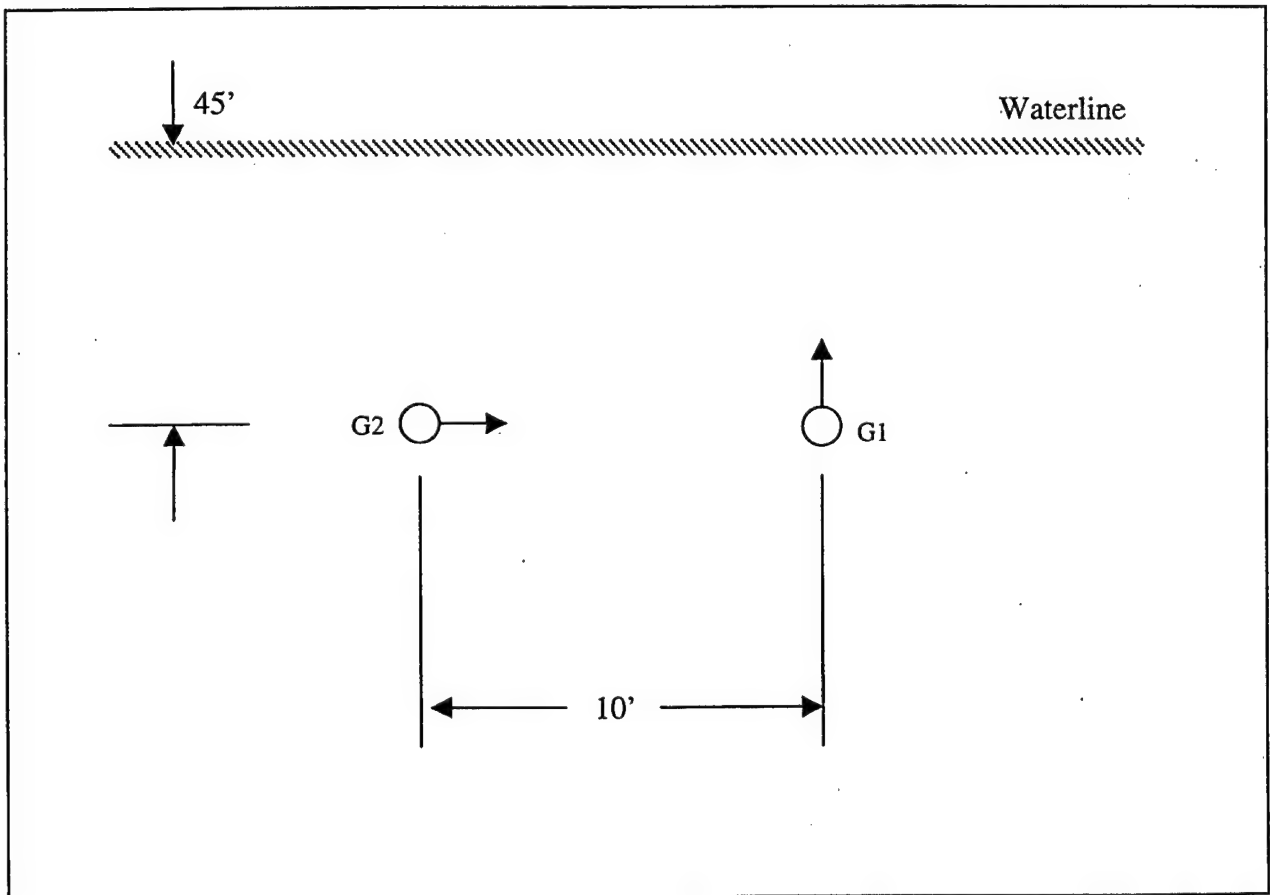
Appendix C5 – Test setup for helium gas tank target tests

Appendix C6 – Test setup for helium gas tank and gunpowder keg target measurements  
(increasing mass)

## APPENDIX C1. AMBIENT NOISE ANALYSIS

This appendix contains the experimental setup for the ambient acoustical noise analysis conducted on September 4, 1998.

**Comments:** Geophone gain = 40db  
Sunny, low tide, 3-4ft waves.  
Unfiltered signals were recorded as shown below



## APPENDIX C2. TEST SETUP FOR VERTICALLY ORIENTED SEISMIC SOURCES

This appendix contains the experimental setup for vertically oriented seismo-acoustic sources on October 20, 1998.

### Source #1

Orientation: Vertical  
Voltage: 10V (20Vpk-pk)  
Frequency: 90Hz  
Cycles: 1

### Source #2

Orientation: Vertical  
Voltage: 10V (20Vpk-pk)  
Frequency: 90Hz  
Cycles: 1

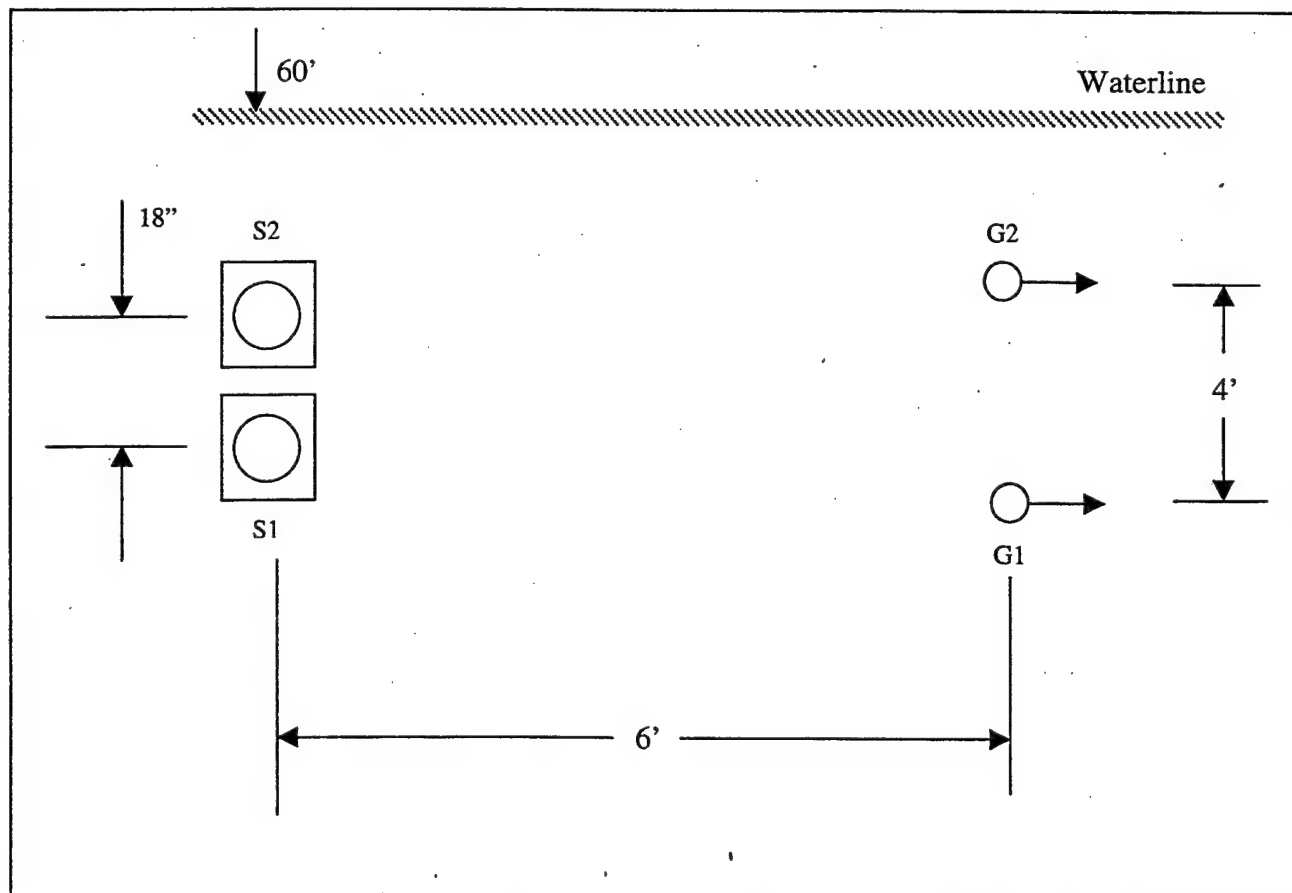
### Geophone #1

Filter: High Pass 40Hz  
Gain: 40db

### Geophone #2

Filter: High Pass 40Hz  
Gain: 40db

**Comments:** Sunny, low tide, 3-4ft waves.



### APPENDIX C3. RAYLEIGH WAVE SEISMIC SOURCE SETUP (PHASING)

This appendix contains the experimental setup for Rayleigh wave excitation on October 2, 1998.

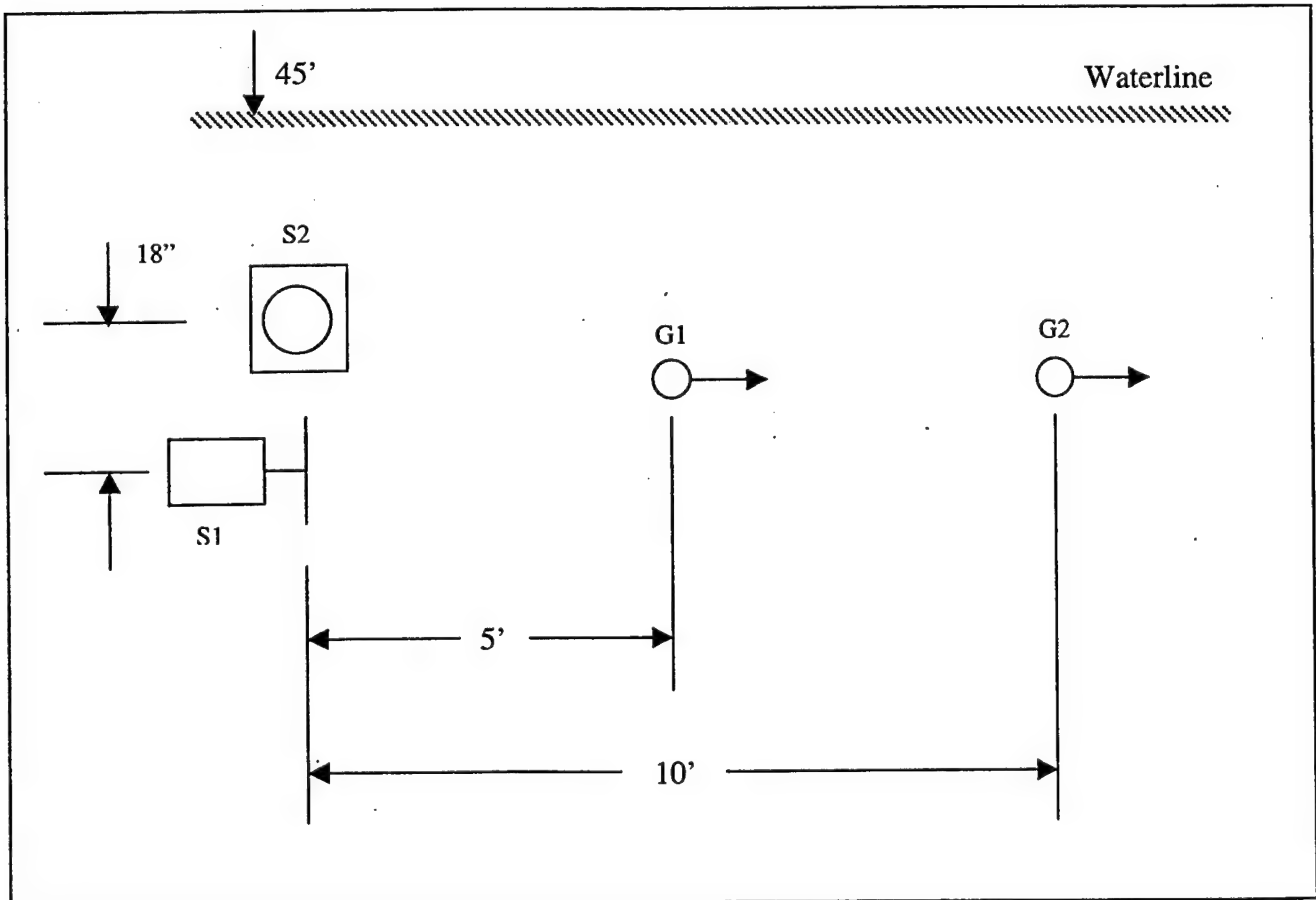
**Source #1**  
Orientation: Horizontal  
Voltage: 6V (12Vpk-pk)  
Frequency: 100Hz  
Cycles: 2  
Phase: 0°

**Source #2**  
Orientation: Vertical  
Voltage: 6V (12Vpk-pk)  
Frequency: 100Hz  
Cycles: 2  
Phase: -90°

**Geophone #1**  
Filter: High Pass 40Hz  
Gain: 40db

**Geophone #2**  
Filter: High Pass 40Hz  
Gain: 40db

**Comments:** Sunny, low-medium tide, 2-3ft waves.



## APPENDIX C4. FREQUENCY OPTIMIZATION AND WAVESPEED SETUP

This appendix contains the experimental setup for determining the optimal drive frequency and its associated wavespeed on October 20, 1998.

### Source #1

Orientation: Vertical  
Voltage: 10V (20Vpk-pk)  
Frequency: 90Hz  
Cycles: 1

### Source #2

Orientation: Vertical  
Voltage: 10V (20Vpk-pk)  
Frequency: 90Hz  
Cycles: 1

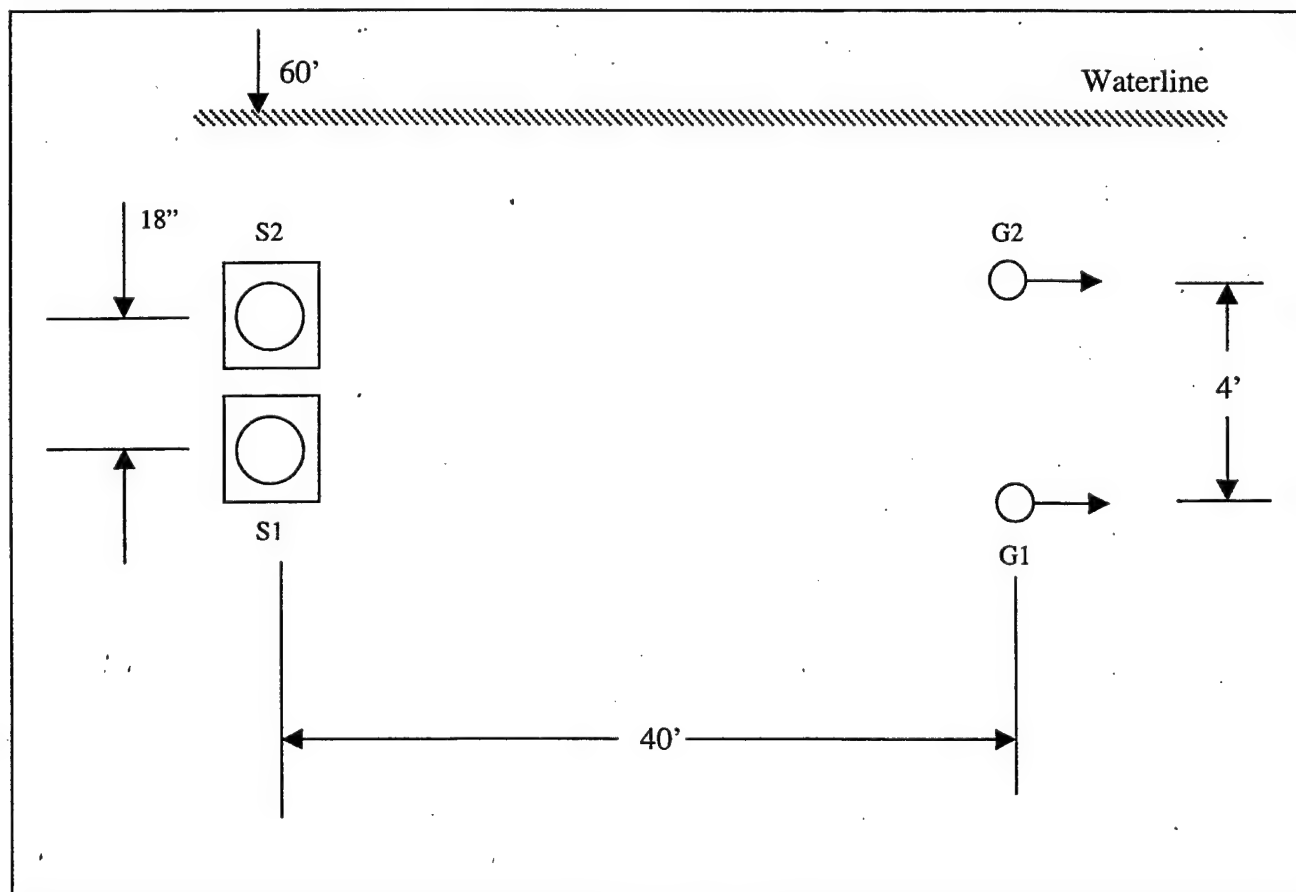
### Geophone #1

Filter: High Pass 40Hz  
Gain: 40db

### Geophone #2

Filter: High Pass 40Hz  
Gain: 40db

**Comments:** Sunny, low tide, 3-4ft waves.



Not to Scale

## APPENDIX C5. TEST SETUP FOR HELIUM GAS TANK TARGET TESTS

This appendix contains the experimental setup for target detection with increasing mass tests conducted on October 23, 1998.

### Source #1

Orientation: Vertical  
Voltage: 10V (20Vpk-pk)  
Frequency: 80Hz  
Cycles: 1

### Source #2

Orientation: Vertical  
Voltage: 10V (20Vpk-pk)  
Frequency: 80Hz  
Cycles: 1

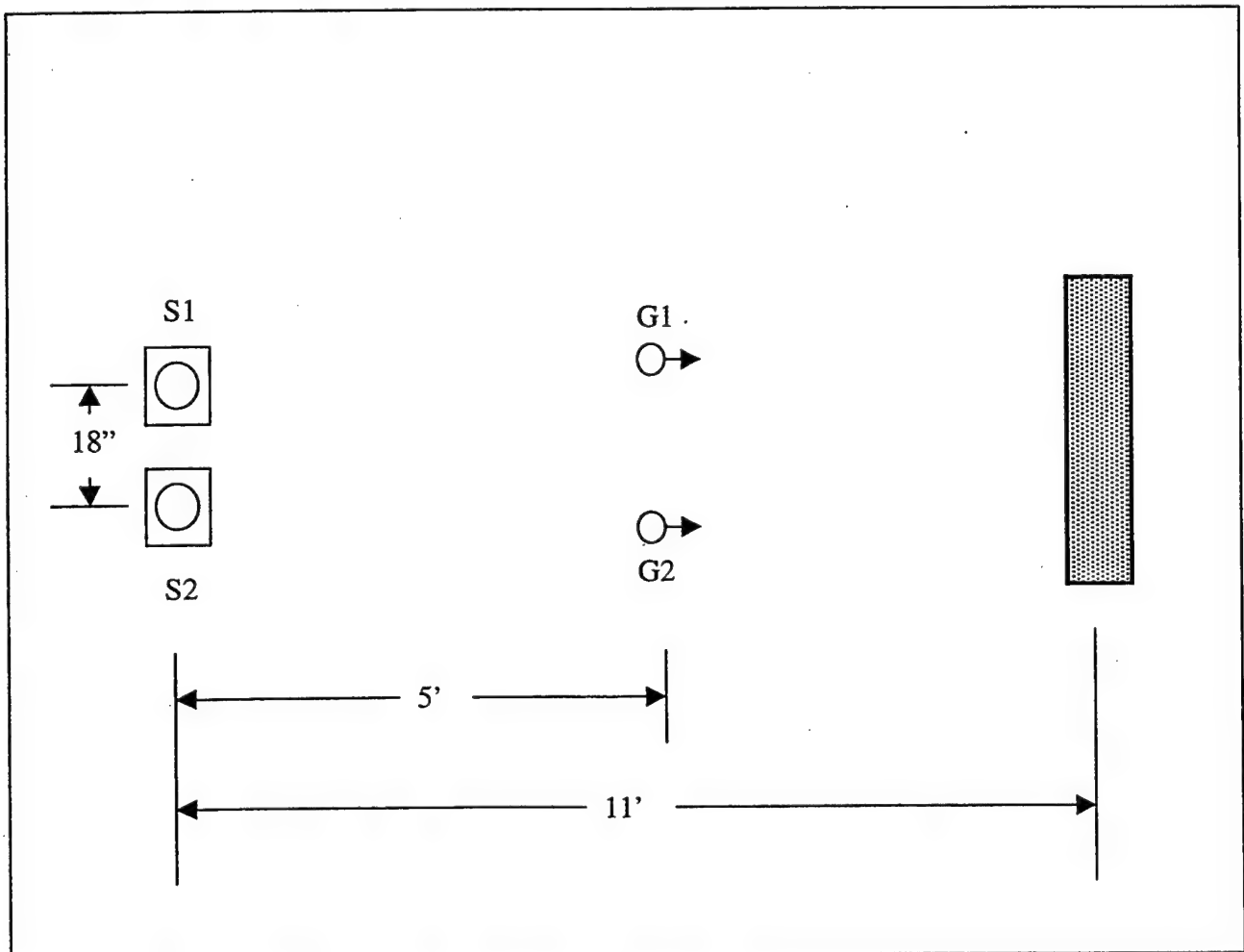
### Geophone #1

Filter: High Pass 40Hz  
Gain: 40db

### Geophone #2

Filter: High Pass 40Hz  
Gain: 40db

**Comments:** Overcast, med-high tide, 4-5ft waves.



## APPENDIX C6. TEST SETUP FOR HELIUM GAS TANK AND GUNPOWDER KEG TARGET TESTS (INCREASING MASS)

This appendix contains the experimental setup for target detection with increasing mass tests conducted on November 6, 1998 and November 10, 1998.

### Source #1

Orientation: Vertical  
Voltage: 10V (20Vpk-pk)  
Frequency: 80Hz  
Cycles: 1

### Source #2

Orientation: Vertical  
Voltage: 10V (20Vpk-pk)  
Frequency: 80Hz  
Cycles: 1

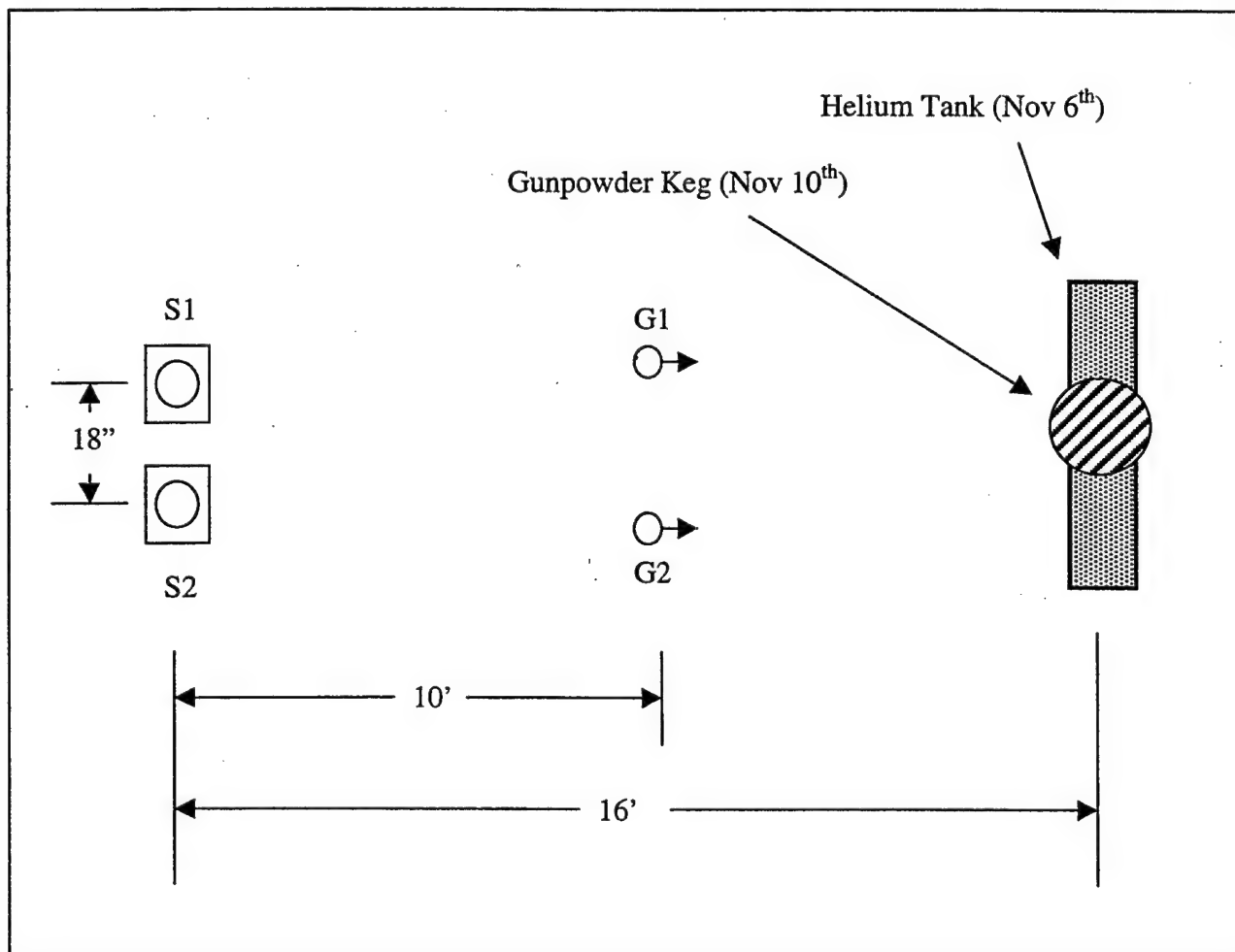
### Geophone #1

Filter: High Pass 40Hz  
Gain: 40db

### Geophone #2

Filter: High Pass 40Hz  
Gain: 40db

**Comments:** Overcast, med-high tide, 4-5ft waves.





## APPENDIX D. COMPUTER PROGRAMS AND SUBROUTINES

This appendix contains the Matlab subroutines and programs that were used during this research for signal processing and data analysis of the recorded beach data. To obtain a copy of the subroutines contact either Professor Thomas G. Muir, Code PH/Mt, or Professor Steven R. Baker, Code PH/Ba at the Naval Postgraduate School, Monterey, California 93943-5000

Appendix D1 – Attenuate.m  
Appendix D2 – Avgsum.  
Appendix D3 – Chan1.m  
Appendix D4 – Chan8.m  
Appendix D5 – Coherence.m  
Appendix D6 – Convert.m  
Appendix D7 – Correlate.m  
Appendix D8 – Displace.m  
Appendix D9 – Filtr.m  
Appendix D10 – Frequency.m  
Appendix D11 – Hankel.m  
Appendix D12 – Hilbrt.m  
Appendix D13 – Hodogram.m  
Appendix D14 – Modification.m  
Appendix D15 – Patch8.m  
Appendix D16 – Powersd.m  
Appendix D17 – Rms8.m  
Appendix D18 – Subhilbrt.m  
Appendix D19 – Subtract.m  
Appendix D20 – Velocity.m  
Appendix D21 – Wavespd.m  
Appendix D22 – Xzplot.m  
Appendix D23 – Theory\_Displace.m



## LIST OF REFERENCES

1. "Landmines – The World Federation of Public Health Associations",  
[<http://www.alpha.org/wfpha/landmines.html>], Nov. 1998.
2. U.S. Navy, Chief of Naval Operations, "United States Naval Mine Warfare Plan" (3<sup>rd</sup> ed), Washington, D.C., 20350, 1996-1997.
3. "Chapter VII – The Maritime Campaign",  
[[http://es.rice.edu/projects/Poli378/Gulf/gwtxt\\_ch7.html](http://es.rice.edu/projects/Poli378/Gulf/gwtxt_ch7.html)], Nov. 1998.
4. "A Moldovan Soldier Probes for Mines at Camp Lejeune",  
[<http://www.defenselink.mil/photos/Aug1996/960818-A-8072J-003.html>], Nov. 1998.
5. "Coastal Battlefield Reconnaissance and Analysis (COBRA)",  
[[http://www.onr.nav.mil/sci\\_tech/ocean/jcm/cobra.html](http://www.onr.nav.mil/sci_tech/ocean/jcm/cobra.html)], Nov. 1998.
6. "Concept: An Active Sonar Using Seismo-Acoustic Interface Waves as the Excitation Carrying Sonar Energy and Information", ONR Slide #Ga-95-231|DES/NLIGA4.
7. Smith, E., Wilson, P., Bacon, F., Manning, J., Behrens, J., Muir, T., "Measurement and Localization of Interface Wave Reflections from a Buried Target", Journal Acoustical Society of America, 103 (5), Pt. 1, May 1998.
8. Gaghan, F.E., *Discrete-Mode Source Development and Testing For a New Seismo-Acoustic Sonar*, Master's Thesis, Naval Postgraduate School, Monterey, CA, Mar. 1998.
9. Kolsky, H., *Stress Waves in Solids*, pp.1-25, Dover Publications, Inc., 1963.
10. Rayleigh, Lord (J.W. Strutt), "On Waves Propagated along the Plane Surface of an Elastic Solid," Proceedings London Mathematical Society, 1885, vol. 17, no. 4.
11. Graff, F.G., *Wave Motion in Elastic Solids*, pp.273-380, Dover Publications, Inc., 1975.
12. Richart, F.E., Hall, J.R., Woods, R.D., *Vibration of Soils and Foundations*, pp.88-92, Prentice-Hall, Inc., 1970.
13. Slide on Scholte Wave Characteristics from D. Rauch, SACLANT ASW Research Center, La Spezia, Italy.
14. Operator's Manual - Electromagnetic Linear Actuator, Aura Systems Inc., El Segundo, CA.

15. Printed with Permission, Aura Systems Inc., El Segundo, CA.
16. Personal communication between D. True, Naval Facilities Engineering Service Center, Naval Construction Battalion Center in Port Hueneme, CA and S.M. Fitzpatrick, Naval Postgraduate School, Jul. 1998.
17. Applied Research Laboratories, University of Texas at Austin, *Characterization of Marine Sediments for Seismic Surveillance and Minehunting*, by Lemair, C., Sep. 1997.
18. Matlab Version 5.2.0.3084 (Signal Processing Toolbox), Jan. 17, 1998, The Mathworks Inc., Natick, MA.
19. ProSeries Model SPS390 Dynamic Signal Analyzer Installation and Operation Manual (Ver. 3.8/Rev. C), Signal Processing Systems, San Diego, CA, 1998.
20. BBN Systems and Technologies Final Report 7677, *Feasibility of Acoustic Landmine Detection*, May 1992.

## INITIAL DISTRIBUTION LIST

1. Defense Technical Information Center.....2  
 8725 John J. Kingman Rd., STE 0944  
 Ft. Belvoir, Virginia 22060-6218
  
2. Dudley Knox Library.....2  
 Naval Postgraduate School  
 411 Dyer Rd.  
 Monterey, California 93943-5101
  
3. Dr. Jeffrey Simmen ..... 1  
 Office of Naval Research, Code 321OA  
 800 N. Quincy St.  
 Arlington, Virginia 22217-5660
  
4. Dr. Douglas Todoroff ..... 1  
 Office of Naval Research, Code 321  
 800 N. Quincy St.  
 Arlington, Virginia 22217-5660
  
5. Professor Thomas G. Muir, Code PH/Mt.....2  
 Department of Physics  
 Naval Postgraduate School  
 Monterey, California 93943-5000
  
6. Professor Steven R. Baker, Code PH/Ba .....2  
 Department of Physics  
 Naval Postgraduate School  
 Monterey, California 93943-5000
  
7. Professor Anthony J. Healey, Code ME/Hy.....2  
 Department of Mechanical Engineering  
 Naval Postgraduate School  
 Monterey, California 93943-5000
  
8. Dr. Raymond Lim .....1  
 Coastal Systems Station, Code R22  
 6703 W. Highway 98  
 Panama City, Florida 32407-7001
  
9. Library, Coastal Systems Station .....1  
 6703 W. Highway 98  
 Panama City, Florida 32407-7001

10. Dr. Richard Gramann .....1  
Applied Research Laboratories  
University of Texas at Austin  
P.O. Box 8029  
Austin, Texas 78713
11. LT Sean M. Fitzpatrick .....2  
12362 Caminito Festivo  
San Diego, California 92131
12. Bill Taylor, Senior Scientist.....1  
Automotive/Industrial Division  
Aura Systems, Inc.  
2335 Alaska Avenue  
El Segundo, California 90245